$RITA_1$

A TOOL FOR EDUCATION AND EXPLORATORY RESEARCH ON SHALLOW WATERS

José Miguel Rodrigues Remédio

B.Sc., Universidade Nova de Lisboa, Portugal, 1987

A thesis submitted to the faculty of the
Oregon Graduate Institute of Science & Technology
in partial fulfillment of the requirements for the degree
Master of Science
in
Environmental Science and Engineering

April 1992

The thesis "$RITA_1$ - a Tool for Education and Exploratory Research on Shallow Waters" by J. Miguel R. Remédio has been examined and approved by the following Examination Committee:

António M. Baptista, PhD.
Assistant Professor
Thesis Adviser

William Fish, PhD.
Assistant Professor

Carl D. Palmer, PhD.
Assistant Professor

M. G. G. Foreman, PhD.
Institute of Ocean Sciences
Victoria, B. C., Canada

ACKNOWLEDGEMENTS

I would like to express my deep gratitude to my thesis adviser Dr. António Melo Baptista, for without his numerous suggestions and encouragement this thesis could never have been written. His friendship for the last five years, both at OGI and previously in Portugal, was greatly appreciated.

Paul Turner and André Fortunato were of great help to me in this project. Our enlightening discussions in addition to their insightful advice greatly improved the quality of my research.

The support of my friends and my family during the preparation of this thesis was invaluable. The love of my daughters Maria and Leonor was a source of motivation and gave me the peace of mind I so much needed. I am especially thankful to the close friends I made in Oregon, for the good times we had together and for everything I learn from them, and to Teresa F. Fernandes, for her constant encouragement.

In addition, I am grateful to the other members of my thesis committee Dr. William Fish, Dr. Carl D. Palmer and Dr. M. G.G. Foreman, for their review of this manuscript and their many comments and suggestions.

This thesis was supported by the grant BM 191-90- Programa Ciência, from the Junta Nacional de Investigação Cientifica e Tecnológica, Portugal, to which I am very grateful. I am also grateful to the Oregon Graduate Institute for the additional financial support provided in the last months of my research.

TABLE OF CONTENTS

LIST OF TABLES

LIST OF FIGURES

ABSTRACT

We formulate, implement, and illustratively apply a model specifically designed to assist graduate-level education and exploratory research on the hydrodynamics and numerics of shallow water circulation. $RITA_1$ (River and Tidal Analysis, 1-D version) uses a flexible finite element wave equation formulation to solve for the one-dimensional shallow water equations. The model allows great flexibility in the choice (a) of the time-discretization scheme, including the ability to handle each physical process differently, and (b) of strategies for the treatment of non-linear terms.

The reference treatment of non-linear terms involves a generic "α-method" in time and a Galerkin finite element method in space. Alternative treatments of non-linear terms include (a) a novel time extrapolation scheme applicable to all or to individual non-linear terms, (b) the element-average of advective acceleration, (c) the use of N+2 upwind weighting functions for the advective acceleration, and (d) an Eulerian-Lagrangian form of the governing equations. $RITA_1$ was tested through extensive numerical experiments, in the context of linear and non-linear tidal propagation, Burgers' equation, and reservoir dynamics.

Selected applications illustrate the potential of the model for exploratory research and education. In particular, we analyze (a) the generation of shallow water tides, (b) the effect on numerical accuracy of the generalized wave equation factor, and (c) the performance of different numerical strategies for the treatment of non-linear terms.

EXTENDED SUMMARY

The numerical modeling of shallow water circulation has progressed very significantly over the past half-century. Indeed, if properly calibrated and validated, leading depth-averaged models can often claim a satisfactory degree of predictive ability within the requirements of many engineering applications. Also, computational costs per grid node and prototype time have decreased drastically, as a consequence of both an explosive evolution of hardware and a steady evolution of numerical techniques.

As in many fast-evolving areas, however, only marginal effort has been dedicated to systematic comparative research, advanced education, and practical training. Reflecting this trend, circulation models are typically developed rigidly around a preferred numerical technique, with the emphasis being placed on computational efficiency rather than on flexible exploration of alternatives.

In this thesis we formulate, implement, and illustratively apply a model specifically designed to assist graduate-level education and exploratory research on the hydrodynamics and numerics of shallow water circulation. This model, $RITA_1$ (River and Tidal Analysis, 1-D version), uses a flexible finite element wave equation formulation to solve for the one-dimensional shallow water equations. $RITA_1$ is served by a flexible user interface and by advanced scientific visualization capabilities, both developed in parallel with this research. The model is also compatible with a series of transport-transformation models that are being developed with similar objectives.

The flexibility of the formulation of $RITA_1$ is particularly important at two levels: (a) problem definition and (b) numerical strategy. Flexible problem definition is fairly common in modern numerical models, and is clearly essential for an effective use of $RITA_1$; a partial measure of the flexibility of $RITA_1$ is provided by the range of illustrative applications reported in this work and elsewhere, which include linear and non-linear tidal propagation, river-reservoir dynamics, and tsunami propagation.

Within the bounds of a finite element wave equation formulation, $RITA_1$ is especially flexible in the choice of (a) the time-discretization scheme, including the ability to discretize different physical processes differently, and (b) the strategy for the treatment of non-linear terms. The emphasis on flexibility for the treatment of non-linear terms is rooted on the belief that treatment of these terms still constitutes a weakness in the state-of-the-art of circulation modeling, drastically affecting, for instance, our ability to simulate shallow or intermittently flooded regions.

The reference treatment of non-linear terms in $RITA_1$ involves a Galerkin finite element method in space and a generic "α-method" in time. Alternative treatments of

these terms include (a) a novel time extrapolation scheme applicable to all or to individual non-linear terms, (b) the average over each element of the advective acceleration, (c) the use of N+2 upwind weighting functions for the advective acceleration, and (d) an Eulerian-Lagrangian re-write of the governing equations.

To test the reliability of $RITA_1$ as a numerical code we performed an extensive set of numerical experiments, in the context of (a) linearized tidal propagation, (b) Burgers' equation, (c) non-linear tidal propagation, and (d) reservoir dynamics. Analytical solutions are available only for problems (a) and (b), but unfortunately these problems have little or no potential for testing the treatment of non-linear processes. For problem (c) we assume the convergence of the reference formulation in $RITA_1$ and generate "refined solutions" by using that formulation with highly resolved grids in space and time. Error-norms are then computed using these "refined solutions". Problem (d) was used to test overall mass preservation. Errors are easy to assess for this problem by comparing net influxes against changes in water volume. Except for the Eulerian-Lagrangian treatment of the governing equations (which will require further investigation), all major model options are considered stable, and are expected to perform reliably.

Selected applications are presented to illustrate the potentialities of $RITA_1$. In particular, we (a) analyze the generation of shallow water tides in a way that is consistent with classroom use in a graduate-level course on estuarine dynamics; (b) explore the performance of different numerical strategies for the treatment of non-linear terms, in a way that is consistent with comparative or exploratory research; and (c) analyze the effect on numerical accuracy of the generalized wave equation factor, in a way that is consistent with classroom use in a graduate-level modeling course. In a separate work[1], we also examine tsunami propagation in sensitivity analysis mode, to identify optimized strategies for the applied, two-dimensional modeling of locally-generated tsunamis in the Cascadia Subduction Zone.

CHAPTER 1

INTRODUCTION

1.1. Context

Rivers, estuaries, lakes and coastal seas support human life in major areas of the globe and it was at the margins of these water bodies, and largely at their expense, that many civilizations appeared and flourished. After almost two centuries of generalized over-exploitation of these natural resources, and of growing needs for water for the most diverse uses, virtually every nation now recognizes that the understanding and management of surface waters is a crucial issue. Indeed, in the last few decades, serious environmental problems have afflicted an increasing number of surface waters all over the world, sometimes to the extent of ecological disasters[2, 3].

Most of what happens in surface waters is strongly affected by their hydrodynamics. For example, the dispersal of pollutants in an estuary, the navigability of a river, the stability of a sand beach, the distribution of organisms in a shallow bay, and the viability of an off-shore oil platform are all among the innumerous processes and activities which are determined by the characteristics of the water circulation. The capability of predicting the hydrodynamics of a water body is therefore of unquestionable importance.

Rivers, estuaries and coastal seas often share an important characteristic: their depth is much smaller than their horizontal dimensions. For this reason, circulation in these water bodies can often be described by the Shallow Water Equations, frequently written in depth-averaged form.

The numerical modeling of shallow waters has progressed very significantly over the past half-century. Leading depth-averaged models[4-7], if properly calibrated and validated, can claim a satisfactory degree of predictive ability within the requirements of many engineering applications. In recent years, computational costs per grid node and per prototype unit have decreased drastically, because of an explosive evolution of hardware and a steady evolution of numerical techniques. This reduction of computational costs has in turn fueled fruitful research and applications in both fully 3-D modeling[8-11] and in long-term, highly resolved, regional modeling[12, 13].

As in many fast-evolving areas, however, only marginal effort has been dedicated to systematic comparative research[a], advanced education, and practical training. Reflecting this trend, circulation models have typically been developed rigidly around a preferred numerical technique, with emphasis being placed on computational efficiency rather than on the flexible exploration of alternative formulations. Although this approach is effective for application-oriented models, we believe that there is a strong need for a circulation model designed to educate and to explore, rather than to solve for specific applications.

The following arguments indicate the pressing need for education and exploratory research models:

- Numerical models are widely utilized and they are now commonly available to users with limited background and experience with numerical methods. Misuse of models in important applications is therefore a clear risk, and one that society can not afford when models guide our management of scarce resources. Education-oriented models used in undergraduate and graduate-level courses and in professional training courses can improve the competence of model users.
- Pressing issues involving surface water systems increasingly require multi-disciplinary approaches, which bring together people with diverse technical expertise. In these multi-disciplinary settings, it is often difficult to establish common terminology and perception of concepts. Education-oriented models, for circulation and a variety of other processes, can help build the much needed common terminology and perception of concepts.
- Numerical modeling has been an extremely prolific area of research. A variety of techniques have been developed, and even those that "don't work" often provide useful insight (or just breadth of knowledge) to advanced modelers and numerical analysts. However, because they have limited practical application, the least used techniques are not readily available in coded form, and are often partially or completely "lost" to the process of educating new generations. An education-oriented model is ideally suited to incorporate such techniques, as a part of a broad range of alternative techniques.
- Since most of the numerical models are rigidly developed around a fixed numerical scheme, and their I/O structures are often mutually incompatible, systematic comparison of numerical modeling methods is rarely performed. Models that allow the flexible choice of the numerical scheme from a broad selection of alternatives, are particularly well suited for such comparison.
- Sensitivity analysis and exploratory research are very important for the design of modeling strategies for particular problems. Preliminary testing of simplified problems can be extremely useful for that purpose. However, the rigidity and

a. The Tidal Flow Forum[14] was a notable exception.

computational cost of most models discourage such practice. Easy-to-use research-oriented models are particularly useful for sensitivity analysis, and can thus improve the quality of problem-solving modeling.

The development on advanced education, and practical training areas can be achieved by the creation of flexible computational structures, including a range of optional numerical schemes and supported by comprehensive, easy to use, visualization tools and user interfaces.

1.2. Scope and objectives

The primary objective of this thesis is to develop, validate, and illustratively apply an education and exploratory research model for circulation in shallow waters. The main target applications for the model are:

- Advanced (graduate-level) education in either the modeling/numerics or the hydrodynamics of shallow waters. The model should be a tool (a) for teachers, who will use it to illustrate concepts in the classroom; and (b) for students, who will consolidate their knowledge through actual experimentation and exploration.
- Comparative research in circulation modeling. In particular, the model should allow detailed comparison, complementary to formal analysis, of a range of approaches to the treatment of non-linear processes.
- Exploratory circulation modeling. In particular, the model should allow one-dimensional sensitivity studies to help design modeling strategies for higher dimension detailed studies.

Both the numerical scheme and the hydrodynamic problem should be easily definable, by means of a user-friendly interface. Up-to-date visualization techniques, including animation, should be used to display the results. To satisfy these goals we developed $RITA_1$ (River and Tidal Analysis, 1-D version), based on a flexible implementation of a finite element wave equation formulation. $RITA_1$ was built as a part of ACE_1[15, 16], an evolving computational structure composed of:

- Selected flow and transport-transformation models[17], most of which are in design or under development, and all of which are oriented towards education and exploratory research.
- A coherent user interface framework, that controls grid generation, model selection and execution, definition of input parameters, and scientific visualization. New model-specific menus are added as those models become available, a task that for $RITA_1$ was accomplished in parallel with but outside this research.
- A flexible scientific visualization platform designed generically enough to serve all target models.

In general, components of ACE_1 have a close correspondence with higher-dimension components of ITACA (Integrated Tools for the Analysis of Coasts and Land-Margins[18]), a computational modular structure designed to support inter-disciplinary research on coastal watersheds[13]. In the case of $RITA_1$, correspondence is with ADCIRC[7, 19], a new two-dimensional, depth-averaged tidal and storm surge model developed jointly at University of Notre Dame and at University of North Carolina.

1.3. Organization and contents

This thesis comprises five chapters and two appendices. Chapter 1 puts the need for an education-oriented circulation model such as $RITA_1$ in context, identifies the scope and objectives of the reported research, and describes the organization of the text.

Chapter 2 describes the formulation of $RITA_1$ in detail. The model uses a flexible finite element wave equation formulation to solve for the one-dimensional shallow water equations. For linear processes our reference formulation uses a generic "α-method" in time, and a Galerkin finite element method with linear shape functions in space; non-linear processes are treated similarly, but the "α-method" is required to lead to explicit representations. Alternatively, $RITA_1$ can treat non-linear processes by using (a) a novel time extrapolation scheme applicable to all or to individual non-linear terms, (b) an element-averaged representation for the advective acceleration, (c) N+2 upwind weighting functions for the advective acceleration, and (d) an Eulerian-Lagrangian re-write of the governing equations.

Chapter 3 describes the validation of $RITA_1$. We report an extensive set of numerical experiments, in the context of (a) linearized tidal propagation, (b) Burger's equation, (c) non-linear tidal propagation, and (d) reservoir dynamics. Analytical solutions are available only for problems (a) and (b), but unfortunately these problems have little or no potential for testing the treatment of non-linear processes in $RITA_1$. For problem (c) we developed "refined" solutions (against which to measure the error) by using the reference formulation in $RITA_1$ with over-refined grids in space and time. Problem (d) was used exclusively to test overall mass preservation, and errors can therefore be assessed comparing net influxes against changes in water volume. Except for the Eulerian-Lagrangian treatment of the governing equations (which will require further investigation), all major model options are considered validated, and are expected to perform reliably.

The use of the model for graduate-level teaching/education and for exploratory research is illustrated in Chapter 4. Selected applications are presented to illustrate the potential uses of the model. In particular, we (a) analyze the effect on numerical accuracy

of the generalized wave equation factor, in a way that is consistent with classroom use in a graduate-level modeling course; (b) explore the performance of different numerical strategies for the treatment of non-linear terms, in a way that is consistent with comparative or exploratory research; and (c) analyze the generation of shallow water tides in a way that is consistent with classroom use in a graduate-level course on estuarine dynamics.

Conclusions and recommendations are presented in Chapter 5. $RITA_1$ represents a useful step towards an integrated set of tools for education and exploratory research on advanced numerics, surface water dynamics, and environmental analysis and modeling. The anticipated use of $RITA_1$ and companion tools (ACE_1 and ELA_1) in selected courses at OGI and other universities should provide the necessary feedback for further developments.

Appendix A describes the analytical solutions used in Chapter 3. Appendix B contains a brief users' manual for $RITA_1$. Like the code itself, this manual is expected to evolve in time. In particular, the users' manual will have to be extended to include the $RITA_1$ options of the user interface of ACE_1.

CHAPTER 2

FORMULATION

$RITA_1$ uses a flexible finite element wave equation formulation to solve the one-dimensional shallow water equations. This chapter describes the model formulation. Section 2.1 briefly reviews the adopted form of the primitive shallow water equations, and describes and motivates the transformation of these equations into "wave equation" and "generalized wave equation" forms, following Lynch[20], Kinnmark[21-23], and others[7, 24-28]. Section 2.2 presents a detailed description of the formulation that we adopted as reference. Finally, Section 2.3 describes selected alternative treatments of the non-linear terms of the governing equations.

2.1. Background

2.1.1. One-Dimensional Shallow Water Equations

We consider the one-dimensional primitive shallow water equations, written as:

continuity:

$$\mathbf{L} \equiv \frac{\partial \eta}{\partial t} + \frac{\partial}{\partial x} Hu = 0 \qquad [2.1]$$

conservation of momentum:

$$\mathbf{M} = \frac{\partial u}{\partial t} + u\frac{\partial u}{\partial x} + g\frac{\partial \eta}{\partial x} + \tau u - \frac{\upsilon}{H}\frac{\partial^2}{\partial x^2} Hu = 0 \qquad [2.2]$$

where (Fig. 1):

- u - velocity [ms^{-1}]
- η - water elevation relative to a reference level [m]
- g - acceleration of gravity [ms^{-2}]
- τ - friction parameter [s^{-1}]
- υ - viscosity [m^2s^{-1}]
- $H \equiv h + \eta$ - total water depth [m]
- h - water depth relative to a reference level [m]

The friction coefficient is defined as:

$$\tau = \frac{gn^2|u|}{R^{1/3}} \qquad [2.3]$$

with:

$R \equiv P/A$ - hydraulic radius [m]

P - wetted perimeter [m]

A - cross-sectional area [m^2]

n - Manning coefficient [$sm^{-1/3}$]

Equations [2.1] and [2.2] may be perceived as describing either (a) a laterally uniform depth-averaged flow (in which case R is approximated by H), or (b) a cross-section averaged flow in a constant-width channel, depending on the meaning assigned to the viscosity and friction coefficients. While either type of flow is over-simplified for most practical situations, these equations support the educational and exploratory research role for which $RITA_1$ was designed.

2.1.2. Wave Equation Formulations

The use of a wave equation formulation to numerically solve for the shallow water equations was first introduced by Lynch[20]. The concept is reviewed below, for the 1-D shallow water equations.

Recognizing that Galerkin finite element methods lead to wiggly (i.e., with parasitic spatial oscillations) solutions to this problem, Lynch resorted to a classical transformation to convert the continuity into a wave-like equation (the Continuity Wave Equation):

$$W \equiv \frac{\partial L}{\partial t} - \frac{\partial M^c}{\partial x} + \tau L = \frac{\partial^2 \eta}{\partial t^2} - \frac{\partial^2}{\partial x^2} Huu - g \frac{\partial}{\partial x} H \frac{\partial \eta}{\partial x} + \upsilon \frac{\partial^3}{\partial x^3} Hu + \tau \frac{\partial \eta}{\partial t} = 0 \qquad [2.4]$$

where

$$M^c \equiv HM + uL = \frac{\partial}{\partial t} Hu + \frac{\partial}{\partial x} Huu + gH \frac{\partial \eta}{\partial x} + \tau Hu - \upsilon \frac{\partial^2}{\partial x^2} Hu = 0 \qquad [2.5]$$

represents the conservative form of the momentum equation.

Formal examination of amplification and propagation errors of the same Galerkin finite element methods, when Equation [2.4] is used instead of Equation [2.1] revealed that short wavelengths responsible for wiggles were damped[20]. These studies were performed on the linearized 1-D equations; however numerical experimentation have confirmed that smooth solutions can be obtained in higher dimensions and for both linear and non-linear problems.

Kinnmark[21--23] extended the work of Lynch by introducing the Generalized Continuity Wave Equation formulation. In this formulation, as in Lynch's, a wave-like equation replaces the continuity equation. However, the new operator is now written as:

$$W^g \equiv \frac{\partial L}{\partial t} - \frac{\partial M^c}{\partial x} + GL \qquad [2.6]$$

leading to:

$$\frac{\partial^2 \eta}{\partial t^2} - \frac{\partial^2}{\partial x^2} Huu - g\frac{\partial}{\partial x} H\frac{\partial \eta}{\partial x} + \upsilon\frac{\partial^3}{\partial x^3} Hu + G\frac{\partial \eta}{\partial t} + \frac{\partial}{\partial x}(G - \tau) Hu = 0 \qquad [2.7]$$

G is an arbitrary numerical parameter with the same units as the friction factor τ (s^{-1}).

In the Continuity Wave Equation, the presence of τ as a coefficient of the first time derivative of η makes the mass matrix corresponding to that equation time-dependent and computationally expensive to solve in an implicit or semi-implicit way. The main advantage of the generalized formulation is that, for a constant $G=\tau$, the mass matrix becomes time-independent, allowing an implicit treatment without significant increase in computational cost. This approach retains the ability to eliminate spurious node-to-node oscillations.

Several authors[24, 27-32] have formally investigated the wave equation formulations or have tested these formulations in the context of realistic multi-dimensional shallow water problems involving non-linear processes. Results consistently support the findings of Lynch and of Kinnmark, and suggest that generalized wave equation finite element methods favorably compare with corresponding primitive equation methods.

One of the remaining questions on the use of the generalized wave equation finite element is the choice of the parameter G. Formal studies[22] suggest that for optimal accuracy and stability G should be similar in magnitude to the friction factor τ. This is partially confirmed by our experimental analysis (Section 4.1.1). In the limit of large values of G, the wave and generalized wave equation formulations approach the behavior of the corresponding primitive equation formulation; hence, spurious node-to-node oscillations should be expected. In the limit of small values of G is too small, mass conservation problems may occur because the system of equations lacks the ability to damp out errors in the continuity equation[22].

From here on we refer the Generalized Continuity Wave Equation simply as wave equation.

2.2. Reference Formulation

The finite element method is used. It is based on a weighted residuals method in which the residuals, weighted by arbitrary weighting functions are minimized over the domain.

The dependent variables are approximated, at an elemental level, by combinations of a set of predetermined basis functions:

$$\eta \approx \sum_{i=1}^{N} \eta_i \phi_i(r) \qquad [2.8]$$

$$u \approx \sum_{i=1}^{N} u_i \phi_i(r) \qquad [2.9]$$

where

- η_i - values of elevation at the nodes [m]
- u_i - values of velocity at the nodes [ms^{-1}]
- N - number of nodes in the domain
- ϕ_i - finite element basis functions
- r - local space-coordinate

In its present version, $RITA_1$ is limited to linear shape functions, defined locally as:

$$\phi_1 = \frac{1}{2}(1-r) \qquad \phi_2 = \frac{1}{2}(1+r) \qquad [-1 \le r \le 1] \qquad [2.10]$$

However, quadratic basis functions could easily be incorporated in the model.

The bathymetry is defined functionally as:

$$h \approx \sum_{i=1}^{N} h_i \phi_i \qquad [2.11]$$

where h_i is the depth at the node i. Other coefficients in the governing equations (υ, τ if the equations are linear, and n if the equations are non-linear) are treated as constants.

Once the residuals are defined, for both the wave and the momentum equations the Galerkin method is used; hence the weighting functions are the same as the basis functions. This approach leads to two systems of N equations, one corresponding to the GCWE, and the other to the momentum equation, solved for the velocities at the nodes. In each time step, the system for the GCWE is solved first. The results are then used for the solution of the momentum equation.

2.2.1. The Generalized Continuity Wave Equation

We write the weighted residual statement as:

$$\int_{\Omega} \varepsilon \phi_k dx = 0 \qquad k = 1, N \qquad [2.12]$$

where the residual, ε, is:

$$\varepsilon = \frac{\partial^2 \eta}{\partial t^2} - \frac{\partial^2}{\partial x^2} Huu - g \frac{\partial}{\partial x} H \frac{\partial \eta}{\partial x} + \upsilon \frac{\partial^3}{\partial x^3} Hu + G \frac{\partial \eta}{\partial t} + \frac{\partial}{\partial x} (G - \tau) Hu \qquad [2.13]$$

All the terms involving space derivatives are integrated by parts, as follows:

$$\int_{\Omega} \phi_k \frac{\partial}{\partial x} \left(\frac{\partial}{\partial x} Huu + gH \frac{\partial \eta}{\partial x} - (G - \tau) Hu - \upsilon \frac{\partial^2}{\partial x^2} Hu \right) dx =$$

$$= \phi_k \left(\frac{\partial}{\partial x} Huu + gH \frac{\partial \eta}{\partial x} - (G - \tau) Hu - \upsilon \frac{\partial^2}{\partial x^2} Hu \right) \Big|_0^L - \qquad [2.14]$$

$$\int_{\Omega} \frac{\partial \phi_k}{\partial x} \left(\frac{\partial}{\partial x} Huu + gH \frac{\partial \eta}{\partial x} - (G - \tau) Hu - \upsilon \frac{\partial^2}{\partial x^2} Hu \right) dx \qquad k = 1, N$$

leading to a general reduction of the order of the space derivatives at the expense of an additional boundary condition.

We note that linear shape functions do not allow the actual treatment of the viscosity term in the wave equation. Indeed, even using integration by parts, second-order derivatives will be involved. Viscosity then appears only in the momentum equation, which constitutes a limitation of our formulation.

Time derivatives are approximated by finite differences using up to three time levels. For the second derivative in time only one scheme is consistent[34]; for all the others terms a general α-method is used. Since the wave equation is solved before the momentum equation, all the linear terms in the wave equation involving velocity and all the nonlinear terms must be treated explicitly. The time discretization scheme is specified for each term by the parameters w_i^{Γ} with Γ identifies the term of the equation and i the time step. All the integrals are computed using 3-point Gauss quadrature.

Developing each term on an elemental basis we have:

- **Second-order time derivative:**

The spatial discretization is:

$$\int_e \phi_k \frac{\partial^2 \eta}{\partial t^2} dx \approx \frac{\partial^2}{\partial t^2} \sum_{i=1}^{2} \eta_i \int_{-1}^{1} \phi_k \phi_i \frac{dx}{dr} dr = \frac{\Delta x_e}{2} \frac{\partial^2}{\partial t^2} \sum_{i=1}^{2} \eta_i \int_{-1}^{1} \phi_k \phi_i dr \qquad k = 1, 2 \qquad [2.15]$$

where:

$$\frac{\partial^2 \eta}{\partial t^2} \approx \frac{1}{(\Delta t)^2}(\eta^{n+1} - 2\eta^n + \eta^{n-1}) \qquad [2.16]$$

and Δx_e is the length of the element.

- **First-order time derivative:**

The G factor is assumed to be constant in space and time. Hence:

$$\int_e \phi_k G \frac{\partial \eta}{\partial t} dx \approx G \frac{\Delta x_e}{2} \frac{\partial}{\partial t} \sum_{i=1}^{2} \eta_i \int_{-1}^{1} \phi_k \phi_i dr \qquad k = 1, 2 \qquad [2.17]$$

where:

$$\frac{\partial \eta}{\partial t} \approx \frac{1}{\Delta t}(w_0^1 \eta^{n+1} + w_1^1 \eta^n + w_2^1 \eta^{n-1}) \qquad [2.18]$$

- **Gravity:**

The gravity term in the wave equation has two components, which result from separating the depth h and the finite amplitude η. The first component is linear; the space discretization is given by:

$$\int_e \frac{\partial \phi_k}{\partial x} g h \frac{\partial \eta}{\partial x} dx \approx \frac{2}{\Delta x_e} g \left(\sum_{i=1}^{2} \sum_{j=1}^{2} h_i \eta_j \int_{-1}^{1} \frac{\partial \phi_k}{\partial r} \phi_i \frac{\partial \phi_j}{\partial r} dr \right) \qquad k = 1, 2 \qquad [2.19]$$

and the time discretization potentially includes values at three time levels:

$$h \frac{\partial \eta}{\partial x} \approx w_0^2 h \frac{\partial}{\partial x} \eta^{n+1} + w_1^2 h \frac{\partial}{\partial x} \eta^n + w_2^2 h \frac{\partial}{\partial x} \eta^{n-1} \qquad [2.20]$$

The second component is non-linear and the mass matrix must be treated explicitly in order to preserve time independency. Then:

$$\int_e \frac{\partial \phi_k}{\partial x} g \eta \frac{\partial \eta}{\partial x} dx \approx \frac{2}{\Delta x_e} g \left(\sum_{i=1}^{2} \sum_{j=1}^{2} \eta_i \eta_j \int_{-1}^{1} \frac{\partial \phi_k}{\partial r} \phi_i \frac{\partial \phi_j}{\partial r} dr \right) \qquad k = 1, 2 \qquad [2.21]$$

and the time discretization only considers the values at time n and n-1:

$$\eta \frac{\partial \eta}{\partial x} \approx w_1^3 \eta^n \frac{\partial}{\partial x} \eta^n + w_2^3 \eta^{n-1} \frac{\partial}{\partial x} \eta^{n-1} \qquad [2.22]$$

- **Advection:**

As in the gravity term, the advection term includes a finite amplitude component. Since one of the objectives of $RITA_1$ is to allow a independent treatment of each term, an explicit treatment is required. For the component which does not depend on the finite amplitude we have:

$$\int_e \frac{\partial \phi_k}{\partial x}\frac{\partial}{\partial x}huudx = \int_e \frac{\partial \phi_k}{\partial x}(2hu\frac{\partial u}{\partial x} + uu\frac{\partial h}{\partial x})\,dx = \int_e \frac{\partial \phi_k}{\partial x}2hu\frac{\partial u}{\partial x}dx + \int_e \frac{\partial \phi_k}{\partial x}uu\frac{\partial h}{\partial x}dx \approx$$
$$\approx \frac{2}{\Delta x_e}\left(\int_e \frac{\partial \phi_k}{\partial r}2hu\frac{\partial u}{\partial r}dr + \int_e \frac{\partial \phi_k}{\partial r}uu\frac{\partial h}{\partial r}dr\right) \qquad k = 1, 2 \qquad [2.23]$$

with:

$$\frac{\partial}{\partial x}huu \approx w_1^4\frac{\partial}{\partial x}h^n u^n + w_2^4\frac{\partial}{\partial x}h^{n-1}u^{n-1} \qquad [2.24]$$

The finite amplitude effect is treated as:

$$\int_e \frac{\partial \phi_k}{\partial x}\frac{\partial}{\partial x}\eta uudx \approx \frac{2}{\Delta x_e}\left(\int_e \frac{\partial \phi_k}{\partial r}2\eta u\frac{\partial u}{\partial r}dr + \int_e \frac{\partial \phi_k}{\partial r}uu\frac{\partial \eta}{\partial r}dr\right) \qquad k = 1, 2 \qquad [2.25]$$

$$\frac{\partial}{\partial x}\eta uu \approx w_1^5\frac{\partial}{\partial x}\eta^n u^n u^n + w_2^5\frac{\partial}{\partial x}\eta^{n-1}u^{n-1}u^{n-1} \qquad [2.26]$$

- **Friction:**

Four friction terms are considered:

a term on τ and h:

$$\int_e \frac{\partial \phi_k}{\partial x}\tau hudx \approx \left(\sum_{i=1}^{2}\sum_{j=1}^{2} h_i u_j \int_{-1}^{1}\frac{\partial \phi_k}{\partial r}\phi_i\phi_j\tau dr\right) \qquad k = 1, 2 \qquad [2.27]$$

$$\tau hu \approx w_1^6\tau^n h^n u^n + w_2^6\tau^{n-1}h^{n-1}u^{n-1} \qquad [2.28]$$

a term on G and h:

$$\int_e \frac{\partial \phi_k}{\partial x}Ghudx \approx G\left(\sum_{i=1}^{2}\sum_{j=1}^{2} h_i u_j \int_{-1}^{1}\frac{\partial \phi_k}{\partial r}\phi_i\phi_j dr\right) \qquad k = 1, 2 \qquad [2.29]$$

$$hu \approx w_1^7 h^n u^n + w_2^7 h^{n-1}u^{n-1} \qquad [2.30]$$

a term on τ and η:

$$\int_e \frac{\partial \phi_k}{\partial x}\tau\eta udx \approx \left(\sum_{i=1}^{2}\sum_{j=1}^{2} \eta_i u_j \int_{-1}^{1}\frac{\partial \phi_k}{\partial r}\phi_i\phi_j\tau dr\right) \qquad k = 1, 2 \qquad [2.31]$$

$$\tau\eta u \approx w_1^8\tau^n\eta^n u^n + w_2^8\tau^{n-1}\eta^{n-1}u^{n-1} \qquad [2.32]$$

a term on G and η:

$$\int_e \frac{\partial \phi_k}{\partial x}G\eta udx \approx G\left(\sum_{i=1}^{2}\sum_{j=1}^{2} \eta_i u_j \int_{-1}^{1}\frac{\partial \phi_k}{\partial r}\phi_i\phi_j dr\right) \qquad k = 1, 2 \qquad [2.33]$$

$$\eta u \approx w_1^9 \eta^n u^n + w_2^9 \eta^{n-1} u^{n-1} \qquad [2.34]$$

Friction can be linearized and considered constant throughout the domain and in time. In this case Equations [2.27], [2.29], [2.31] and [2.33] reduce to:

$$\int_e \frac{\partial \phi_k}{\partial x}(G-\tau)\, hu dx \approx (G-\tau) \sum_{i=1}^{2}\sum_{j=1}^{2} h_i u_j \int_{-1}^{1} \frac{\partial \phi_k}{\partial r}\phi_i \phi_j dr \qquad k = 1,2 \qquad [2.35]$$

$$\int_e \frac{\partial \phi_k}{\partial x}(G-\tau)\, \eta u dx \approx (G-\tau) \sum_{i=1}^{2}\sum_{j=1}^{2} \eta_i u_j \int_{-1}^{1} \frac{\partial \phi_k}{\partial r}\phi_i \phi_j dr \qquad k = 1,2 \qquad [2.36]$$

2.2.2. The Momentum Equation

The residual is now:

$$\varepsilon = \frac{\partial u}{\partial t} + u\frac{\partial u}{\partial x} + g\frac{\partial \eta}{\partial x} + \tau u - \frac{\upsilon}{H}\frac{\partial^2}{\partial x^2} Hu \qquad [2.37]$$

and the weighted residual statement over the domain reads:

$$\int_\Omega \varepsilon \phi_k dx = 0 \qquad k = 1, N \qquad [2.38]$$

The viscosity term is integrated by parts to balance the order of the derivatives:

$$\int_\Omega \phi_k \frac{\upsilon}{H}\frac{\partial^2}{\partial x^2} Hu = \phi_k \frac{\upsilon}{H}\frac{\partial}{\partial x} Hu \Big|_0^L - \upsilon \int_\Omega \frac{\partial}{\partial x}\frac{\phi_k}{H}\frac{\partial}{\partial x} Hu dx \qquad k = 1, N \qquad [2.39]$$

Each term is treated in time using a maximum of two time steps. The time discretization scheme is specified for each term by the parameters m_i^Γ with Γ specifying the term of the equation and i the time step; the choice between implicit and explicit treatment of each term is done considering that the time independence of the mass matrix must be preserved. At an elemental basis, we have for each term:

- **Local acceleration:**

$$\int_e \phi_k \frac{\partial u}{\partial t} dx \approx \frac{\Delta x_e}{2} \int_{-1}^{1} \phi_k \frac{\partial u}{\partial t} dr = \frac{\Delta x_e}{2}\frac{\partial}{\partial t} \sum_{i=1}^{2} u_i \int_{-1}^{1} \phi_k \phi_i dr \qquad k = 1,2 \qquad [2.40]$$

with:

$$\frac{\partial u}{\partial t} \approx \frac{1}{\Delta t}(u^{n+1} - u^n) \qquad [2.41]$$

- **Advection:**

$$\int_e \phi_k u \frac{\partial u}{\partial x} dx = \int_{-1}^{1} \phi_k u \frac{\partial u}{\partial r} dr \approx \sum_{i=1}^{2} \sum_{j=1}^{2} u_i u_j \int_{-1}^{1} \phi_k \phi_i \frac{\partial \phi_j}{\partial r} dr \qquad k = 1, 2 \qquad [2.42]$$

with:

$$u \frac{\partial u}{\partial x} \approx u^n \frac{\partial}{\partial x} u^n \qquad [2.43]$$

- **Gravity:**

$$\int_e \phi_k g \frac{\partial \eta}{\partial t} dx = g \int_{-1}^{1} \phi_k \frac{\partial \eta}{\partial r} dr \approx g \sum_{i=1}^{2} \eta_i \int_{-1}^{1} \phi_k \frac{\partial \phi_i}{\partial r} dr \qquad k = 1, 2 \qquad [2.44]$$

with:

$$\frac{\partial \eta}{\partial x} \approx m_0^2 \frac{\partial}{\partial x} \eta^{n+1} + m_1^2 \frac{\partial}{\partial x} \eta^n \qquad [2.45]$$

- **Friction:**

$$\int_e \phi_k \tau u dx \approx \frac{\Delta x_e}{2} \sum_{i=1}^{2} u_i \int_{-1}^{1} \frac{\partial \phi_k}{\partial r} \phi_i \tau dr \qquad k = 1, 2 \qquad [2.46]$$

with:

$$\tau u \approx \tau^n u^n \qquad [2.47]$$

For linear friction this term is linear and can be re-written as:

$$\int_e \phi_k \tau u dx \approx \frac{\Delta x_e}{2} \tau \sum_{i=1}^{2} u_i \int_{-1}^{1} \phi_k \phi_i dr \qquad k = 1, 2 \qquad [2.48]$$

with:

$$\tau u \approx m_0^3 \tau u^{n+1} + m_1^3 \tau u^n \qquad [2.49]$$

- **Viscosity:**

$$\upsilon \int_e \frac{\partial}{\partial x} \frac{\phi_k}{H} \frac{\partial}{\partial x} H u dx \approx \frac{2}{\Delta x_e} \upsilon \left(\sum_{i=1}^{2} \sum_{j=1}^{2} (H_i \eta_j + \eta_i H_j) \int_{-1}^{1} \frac{\partial}{\partial r} \frac{\phi_k}{H} \phi_i \frac{\partial \phi_j}{\partial r} dr \right) \qquad k = 1, 2 \qquad [2.50]$$

with:

$$\frac{\upsilon}{H} \frac{\partial}{\partial x} H u \approx \frac{\upsilon}{H^n} \frac{\partial}{\partial x} H^n u^n \qquad [2.51]$$

2.2.3. Boundary Conditions

The domain the value of either the elevation or the velocity must be specified at each boundary. The values specified can be the same at the two boundaries (e.g. two elevations or two velocities) or they can be different (i.e. the velocity at one boundary and the elevation at the other).

The elevations prescribed in the boundaries are strictly obeyed by the solution of the wave equation; the same happens to the values of velocity in the momentum equation. Those are essential boundary conditions. If an elevation (or velocity) is prescribed for a certain boundary, that boundary is solved as a natural boundary condition in the momentum equation (or in the wave equation, when velocity is prescribed); a boundary term comes "naturally" from the integration by parts (Equations [2.14] and [2.39]).

The surface integral from Equation [2.14] is treated as proposed by Lynch[20], substituting in the conservative momentum equation (Equation [2.5]):

$$\phi_k \left(\frac{\partial}{\partial x}Huu + gH\frac{\partial \eta}{\partial x} - (G-\tau)Hu\right)\Big|_0^L = -\phi_k \left(\frac{\partial}{\partial t}Hu + GHu\right)\Big|_0^L \qquad [2.52]$$

Since this only applies when flow (Q=B*Hu, where B is the width) is prescribed, one has:

$$\frac{\partial}{\partial t}Hu\Big|^{n+1} \approx \frac{Q^{n+1}-Q^n}{B\Delta t} \qquad [2.53]$$

where Δt is the time step.

The boundary term from Equation [2.39] is treated as:

$$\frac{\upsilon}{H}\frac{\partial}{\partial x}Hu\Big|_0^L \approx \frac{\upsilon}{H_N}\frac{H_N u_N - H_{N-1}u_{N-1}}{\Delta x_{N-1}} - \frac{\upsilon}{H_1}\frac{H_2 u_2 - H_1 u_1}{\Delta x_1} \qquad [2.54]$$

A transmissive boundary[35] can also be prescribed in $RITA_1$: it works as an elevation specified boundary, but the value prescribed is computed based on the assumption that the wave travels without change of form across the boundary. In that case we have:

$$\frac{D\eta}{Dt} \equiv \frac{\partial \eta}{\partial t} \pm c\frac{\partial \eta}{\partial x} = 0 \qquad [2\text{-}55]$$

with $c = \sqrt{gh}$.

For the downstream (left side) boundary we have:

$$\frac{\partial \eta}{\partial t} = c\frac{\partial \eta}{\partial x} \qquad [2\text{-}56]$$

which can be approximated by:

$$\frac{\eta_1^{n+1} - \eta_1^n}{\Delta t} = -\sqrt{g\bar{h}}\frac{\eta_1^n - \eta_2^n}{\Delta x_1} \qquad [2\text{-}57]$$

$$\frac{\eta_1^{n+1} - \eta_1^n}{\eta_1^n - \eta_2^n} = -\frac{\Delta t\sqrt{g\bar{h}}}{\Delta x_1} \qquad [2.58]$$

leading to:

$$\eta_1^{n+1} = \eta_1^n - (\eta_1^n - \eta_2^n)\frac{\Delta t\sqrt{g\bar{h}}}{\Delta x_1} \qquad [2.59]$$

where $\bar{h}$ denotes the average depth at the boundary element. Similarly, for the upstream boundary we have:

$$\eta_N^{n+1} = \eta_N^n - (\eta_N^n - \eta_{N-1}^n)\frac{\Delta t\sqrt{g\bar{h}}}{\Delta x_{N-1}} \qquad [2.60]$$

2.2.4. Initial Conditions

Initial conditions should be prescribed as values for elevation and velocity at all nodes at time zero. Since the time discretization for the wave equation uses three time levels, additional information should also be provided at the time immediately preceding time zero. In short, elevation and velocities must be prescribed for all nodes at two consecutive time steps. The values can be assumed constant, in space and time ("cold start"), or be derived from the results of a previous run of the model or from an analytical solution, if available.

2.3. Alternative Schemes

2.3.1. Extrapolation in Time

The reference formulation of $RITA_1$ deals with all non-linear terms explicitly, to allow (a) the decoupling of the wave equation from the momentum equation and (b) the time-independence of the mass matrices of the algebraic systems associated to both equations. However, both these objectives can be achieved by introducing a pseudo-implicit treatment of the non-linear terms. The approach is novel, has inherent potential, and should be applicable to all non-linear terms. It consists in "estimating" the elevations and velocities at time n+1 by linear extrapolation from times n and n-1, i.e.

$$\tilde{\eta}^{n+1} = 2\eta^n - \eta^{n-1} \qquad [2.61]$$

$$\tilde{u}^{n+1} = 2u^n - u^{n-1} \qquad [2.62]$$

and using the resulting values and their derivatives to estimate the non-linear terms at n+1.

Using this technique we can have for the time discretization of the non-linear terms in the wave equation:

- **Gravity:**

$$g\eta\frac{\partial\eta}{\partial x} \approx w_0^3\tilde{\eta}^{n+1}\frac{\partial\tilde{\eta}^{n+1}}{\partial x} + w_1^3\eta^n\frac{\partial}{\partial x}\eta^n + w_2^3\eta^{n-1}\frac{\partial}{\partial x}\eta^{n-1} \qquad [2.63]$$

- **Advection:**

$$\frac{\partial}{\partial x}huu \approx w_0^5\frac{\partial}{\partial x}h\tilde{u}^{n+1}\tilde{u}^{n+1} + w_1^5\frac{\partial}{\partial x}hu^nu^n + w_2^5\frac{\partial}{\partial x}hu^{n-1}u^{n-1} \qquad [2.64]$$

$$\frac{\partial}{\partial x}\eta uu \approx w_0^5\frac{\partial}{\partial x}\tilde{\eta}^{n+1}\tilde{u}^{n+1}\tilde{u}^{n+1} + w_1^5\frac{\partial}{\partial x}\eta^nu^nu^n + w_2^5\frac{\partial}{\partial x}\eta^{n-1}u^{n-1}u^{n-1} \qquad [2.65]$$

- **Friction:**

A non-linear friction coefficient $\tilde{\tau}^{n+1}$ can be estimated using $\tilde{\eta}^{n+1}$ and $\tilde{u}^{n+1}$.

$$\tau hu \approx w_0^6\tilde{\tau}^{n+1}h\tilde{u}^{n+1} + w_1^6\tau^nhu^n + w_2^6\tau^{n-1}hu^{n-1} \qquad [2.66]$$

$$hu \approx w_0^7h\tilde{u}^{n+1} + w_1^7hu^n + w_2^7hu^{n-1} \qquad [2.67]$$

$$\tau\eta u \approx w_0^8\tilde{\tau}^{n+1}\tilde{\eta}^{n+1}\tilde{u}^{n+1} + w_1^8\tau^n\eta^nu^n + w_2^8\tau^{n-1}\eta^{n-1}u^{n-1} \qquad [2.68]$$

$$\eta u \approx w_0^9\tilde{\eta}^{n+1}\tilde{u}^{n+1} + w_1^9\eta^nu^n + w_2^9\eta^{n-1}u^{n-1} \qquad [2.69]$$

and in the momentum equation:

- **Advection:**

$$u\frac{\partial u}{\partial x} \approx m_0^1\tilde{u}^{n+1}\frac{\partial\tilde{u}^{n+1}}{\partial x} + m_1^1u^n\frac{\partial}{\partial x}u^n \qquad [2.70]$$

- **Non-linear friction:**

$$\tau u \approx m_0^3\tilde{\tau}^{n+1}\tilde{u}^{n+1} + m_1^3\tau^nu^n \qquad [2.71]$$

- **Viscosity:**

$$\frac{\upsilon}{H}\frac{\partial^2}{\partial x^2}Hu \approx m_0^4\frac{\upsilon}{(h+\tilde{\eta}^{n+1})}\frac{\partial^2}{\partial x^2}(h+\tilde{\eta}^{n+1})\,\tilde{u}^{n+1} + m_1^4\frac{\upsilon}{H^n}\frac{\partial^2}{\partial x^2}H^nu^n \qquad [2.72]$$

2.3.2. The Use of "Upwind" Weighting Functions

Upwinding has been often used[36-40], although with mixed success, in the solution of both the transport and the shallow-water equations. The concept is simple: when dealing with advection, most weight should be given to the information that is upstream (rather than downstream) of the node of interest.

To accomplish such an objective the standard Galerkin scheme must be modified to permit the use of non-symmetric weighting functions. As the direction from which the

fluid is approaching a node can vary, those weighting functions must be redefined when the flow changes direction.

This approach has been traditionally applied by using weighting functions which are modified by polynomials one order higher than the basis functions ("n+1 upwind"[36]). Westerink[37] introduced the use of weighting functions which are modified generically by polynomials two orders higher than the basis functions ("n+2 upwind"). The method was used for the finite element solution of the time dependent transport equation and it was showed that the "n+2 upwind" results in a much improved solution compared to both the standard and the "n+1 upwind" solutions.

As an alternative to the reference formulation of $RITA_1$, we extend to the shallow water equations the "n+2 upwind". It is only applied to the advective term on the momentum equation, since the second derivative in space that appears in the advective term of the wave equation reduces the convective character of the term, and the use of upwinding results less interesting.

The modified weighting functions are defined as:

$$\varphi_i(r) = \phi_i(r) + F_i(r) \qquad [2.73]$$

where $F(r)$ is a cubic correction function generically defined as:

$$F(r) = \beta r^3 + \alpha r^2 + \delta r + \sigma \qquad [2\text{-}74]$$

Forcing:

$$F(-1) = F(1) = 0 \qquad [2\text{-}75]$$

we get:

$$F_i(r) = \begin{cases} -(\alpha+\beta r)(r^2-1) & \text{downstream-node} \\ (\alpha+\beta r)(r^2-1) & \text{upstream-node} \end{cases} \qquad [2.76]$$

the coefficients α and β are generic, and determine the "degree" of upwinding. If $\beta = 0$ we revert to a more common "n+1 upwind", and if $\alpha = \beta = 0$ we revert to the centered Galerkin that constitutes the reference in $RITA_1$.

On an elemental level, the advective term in the momentum equation (Equation [2.42]) becomes:

$$\int_e \varphi_k u \frac{\partial u}{\partial x} dx \approx \sum_{i=1}^{2}\sum_{j=1}^{2} u_i u_j \int_{-1}^{1} \varphi_k \phi_i \frac{\partial \phi_j}{\partial r} dr = \sum_{i=1}^{2}\sum_{j=1}^{2} u_i u_j \int_{-1}^{1} (\phi_k + F_k)\phi_i \frac{\partial \phi_j}{\partial r} dr =$$
$$= \sum_{i=1}^{2}\sum_{j=1}^{2} u_i u_j \int_{-1}^{1} \phi_k \phi_i \frac{\partial \phi_j}{\partial r} dr + \sum_{i=1}^{2}\sum_{j=1}^{2} u_i u_j \int_{-1}^{1} F_k \phi_i \frac{\partial \phi_j}{\partial r} dr \qquad k = 1, 2 \qquad [2.77]$$

We should note that this technique constitutes an alteration from the reference Galerkin method. Indeed the last two terms in Equation [2.77] represent respectively the reference Galerkin method and a correction term.

2.3.3. Element-based Technique

In the reference formulation, all non-linear terms vary over each element consistently with the linear variation of velocities and elevations over the same element; in particular, the advective term in the momentum equation, $u\partial u/\partial x$, varies linearly over each element (since u is linear and $\partial u/\partial x$ is constant) while in the wave equation the corresponding term ($\partial Huu/\partial x$)varies quadratically.

Luettich *et al.*[7] suggest that better-behaved (smoother and more stable) numerical solutions may be obtained if the advective term is averaged over the element, in both the momentum and the wave equations. This approach, which Luettich *et al*[7] recommend only for the advective term, leads to a formulation that differs from the reference one by substituting Equations [2.23] and [2.25] by:

$$\frac{2}{\Delta x_e}\int_e \frac{\partial \phi_k}{\partial r} hu \frac{\partial u}{\partial r} dr \approx \frac{2}{\Delta x_e} \langle hu \frac{\partial u}{\partial r} \rangle_e \int_e \frac{\partial \phi_k}{\partial r} dr \qquad k = 1, 2 \qquad [2.78]$$

$$\frac{2}{\Delta x_e}\int_e \frac{\partial \phi_k}{\partial r} \eta u \frac{\partial u}{\partial r} dr \approx \frac{2}{\Delta x_e} \langle \eta u \frac{\partial u}{\partial r} \rangle_e \int_e \frac{\partial \phi_k}{\partial r} dr \qquad k = 1, 2 \qquad [2.79]$$

and Equation [2.42] by:

$$\int_e \phi_k u \frac{\partial u}{\partial r} dr \approx \langle u \frac{\partial u}{\partial r} \rangle_e \int_e \phi_k dr \qquad k = 1, 2 \qquad [2.80]$$

where $\langle Y \rangle_e$ represents the average of Y over the element.

2.3.4. An Eulerian-Lagrangian Method

The flow process has wave-like properties consistent with the hyperbolic nature of the governing equations. The method of characteristics (MOC) is a natural method of solution. This method, being purely lagrangian, brings some practical difficulties in keeping track of the computational grid points and the interpretation of results become somewhat difficult[41].

The problems associated to the lagrangian nature of the MOC can be solved by formulating the MOC over a fixed computational grid. The total derivatives of the dependent variables are obtained by using the MOC (lagrangian process); at each time step the values of the variables are stored on a fix space-time network (eulerian process). This class of methods are known as Eulerian-Lagrangian methods (ELM) and have been effectively

used to solve both the transport[42] and the shallow water equations[43]. They have never been used, though, in the context of a wave equation model.

$RITA_1$ was used to test and explore an ELM scheme for the momentum equation. The order of solution of the equations is the same as in the reference formulation.

A total derivative of the velocity is defined:

$$\frac{Du}{Dt} = \frac{\partial u}{\partial t} + u\frac{\partial u}{\partial x} \qquad [2.81]$$

hence:

$$\frac{Du}{Dt} = -g\frac{\partial \eta}{\partial x} - \tau + \frac{\upsilon}{H}\frac{\partial^2}{\partial x^2}Hu \qquad [2.82]$$

Now, the total derivative can be approximated as:

$$\frac{Du}{Dt} \approx \frac{u^{n+1} - u^{\xi}}{\Delta t} \qquad [2.83]$$

where the superscript ξ denotes the foot (at time n) of a characteristic line that follows the flow. The generalized wave equation remains unaffected

To solve the modified momentum equation we use a standard Galerkin method. The location of the foot of the characteristic lines is computed iteratively with a second order Runge-Kutta method, as the position of the characteristic lines is a function of the dependent variable of interest. For the Runge-Kutta tracking, the time step is divided into four sub-steps, and the tracking is performed sequentially over them (Fig. 2). Term by term we have:

- **Total derivative:**

$$\int_e \phi_k \frac{Du}{Dt} dx \approx \frac{\Delta x_e}{2} \int_{-1}^{1} \phi_k \frac{Du}{Dt} dr = \frac{\Delta x_e}{2} \frac{D}{Dt} \sum_{i=1}^{2} u_i \int_{-1}^{1} \phi_k \phi_i dr \qquad [2.84]$$

$$\frac{Du}{Dt} \approx \frac{1}{\Delta t}(u^{n+1} - u^{\xi}) \qquad [2.85]$$

- **Gravity:**

$$\int_e \phi_k g \frac{\partial \eta}{\partial x} dx \approx g \int_{-1}^{1} \phi_k \frac{\partial \eta}{\partial r} dr = g \sum_{i=1}^{2} \eta_i \int_{-1}^{1} \phi_k \frac{\partial \phi_i}{\partial r} dr \qquad [2.86]$$

$$\frac{\partial \eta}{\partial x} \approx m_0^2 \frac{\partial}{\partial x}(\eta^{n+1}) + m_1^2 \frac{\partial}{\partial x}(\eta^{\xi}) \qquad [2.87]$$

- **Friction:**

Non-linear:

$$\int_e \phi_k \tau u dx \approx \frac{\Delta x_e}{2} g \int_{-1}^{1} \phi_k \tau u dr \qquad k = 1, 2 \qquad [2.88]$$

$$\tau u \approx \tau^{\xi} u^{\xi} \qquad [2.89]$$

Linear:

$$\int_e \phi_k \tau u dx \approx \frac{\Delta x_e}{2} \tau \sum_{i=1}^{2} u_i \int_{-1}^{1} \phi_k \phi_i dr \qquad k = 1, 2 \qquad [2.90]$$

$$\tau u \approx m_0^3 \tau u^{n+1} + m_1^3 \tau u^{\xi} \qquad [2.91]$$

- **Viscosity:**

$$\upsilon \int_e \frac{\partial}{\partial x} \frac{\phi_k}{H} \frac{\partial}{\partial x} H u dx \approx \frac{2}{\Delta x_e} \upsilon \left(\sum_{i=1}^{2} \sum_{j=1}^{2} (H_i \eta_j + \eta_i H_j) \int_{-1}^{1} \frac{\partial}{\partial r} \frac{\phi_k}{H} \phi_i \frac{\partial \phi_j}{\partial r} dr \right) \qquad k = 1, 2 \quad [2.92]$$

$$\frac{\upsilon}{H} \frac{\partial^2}{\partial x^2} H u \approx \frac{\upsilon}{H^{\xi}} \frac{\partial^2}{\partial x^2} H^{\xi} u^{\xi} \qquad [2.93]$$

We should note that once the ELM is used to solve the momentum equation, the time extrapolation scheme presented in Section 2.3.1 cannot be used. In the context of ELMs, a time extrapolation method for the friction or viscosity terms only makes sense if performed along the characteristic lines. This feature should be incorporated in future versions of $RITA_1$.

CHAPTER 3

VALIDATION

In this chapter we describe the validation of $RITA_1$. Our objective is to demonstrate that the main options of the model are working properly, providing reliable solutions to common problems. For that purpose, we present a L_2 error-norm analysis in which the results of $RITA_1$ are compared against either analytical solutions (Sections 3.1.1 and 3.1.2) or numerical solutions obtained using a highly resolved grid in time and spatial (Section 3.1.3). We also describe a simple test of mass conservation (Section 3.2). A more detailed study of the behavior of selected numerical schemes and comparisons among alternative methods can be found in Chapter 4.

3.1. L_2 error-norm analysis

An error analysis of $RITA_1$ is done by comparing solutions obtained for several test cases, using different numerical schemes, with:

1. analytical solutions - this is done for the linear shallow water equations and for the Burgers' equation;
2. "refined" solutions - assuming the consistency and convergence of the basic formulation(s) of the model, we expect to increase accuracy as we increase both the spatial and temporal discretization. Thus, the use of an highly resolved computational grid should lead to a solution very close to the exact solution. That solution is then used as a reference for the error studies.

The numerical schemes tested are:

1. the reference formulation (RF) for the linear case;
2. RF and time extrapolation (TE) for the finite amplitude and non-linear friction;
3. RF, TE, element-based (EB) and upwind (UPW) for advection, advection and viscosity and fully non-linear equations (all terms but viscosity).

3.1.1. Linear tidal propagation

The linear forms of Equations [2.7] and [2.2] are:

$$\frac{\partial^2\eta}{\partial t^2} - g\frac{\partial}{\partial x}h\frac{\partial\eta}{\partial x} + G\frac{\partial\eta}{\partial t} + \frac{\partial}{\partial x}(G-\tau)hu = 0 \qquad [3.1]$$

$$\frac{\partial u}{\partial t} + g\frac{\partial\eta}{\partial x} + \tau u = 0 \qquad [3.2]$$

Analytical solutions for the linear propagation of a tidal wave (Equations [3.1] and [3.2]) in a closed-end channel were derived by Lynch and Gray[44] and are reviewed in Appendix A.

We will consider a M_{16} tidal wave with an amplitude of 1.5 m, propagating in a shallow embayment 80 km long and with an inclined bottom. The slope is linear with depths changing from 15 m at the mouth to 5 m at the closed end. The "average" celerity of the waves in the channel is approximately 10 ms^{-1}. Because the M_{16} tidal wave has a period of 1.55 hours the resulting "average" wavelength is 55.8 km.

A sensitivity analysis of the accuracy of the reference linear model to both the space and time discretization was performed. The sensitivity to Δx was tested with Δx of 50, 100, 500, 2500 and 10000 m, and Δt=4.8 s. The sensitivity to Δt was tested with Δt of 4.8, 9.6, 48.0, 240.0 and 960.0 s, using Δx=500 m.

The simulations were carried for 9.3 h (six M_{16} periods) starting from analytically computed initial conditions. Since the analytical solution only equals the numerical solution in the limit as Δx, Δt -> 0 the simulations may need some time to reach a steady state; however in this study the numerical solutions were assumed to reach steady state instantaneously (i.e., no warm-up time is allowed). The relevant parameters of the reference numerical method are shown in Table 1. A linear friction coefficient was used (τ=0.00025 s^{-1}).

An error norm was defined as:

$$L_2 = \sqrt{\frac{\sum_{k=1}^{T}\left(\sum_{i=1}^{N}(n_i^k - a_i^k)^2\right)}{TN}} \qquad [3.3]$$

with:

T - number of time steps

N - number of nodes

n_i^k - numerical value of the variable at time step k and node i

a_i^k -analytical value of the variable at time step k and node i

Error norms were computed for both elevation and velocity. Results are shown in Figs. 3-5, where the error-norms are mapped respectively as a function of Δx, Δt and aver-

age Courant number (Cu). The average Cu ($Cu=c^*\Delta t/\Delta x$, c being the celerity) is defined based on the celerity for to the average depth in the domain.

For a constant Δt, Cu decreases with the increasing Δx used in the sensitivity studies. This inverse dependence of Cu on Δx explains the form of the curves shown in Fig. 3: for small values of Δx (corresponding to large Courant numbers) the method is insensitive to Δx, or may even show a decrease in the error norm with an increase in Δx. This is because the value of Cu decreases and has an effect on accuracy that compensates the effect we expect from an increase on Δx. As Δx increases Cu becomes small and has a smaller effect on accuracy, in comparison with what happens when Cu has greater values.

For constant Δx (Figures 4 and 5), the error decreases with the decrease of Δt (or Cu), showing the expected convergence of the method. The absolute values of the error indicate very good accuracy for values of Cu less than one.

3.1.2. Burgers' equation

Burgers' equation has the form:

$$\frac{\partial u}{\partial t} = \nu\frac{\partial^2 u}{\partial x^2} - u\frac{\partial u}{\partial x} \qquad [3.4]$$

and will be solved in a dimensionless flat domain, with $x \in [0,1]$.

The analytical solution[45] (Appendix A) will be compared with numerical results obtained with four alternative numerical methods for the treatment of advection. Since the elevation does not appear in Burgers' equation, this experiment can only provide information about the solution of the momentum equation. Also, only the advective and viscous terms were tested.

Four numerical simulations were run on a regular grid with $\Delta x=0.02$. Each simulations corresponded to a different numerical method (Table 2). The physical parameters (see Appendix A) were $c=0.6\ s^{-1}$, $\alpha=0.4$, $\beta=0.125$ and $\upsilon=0.003\ s^{-1}$. To have a small Courant number (Cu=0.03), Δt was set to 0.001 s. The corresponding Peclet number ($Pe=Cu\Delta x^2/\upsilon\Delta t$) is 2.0.

The simulations were carried out for 1.5 s and the error norms were computed as defined by Equation [3.3]. The velocity profiles in the domain, given by the analytical solution and the four numerical schemes, for t=1 s, are presented in Fig. 6. The error norms are presented in Table 3; the characteristic errors are smaller than $0.01\ s^{-1}$. Since the characteristic velocity can be assumed to be of the order of the $0.6\ s^{-1}$, all methods show acceptable accuracy for the low Cu adopted.

3.1.3. Non-linear tidal propagation

Assuming that the numerical formulation of the model is convergent, numerical solutions using a highly resolved grid (in space and time) are quasi-exact, and can be used to evaluate L_2-error norms for simulations based on coarser grids.

"Refined solutions" were obtained for each non-linear term (finite amplitude, friction, advection) individually, and also to the case in which all the non-linear terms are present simultaneously. The selected test case was chosen to be a M_2 tidal wave propagating in the same shallow channel as in Section 3.1.1. For the reference $RITA_1$ formulation the model was run using a grid with Δx=100m and Δt=1s. This discretization corresponds to a very low "average" Courant number (Cu=0.1) and a very large dimensionless wavelength ($L/\Delta x$=4410). The initial conditions for the refined runs, as well as for all other runs in this section were obtained from the linear analytical solution used in Section 3.1.1. All runs were carried out for 49.6 h (four M_2 cycles), with a warm-up time of 37.2 h (three M_2 cycles). The time series of elevations and velocities obtained from the refined run with all three non-linear terms, at a station in the middle of the channel (Fig. 7) shows that a "dynamic steady state" is quickly established.

Parameter G was set to 0.00025 s^{-1} for all runs. This value of G is either equal to the linear friction coefficient (Sections 3.1.3.1 and 3.1.3.3) or represents a characteristic non-linear friction coefficient (Sections 3.1.3.2 and 3.1.3.4). In the wave equation, the values of the time discretization parameters for the first time derivative term and for the linear gravity term remained constants for all runs (w_0^1=1.0, w_1^1=-1.0, w_2^1=0.0; and w_0^2=0.35, w_1^2=0.3, w_2^2=0.35). In the momentum equation, the time-discretization of the gravity term was also always constant (m_0^2=0.5, m_1^2=0.5).

To obtain all the refined solutions the reference formulation (RF) was used. The numerical parameters are given in Tables 4-7, together with the parameters for the alternative methods used in the runs with coarser grids. The numerical solutions presented in this section (excluding the refined solutions) were obtained using a uniform grid with Δx=2500 m. For the M_2 tidal wave, this leads to an "average" dimensionless wavelength $L/\Delta x$ of 177. Each method considered was used over a range of "average" Cu (Table 8.) The error-norm defined by Equation [3.3] was computed for each simulation and plotted versus the Cu.

3.1.3.1. Finite amplitude

To isolate the finite amplitude from other non-linear effects we solve for:

$$\frac{\partial^2 \eta}{\partial t^2} - g\frac{\partial}{\partial x}H\frac{\partial \eta}{\partial x} + G\frac{\partial \eta}{\partial t} + \frac{\partial}{\partial x}(G-\tau)\,hu = 0 \qquad [3.5]$$

$$\frac{\partial u}{\partial t} + u\frac{\partial u}{\partial x} + g\frac{\partial \eta}{\partial x} + \tau u = 0 \qquad [3.6]$$

Only the RF and the TE methods are of interest for this case; relevant parameters are given in Table 4. The linear friction coefficient was set to τ=0.00025 s^{-1}.

The time series of the errors in elevation and velocity at a mid-channel station, are presented in Figs. 9-12, for values of Cu of respectively 0.12, 0.96, 2.4 and 9.6. In Fig. 8 the L_2 error-norms are plotted vs. Cu. The RF and TE methods show a very similar behavior for low Cu. However, the RF method is stable for Cu as large as 9.6, while the TE method becomes unstable at Courant numbers above 2.4. Both methods have a maximum absolute error in elevation and velocity, of approximately 3 mm and 3 mms^{-1}, respectively, for Cu=0.12 (this correspond to average errors of approximately 0.3%); the errors can be as large as 75 mms^{-1} in velocity and 50 mm in elevation for Cu=2.4. Even though the RF method is still stable for Cu=9.6, the errors can be as large as 30% in both elevation and velocity.

The error sensitivity to the value of Cu was expected, and the good agreement between the coarser and the refined solutions for small values of Cu suggests the validity of the implementation of both the RF and the TE methods, for Equations [3.5] and [3.6].

3.1.3.2. Friction

Sensitivity studies to alternative treatments (RF and TE methods) of the non-linear friction term require the solution of:

$$\frac{\partial^2 \eta}{\partial t^2} - g\frac{\partial}{\partial x}h\frac{\partial \eta}{\partial x} + G\frac{\partial \eta}{\partial t} + \frac{\partial}{\partial x}(G - \tau)\,hu = 0 \qquad [3.7]$$

$$\frac{\partial u}{\partial t} + g\frac{\partial \eta}{\partial x} + \tau u = 0 \qquad [3.8]$$

Only the RF and the TE methods are of interest for this case. The relevant parameters are given in Table 5; friction is described by a Manning coefficient n=0.025 $sm^{-1/3}$.

The L_2-error norms are plotted vs. Cu (Fig. 13). Results indicate that the RF method is stable for Cu as large as 9.6 while the TE method becomes unstable at a Cu between 4.8 and 9.6. As in the previous section, the errors increase with the value of the Cu. The slopes of the log-log plots (Fig. 13) are similar for both methods and are similar to those of Fig. 8. This similarity indicates a dependency of the error on Cu. The TE method shows a slightly smaller error than the RF method, especially in velocity. Examination of the time series of the errors for several values of Cu (Figs. 14-17) shows that the TE method smooths the error (see Section 4.1.3. for further discussion). The implementation of both methods is correct for the solution of Equations [3.7] and [3.8].

3.1.3.3. Advection

Sensitivity experiments on the advection term utilized he governing equations:

$$\frac{\partial^2 \eta}{\partial t^2} - \frac{\partial^2}{\partial x^2} huu - g\frac{\partial}{\partial x} h\frac{\partial \eta}{\partial x} + G\frac{\partial \eta}{\partial t} + \frac{\partial}{\partial x}(G-\tau)\,hu = 0 \qquad [3.9]$$

$$\frac{\partial u}{\partial t} + u\frac{\partial u}{\partial x} + g\frac{\partial \eta}{\partial x} + \tau u = 0 \qquad [3.10]$$

For this case the methods RF, TE, UPW and EB presented in Chapter 2 are of interest. Their numerical parameters are given in Table 6. All the simulations in this section were done with a linear friction coefficient of τ=0.00025 s^{-1}.

Errors (Fig. 18) are generally small for all methods, but no method is stable for a Courant number greater than 1.92 (and even for that value of Cu the results show already signs of unstable behavior - Fig. 21) All methods seem to give very close results. Although Cu appears to be very restrictive to stability, the relatively small error norms obtained with all methods for low Cu suggest the validity of the implementation for Equations [3.9] and [3.10].

3.1.3.4. Fully non-linear case

The fully non-linear case requires the solution of:

$$\frac{\partial^2 \eta}{\partial t^2} - \frac{\partial^2}{\partial x^2} Huu - g\frac{\partial}{\partial x} H\frac{\partial \eta}{\partial x} + G\frac{\partial \eta}{\partial t} + \frac{\partial}{\partial x}(G-\tau)\,Hu = 0 \qquad [3.11]$$

$$\frac{\partial u}{\partial t} + u\frac{\partial u}{\partial x} + g\frac{\partial \eta}{\partial x} + \tau u = 0 \qquad [3.12]$$

The relevant numerical parameters for the four methods considered are given in Table 7. The TE scheme is only applied to the advective terms.

The error norms obtained from the simulations are shown in Fig. 22; time-series of errors can be seen in Figs. 23-25. The RF, UPW and EB methods become unstable for Cu>1.2.; the TE method is already unstable for Cu=1.2. All methods have reasonably small errors for small values of Cu, which we take as an indication of proper implementation of the solution technique for Equations [3.11] and [3.12].

3.2. Mass conservation tests

Mass conservation is a very important feature in numerical hydrodynamic models. The main numerical methods included in $RITA_1$ were tested for mass conservation by means of a simple numerical experiment.

Our test case was based on the reservoir schematically shown in Fig. 26. Starting from initial conditions of zero elevation and zero velocity throughout the domain, the flow from upstream increases from zero to a constant value of 500 m^3s^{-1} in about three hours. Downstream, a sinusoidal function controls the flow leaving the domain; the fluctuation has a cycle of 6 h, a maximum of 1000 m^3s^{-1} and a minimum of zero. The problem was simulated for 48 h using the four numerical schemes identified in Table 7. A uniform grid with 101 nodes and Δx=500 m was used; the time step was set to 25 s.

The cumulative volume losses are computed over time and are defined as:

$$\Delta V(k) = V_b^k - (V_d^k - V_0) \qquad [3.13]$$

where V_b^k is the cumulative net volume through the boundaries and V_d^k the volume in the domain, both after k time steps, and V_0 is the initial volume of the reservoir, i.e.:

$$Vb^k = \Delta t \sum_{j=1}^{k} \left((\eta_1^j + h_1)\, u_1^j - (\eta_{101}^j + h_{101})\, u_{101}^j \right) \qquad [3.14]$$

$$Vd^k = \sum_{i=1}^{100} \frac{\eta_i^k + h_i + \eta_{i+1}^k + h_{i+1}}{2} \Delta x_i \qquad [3.15]$$

The fluctuation of volume in the reservoir can be seen in Fig. 27 together with the volume loss as a function of time for each numerical scheme. The errors are of the order of 10^{-7}% of the total volume, for all formulations tested. The behavior of the UPW method is remarkably different from that of all the other methods: the error exhibits no periodicity and has a definitely non-zero (although very small) average over time.

3.3. Conclusions

Small error-norms obtained for small Courant numbers in comparisons with analytical solutions and finely discretized domains and the excellent mass balances obtained in the reservoir problem validate $RITA_1$. The relative importance of the linear and non-linear terms for the inclined-bottom channel (Figs. 30 and 31) suggests that friction is the dominant non-linear process. Thus, the apparent lack of sensitivity of the results to the method used, while studying the solution for finite amplitude and advection, may be due mainly to the relatively small importance of these terms in the case studied.

CHAPTER 4

APPLICATION

The value of $RITA_1$ as a tool for studying both physical processes and numerical methods associated with the shallow water equations is illustrated in this chapter. In Section 4.1 we use $RITA_1$ to explore numerical aspects of particular interest: (a) the sensitivity of the method to the parameter G in the wave equation and (b) the comparison of alternative treatments of non-linear terms, with emphasis on friction. In Section 4.2 we illustrate the use of $RITA_1$ as an educational tool through a classroom-oriented study of the generation of shallow-water tides.

4.1. Numerical Studies

4.1.1. Sensitivity of wave equation solutions to G

In this section a very simple test is performed to examine the sensitivity of the reference formulation to the value of G. Simulations refer to the case described in Section 3.1.3.4, using a range of values for G, for a set of average Courant numbers (see section 3.1.1). An RF numerical scheme was used with the time discretization specified in Table 7.

The L_2-error norms were computed as in Section 3.1.3.4 and are presented as a function of the value of G for several Cu (Fig. 28). In Fig. 29 we show the time series of the differences between the results of each simulation and the corresponding refined solution, at a mid-channel station.

The results show, for small average Courant numbers, a sharp increase in accuracy as the value of G increases to the characteristic value of the friction coefficient τ (computed from a characteristic velocity and an average depth). For values of G greater than the characteristic value of friction the accuracy decreases slowly as G increases. As the Courant number increases, the accuracy decreases, for all values of G; however this accuracy decrease seems more accentuated for G greater than the characteristic friction. The accuracy on elevation and velocity exhibit different dependence of the optimal G on the Courant number. While the velocity accuracy seems to have an optimal G very close to the characteristic value of friction and is independent of the value of the Courant number, the elevation accuracy shows an optimal G varying with Cu. The optimal G approaches the characteristic value of friction, at greater values, as the Courant number increases.

As a general rule, for Courant numbers greater than 1, an optimal accuracy is expected (for both elevation and velocity), when the value of G is close to the value of the

characteristic friction. However, when dealing with small Courant numbers the optimal G can be more than an order of magnitude greater than the characteristic friction.

4.1.2. The numerical treatment of friction

One of the more interesting and immediate uses of $RITA_1$ is in the comparative study of numerical schemes for the treatment of non-linear terms. In this section we explore the time-extrapolation method applied to the non-linear friction term, and compare its accuracy against the lumping technique used by Luettich et al.[7]. These authors use a semi-implicit time-discretization scheme centered at n+1/2 for the treatment of friction in the momentum equation. The friction coefficient τ is computed at time n and used at n+1. Relative to the reference formulation of $RITA_1$, Equation [2-49] is approximated by:

$$\tau u \approx m_0^3 \tau^n u^{n+1} + m_1^3 \tau^n u^n \qquad [4.1]$$

The mass matrix corresponding to the momentum equation becomes time dependent and the solution requires the factorization of the matrix at each time step. The computational effort is reduced by lumping the non-diagonal part of the matrix and treating it explicitly. The implicit treatment would likely decrease the error and increase the stability, compensating for the loss in accuracy due to lumping.

To compare the method of Luettich et al. with time-extrapolation methods in $RITA_1$ we retain as a reference the problem solved in Section 3.1.3. We recall from Figs. 30 and 31 that friction is clearly the dominant non-linear process in this problem.

In the previous chapter we observed that the time extrapolation method for non-linear friction seems to enhance accuracy relative to the reference method. The same case studied in Section 3.1.3.2 was simulated by using different time discretization schemes (or different values for m_0^3, the weight for the non-linear friction term at time n+1, in the momentum equation), in a time-extrapolation fashion. The L_2-error norms are presented as function of the Courant number in Fig. 32. A small gain in accuracy is obtained with the time extrapolation method. The gain of accuracy in elevation consistently increases with the weight given to the value of the non-linear friction terms at time n+1, for all Cu. The gain in accuracy of velocity is greater for Cu in the range 0.5-1.2 and the Crank-Nicholson scheme performs better than any of the others. The time series of the errors at a station localized at mid-channel, and relative to an average Cu of 0.96, can be seen in Fig. 33.

To compare the results for the time extrapolation method with those for the lumping technique of Luettich et al., both models ADCIRC[7] and $RITA_1$ were used to simulate an M_2 tidal wave, with an amplitude of 1.5 m and forcing phase zero, propagating in a closed-end rectangular channel (80 km long), with a constant depth of 10 m. Since ADCIRC does not allow the treatment of non-linear friction without the inclusion of finite

amplitude, the $RITA_1$ simulations also considered both non-linear terms (non-linear friction and finite amplitude). All simulations started from zero initial conditions and were carried out for four days; the warm-up period was set to three days. Results were obtained with $RITA_1$ using three different numerical schemes: the reference method, and two different time-extrapolation methods in which the non-linear friction term is treated either with a Crank-Nicholson scheme centered at time n+1/2 or fully implicitly.

The results obtained with the time extrapolation method are compared to the results of ADCIRC (Fig. 34), in the form of L_2-norms as a function of Cu. For large Cu the values obtained with $RITA_1$ have a different behavior than the ones presented in Fig. 32.

As we can see in Fig. 34, the lumping used in ADCIRC is very insensitive to the Courant number, when Cu<2. $RITA_1$ is more accurate for Cu<1, regardless the choice of specific non-lumping method. For 1<Cu<2, the lumping technique shows greater accuracy. This can be interpreted as a balance between sources of error: both lumping and time extrapolation attempt to increase accuracy and stability by extrapolating in time the value of the friction terms, in the case of $RITA_1$, and the value of the non-linear friction coefficient and part of the local acceleration term, in the case of ADCIRC. Although the errors decrease by increasing the degree of implicity, the errors increase as a result of the extrapolation in time. The L_2-norms obtained for simulations done with ADCIRC, using three different grids are shown in Fig. 35. For Δx=5000 m, the results show the same behavior with a minimum error greater than the one obtained when using Δx=2500 m. For the simulations with Δx=1250 m, we expect the minimum error (corresponding to the smaller values of Cu) would be smaller than the one obtained with Δx=2500 m. More simulations (with smaller Cu) are required to confirm this expectation.

In general, the results suggest that for small values of Cu, a time-extrapolation technique applied to the non-linear friction term provides greater accuracy than the lumping technique. However, for computationally intensive problems, the increase in accuracy must be weighted against the computational cost advantages associated with lumping.

4.2. The Generation of Shallow Water Tides

The propagation of tides in shallow-waters is a complex problem of significant practical importance. $RITA_1$ and the associated visualization interface can be used very effectively either in a classroom context or as a tool for personal learning, to explore and demonstrate several aspects of the problem. We will deal in this section with the role of specific propagation mechanisms on the generation of harmonic and compound tides.

Tides in the oceans are related to the periodic motion of celestial bodies. In deep sea, the tides can be described as the sum of harmonic constituents whose frequencies are dictated by the motion of the moon and sun relative to the earth surface. In deep sea, the effect of the non-linear terms of the equations of motion are negligible; thus, the propagation of tides is a quasi-linear process and no significant interaction occurs between different tidal constituents. These tidal constituents are called astronomical tides.

As the tidal waves enter shallower regions, the effect of non-linear processes becomes very significant: elevations are now an important percentage of the total water depth, friction at the bottom can be very important, and advection eventually becomes non-negligible. These non-linear processes allow the different tidal constituents to interact with each other and, in the process, energy is transferred to related frequencies, originating another type of tidal constituent: the shallow water tides.

The elevation and velocity of the water surface at any given point can still be represented as a summation of cosines (or sines) with different amplitudes and frequencies:

$$\eta = \sum_{i}^{N} \eta_{0i} \cos(\omega_i t - \phi_{0i}) \qquad [4.2]$$

$$u = \sum_{i}^{N} u_{0i} \sin(\omega_i t - \theta_{0i}) \qquad [4.3]$$

with:

ω_i - frequency of the constituent i [rad.s^{-1}]
η_{0i} - elevation amplitude of the constituent i [m]
u_{0i} - velocity amplitude of the constituent i [ms^{-1}]
ϕ_{0i} - elevation phase of the constituent i [rad]
θ_{0i} - velocity phase of the constituent i [rad].

Through the analysis of the governing equations one can identify the non-linear terms and study their effects on the generation of shallow water tides. This is done by substituting Equations [4.2] and [4.3] into the equations that describe the case in study.
Three non-linear terms are considered in the equations of motion:

1. advection, with the general form uu,
2. finite amplitude, with the form ηu,
3. friction, with the form ulul (we do not consider the effect of the finite amplitude that comes from the denominator of τ).

In the next sections, each non-linear term is analyzed alone and in combination with others, both by mathematical handling of the governing equations and by interpretation of the results provided by $RITA_1$. Two test cases are considered:

1. a longitudinal slice of a closed-end channel, 80 km long and 10m deep and
2. a longitudinal slice of a closed-end channel, 80 km long and with the depth varying linearly from 15 m at the mouth to 5 m at the closed end.

For each case, and for each set of selected terms, $RITA_1$ is used to solve the hydrodynamics equations, using two different boundary conditions at the mouth of the channels. The boundary conditions consist of prescribed elevations defined as values for the following astronomical tides:

1. a M_2 tide with amplitude of 1.5 m and zero phase; and
2. a combination of M_2, S_2 and O_1 tides; forcing amplitudes are 1.5, 0.84 and 0.375 m, and all forcing phases are zero.

A space-time grid with Δx=500 m and Δt=60 s was used to support all $RITA_1$ simulations. The reference numerical scheme was used in all the simulations.

After several tidal periods of warm-up from analytically-generated initial conditions, 1024 h long hourly records of elevation were "collected" at two stations: at the wall (A), and at mid-channel (B). All records were analyzed with a least-squares sinusoidal regression method, to identify amplitudes and phases of the 16 tidal constituents listed in Table 9. The results of the tidal analysis are given as amplitude (η_0, in meters), phase (ϕ, in hours) and relative amplitude (χ in percentage of the M_2 amplitude), for each constituent of interest.

4.2.1. Frictionless linear case

We first consider a simple balance of the local acceleration and the gravity terms. No finite amplitude effects are included and the governing equations reduce to:

$$\frac{\partial \eta}{\partial t} + \frac{\partial}{\partial x} hu = 0 \qquad [4.4]$$

$$\frac{\partial u}{\partial t} + g\frac{\partial \eta}{\partial x} = 0 \qquad [4.5]$$

Since all the governing processes are strictly linear the different waves cannot interact and no new tidal constituents can be generated.

The results of the simulations for the flat bottom channel are presented in Tables 10 and 11 and in Figs. 36 and 37. A significant, constituent-dependent, tidal amplification was observed at stations A and B. No energy was detected at any frequency other than the forcing frequencies. This result was expected and can be effectively used to illustrate the

notion that linear propagation mechanisms cannot transfer energy from one frequency to another. We also note that each tidal constituent is in phase over the entire channel. This is a characteristic of standing waves.

For the channel with inclined bottom (Tables 12 and 13, Figs. 38 and 39) the same type of constituent-dependent tidal amplification at stations A and B is obtained. The values of elevation are slightly lower, at both stations, than the ones obtained for the flat bottom channel. This is due only to the relative situation of the flat bottom case in relation to a resonance mode.

4.2.2. Linear friction case

We now introduce linear friction (τ=0.00025 s^{-1}) in the system; the governing equations become:

$$\frac{\partial \eta}{\partial t} + \frac{\partial}{\partial x} uh = 0 \qquad [4.6]$$

$$\frac{\partial u}{\partial t} + g\frac{\partial \eta}{\partial x} + \tau u = 0 \qquad [4.7]$$

As in the previous section, all the governing processes are strictly linear and the forcing constituents cannot interact to generate new constituents.

The results of the simulations for the flat bottom channel are presented in Tables 14 and 15 and in Figs. 40 and 41. Results for the inclined bottom channel are shown in Tables 16 and 17 and in Figs. 42 and 43. The tidal amplification at stations A and B observed for the frictionless case is reduced or even reversed. The elevations at station A are consistently lower than the ones at station B; in both stations the elevations are slightly greater in the inclined bottom case. Results are consistent with the role of frictional effects, which are cumulatively felt along the channel; the difference between the results obtained for the flat and the inclined bottom cases are due to the length of the bottom rather than to the actual change in depth.

4.2.3. Finite amplitude

Considering the effect of finite amplitude, while keeping a linearized representation for friction (τ=0.00025 s^{-1}), the governing equations become:

$$\frac{\partial \eta}{\partial t} + \frac{\partial}{\partial x} Hu = 0 \qquad [4.8]$$

$$\frac{\partial u}{\partial t} + g\frac{\partial \eta}{\partial x} + \tau u = 0 \qquad [4.9]$$

The non-linear term is:

$$\frac{\partial}{\partial x}Hu = \frac{\partial}{\partial x}(h+\eta)\,u \qquad [4.10]$$

Using the expressions for u and η stated in Equations [4.2] and [4.3], we recognize that a product involving a sine and a cosine will result from this non-linear term.

If the ocean boundary is forced with only one constituent, say the M_2, energy will be transferred to a constituent with twice the frequency, and to S_0:

$$\begin{aligned}\cos(\omega_{M2}t+\phi)\sin(\omega_{M2}t+\theta) &= \\ = (\cos\phi\cos t\omega_{M2} - \sin\phi\sin t\omega_{M2})\,(\sin t\omega_{M2}\cos\theta + \sin\theta\cos t\omega_{M2})&\end{aligned} \qquad [4.11]$$

Or, as:

$$\begin{aligned} A &= \cos\phi \qquad B = \sin\phi \\ C &= \cos\theta \qquad D = \sin\theta \end{aligned} \qquad [4.12]$$

we get:

$$\begin{aligned}&(A\cos t\omega_{M2} - B\sin t\omega_{M2})\,(C\sin t\omega_{M2} + D\cos t\omega_{M2}) = \\ &= AC\sin t\omega_{M2}\cos t\omega_{M2} + AD\cos^2 t\omega_{M2} - BC\sin^2 t\omega_{M2} - BD\sin t\omega_{M2}\cos t\omega_{M2} = \\ &= 0.5\,((AD+BC)\cos 2t\omega_{M2} + (AC+BD)\sin 2t\omega_{M2} + (AD-BC)\cos 0)\end{aligned} \qquad [4.13]$$

Noting that:

$$\begin{aligned} 2\omega_{M2} &= \omega_{M4} \\ 0 &= \omega_{S0} \end{aligned} \qquad [4.14]$$

we can see that indeed the original M_2 potentially generates two new constituents: the M_4 and the S_0. The S_0 will not produce energy at new frequencies but the M_4 will interact with the original M_2 and with itself as follows (for the sake of simplicity we neglect the phases, since as we see in equation [4-13] they only affect the amplitudes of the new constituents and not their frequency):

$$\begin{aligned}&\cos(\omega_{M4}t)\sin(\omega_{M2}t) = \\ &= \frac{1}{2}(\sin((\omega_{M4}+\omega_{M2})t) - \sin((\omega_{M4}-\omega_{M2})t)) = \\ &= \frac{1}{2}(\sin(\omega_{M6}t) - \sin(\omega_{M2}t))\end{aligned} \qquad [4.15]$$

$$\begin{aligned}&\cos(\omega_{M2}t)\sin(\omega_{M4}t) = \\ &= \frac{1}{2}(\sin((\omega_{M2}+\omega_{M4})t) - \sin((\omega_{M2}-\omega_{M4})t)) = \\ &= \frac{1}{2}(\sin(\omega_{M6}t) + \sin(\omega_{M2}t))\end{aligned} \qquad [4.16]$$

$$\cos(\omega_{M4}t)\sin(\omega_{M4}t) = \frac{1}{2}\sin(2\omega_{M4}t) = \frac{1}{2}\sin(\omega_{M8}t) \qquad [4.17]$$

Two new constituents were generated, both with frequencies which are multiple of the M_2 frequency. This new constituents will also interact and other are generated, with progressively higher frequencies and smaller energies. The frequencies of the new constituents are always multiples of the frequency of the original constituent. They are called overtides.

If the ocean boundary is forced with two constituents, say M_2 and S_2, energy will be transferred to the overtides of each of the original constituents but, in addition, another type of shallow water tides will be also generated. These new constituents are called compound tides, and are generated through the interaction at two different astronomical tides:

$$\begin{aligned} &\cos(\omega_{M2}t)\sin(\omega_{S2}t) = \\ &= \frac{1}{2}\left(\sin\left((\omega_{M2}+\omega_{S2})t\right) - \sin\left((\omega_{M2}-\omega_{S2})t\right)\right) = \\ &= \frac{1}{2}\left(\sin(\omega_{MS4}t) - \sin(\omega_{MS0}t)\right) \end{aligned} \qquad [4.18]$$

Again, two new constituents were generated, both with frequencies which are now combinations of the M_2 and S_2 frequencies. These new constituents will interact with the original ones and other constituents are generated.

The general algorithm of generation of new constituents through finite amplitude can be stated as:

$$\omega_k = |\omega_i \pm \omega_j| \qquad [4.19]$$

where ω_i, ω_j denote the forcing frequencies and ω_k the shallow-water frequencies.

Table 18 presents some shallow water tides resulting from one or two astronomical tides, through the finite amplitude non-linear process. The results of the simulations are presented in Tables 19 and 20 and in Figs. 44 and 45 (flat bottom channel) and in Tables 21 and 22 and in Figs. 46 and 47 (inclined bottom channel).

The numerical results are consistent with the behavior expected from the above analysis: when the M_2 is the only forcing tidal constituent, energy is transferred only to its overtides and to the S_0 constituent; when more than one forcing tide is present, both overtides and compound tides are generated.

The results of the simulations also provide interesting additional insight. For instance, we note that:

1. The transfer of energy appears to be more important in the inclined bottom channel, which can be attributed to the stronger amplification of the waves that occurs in this case (Section 4.2.2).
2. The M_4 (the first harmonic of the dominant forcing frequency M_2) and the MS_4 (the first order effect of the interaction of the M_2 and S_2 frequencies) are consistently important constituents while the zero-frequency constituent captures an insignificant amount of energy; i.e., the finite amplitude contributes only marginally to a residual slope in the water surface of the channels.
3. The second and higher harmonics of the M_2 and S_2 (M_6, S_6, M_8, S_8, etc.) are essentially negligible, while the MO_3 and SO_3 (the first order effect of the interaction of the semi-diurnal and the diurnal forcing frequencies) are more weakly represented than the MS_4, but not negligible.

4.2.4. Non-linear friction

For a non-linear friction without finite amplitude effects, the governing equations becomes:

$$\frac{\partial \eta}{\partial t} + \frac{\partial}{\partial x} hu = 0 \qquad [4.20]$$

$$\frac{\partial u}{\partial t} + g\frac{\partial \eta}{\partial x} + \tau u = 0 \qquad [4.21]$$

The non-linear friction τ, is defined as:

$$\tau = \frac{n^2|u|}{h^{4/3}} \qquad [4.22]$$

with $n=0.025\ sm^{-1/3}$.

The non-linearity now has the form ulul. Substituting u by it expression as stated in Equation [4.3] and using Tschebyscheff polynomials we obtain non linear terms involving[46]:

$$\left(\sum_i^N u_{0i} \sin(\omega_i t + \theta_i)\right)^3 \qquad [4.23]$$

The general equation for generation of new constituents through non-linear friction is:

$$\omega_k = |2\omega_i \pm \omega_j| \qquad [4.24]$$

In Table 23, some shallow water tides resulting from one or two astronomical tides, through the non-linear friction process are presented. The results of the simulations

are presented in Tables 24 and 25 and in Figs. 48 and 49 (flat bottom channel) and in Tables 26 and 27 and in Figs. 50 and 51 (inclined bottom channel). As in the previous cases, the numerical results are consistent with the behavior expected by the analysis above. We observe that:

1. The transfer of energy does not seem to depend consistently on the form of the bottom, unlike in the finite amplitude case. Since the amplification is much more accentuated in the inclined bottom channel we suspect that some cancelation of effects occurs.
2. The S_0 captures significantly more energy than when only finite amplitude is considered; i.e., the non-linear friction contributes to a residual slope in the water surface of the channels.
3. When only the M_2 is forcing the system, only the S_0 and the M_6 capture significant energy. In this case the S_0 is far more important than the M_6 at station A and the opposite is true at station B.
4. The $2MS_2$, $2MS_6$, M_6 and $2SM_2$ are dominant in a fairly full spectrum of shallow-water constituents, for both channels, when the system is forced by the three astronomical tides.

4.2.5. Finite amplitude and non-linear friction

In this section, we consider simultaneously the non-linear effects studied separately in the two previous sections. The governing equations are:

$$\frac{\partial \eta}{\partial t} + \frac{\partial}{\partial x} Hu = 0 \qquad [4.25]$$

$$\frac{\partial u}{\partial t} + g\frac{\partial \eta}{\partial x} + \tau u = 0 \qquad [4.26]$$

with:

$$\tau = \frac{n^2|u|}{H^{4/3}} \qquad [4.27]$$

The shallow water tides that are generated in these conditions are expected to be similar to the ones generated by finite amplitude only, plus the ones generated through non-linear friction. Since we are now considering a finite amplitude effect in the friction term (Equation [4.27]), we should keep in mind that the amplitudes of the constituents generated through non-linear frictional processes are not expected to equal to those obtained in the previous section.

The results of the simulations for the flat bottom channel are presented in Tables 28 and 29 and in Figs. 52 and 53. Tables 30 and 31 and Figs. 54 and 55 show the results for the inclined channel. The results appear to be only slightly different from the sum of those obtained in the two previous sections.

4.2.6. Advection

Considering the advective term as single non-linear mechanism, the equations of motion become:

$$\frac{\partial \eta}{\partial t} + \frac{\partial}{\partial x} uh = 0 \qquad [4.28]$$

$$\frac{\partial u}{\partial t} + u\frac{\partial u}{\partial x} + g\frac{\partial \eta}{\partial x} + \tau u = 0 \qquad [4.29]$$

Friction is linear and characterized by τ=0.00025 s^{-1}. The non-linear term leads to a generic algorithm of generation of shallow water tides which is similar to that identified by Equation [4.19]. Indeed, in terms of the definition of the frequencies to where energy is transferred, it does not matter if the transference is done through elevation (when finite amplitude is the only non-linear process considered) or velocity (when advection is present with the non-linear character coming from the product of velocities).

The results of the simulations for the flat bottom channel are presented in Tables 32 and 33 and in Figs. 56 and 57 while the results for the inclined bottom channel are shown in Tables 34 and 35 and in Figs. 58 and 59. The numerical results are consistent with the behavior expected by the analysis performed for the case in which finite amplitude was the only non-linear effect.

Even though the main conclusions of Section 4.2.3 apply in this case, a significant difference was found in the importance of the S_0 constituent. While the zero-frequency constituent does not capture significant energy through finite amplitude non-linear effects, it assumes considerable importance when advection is accounted for; i.e., advection contributes in a major way to a residual slope in both channels.

4.2.7. Advection, finite amplitude and non-linear friction

Finally, considering simultaneously all the non-linear terms we have the governing equations:

$$\frac{\partial \eta}{\partial t} + \frac{\partial}{\partial x} Hu = 0 \qquad [4.30]$$

$$\frac{\partial u}{\partial t} + u\frac{\partial u}{\partial x} + g\frac{\partial \eta}{\partial x} + \tau u = 0 \qquad [4.31]$$

where τ is computed by Equation [4.27] with n=0.025 $sm^{-1/3}$. The results of the simulations are presented in Tables 36 and 37 and in Figs. 60 and 61 (flat bottom channel) and in Tables 38 and 39 and in Figs. 62 and 63 (inclined bottom channel).

Dominant shallow water constituents are, for both channels, the M_4 and S_0 when only the M_2 was forced at the boundary, and the $2MS_2$ (primarily due to friction), the S_0 (primarily due to advection), and the M_4 and MS_4 (contributed by all terms) when the M_2, S_2 and O_1 are all imposed at the open boundary.

As in Section 4.2.5 we expect to observe the generation of shallow water tides roughly corresponding to the ones generated by each of the non-linear processes taken by itself. In this case, we should not only consider the finite amplitude effect on the non-linear friction but also in the advective term.

$RITA_1$ results indicate in this case a small deviation from a simple sum of the effects of the three non-linear terms taken in separate. In the comparison done in Section 4.2.5 the amplitudes of the constituents seemed to be approximately added together. In the presence of all three non-linear effects we note that some shallow water constituents (e.g., S_0) decrease in amplitude showing an interesting cancellation effect.

4.2.8. Conclusions

Throughout the last sections we have explored the generation of shallow water tides taking advantage of the capabilities of $RITA_1$ and, more generically, of ACE_1. The educational value of the process has significant potential and suggests the usefulness of our computational structure for the teaching and learning of physical phenomena. The animated video sequence that supports this work is also an example of how the advances on computer hardware can assist education.

We observed, using numerical simulations, the non-linear mechanisms of generation of overtides and compound tides. From a didactic standpoint we can summarize the content of the last sections as follows:

1. Only through non-linear processes it is possible for the energy associated to tidal constituents to be transferred to other frequencies, corresponding to shallow water tides. This is a well-known fact, that becomes perhaps more clear through analysis such as the one now performed.
2. The type of shallow water tides that are generated, for a well defined case, depend on the dominant non-linear process active in the system. The frequencies of the overtides and compound tides can be determined as func-

tions of the frequencies of the forcing frequencies to the system; results from numerical simulations using $RITA_1$ obey the general rules obtained analytically from the governing equations.

3. The conjugate effect of several non-linear processes acting simultaneously in the system shows a significant synergistic response. Interesting cases of cancelation of effects, extremely difficult to detect otherwise, can be observed by numerical simulation.

The experiments which were object of this section could be further improved. In particular:

1. A larger list of constituents should be used. The constituents $K_1=M_2-O_1$, $M_{SF}=S_2-M_2$ and $SO_1=S_2-O_1$ could have been generated in the cases studied in this section and they were not detected since the harmonic analysis only detects specified constituents. Complementary spectral analysis could detect energy in unspecified constituents.
2. Quadratic bottom friction generates more terms than the ones considered (Equation [4.23]);
3. The analysis of the results based on the comparison of ratios of compound tides against the ratio of the generating astronomical tides (e.g. MO_3/MS_4 vs. O_1/S_2) could provide interesting insight;
4. The analysis of the velocities can provide different results than those obtained for elevations;
5. A larger set of cases should be used. In particular the use of domains with non-uniform Δx should be studied.

CHAPTER 5

CONCLUSIONS

Computer hardware has achieved an extraordinary degree of sophistication in the last few years and hydrodynamic modelling has taken substantial advantage of those advances. However, systematic comparative research and the education and advanced practical training of modelers have been somewhat neglected. To address these issues we developed $RITA_1$ as a tool for education and exploratory research rather than for problem-solving.

One of the objectives in developing the model was to assure its flexibility by incorporating alternative numerical schemes and defining these schemes in a generic way. In doing this, we allow the user to more precisely tailor the characteristics of the method according to his/her particular interests. In Chapter 2, a reference finite element formulation was presented: it is based on the Generalized Continuity Wave Equation, known for its ability to suppress spurious spatial oscillations that afflict the numerical solutions of primitive equations formulations. As deviations from the reference formulation, four alternatives are presented for the treatment of non-linear terms:

1. A time extrapolation method, which allows a certain degree of impliticity on the treatment of non-linear terms without changing the stationarity of the mass matrices;
2. An element-based method, which attempts to reduce the non-linear character of the advective term hence relaxing the stability criteria;
3. A"n+2 upwind" method, in which a more "natural" treatment of the advection is allowed, by means of using non-symmetric weighting functions; and
4. An Eulerian-Lagrangian method. This method was not validated or applied in any simulations; only the interest inherent to the formulation justified its inclusion in Chapter 2.

Our implementation of the numerical algorithms was partially validated by comparison of the numerical results provided by the model with analytical solutions and solutions obtained with an extremely refined time and space discretization (Chapter 3). All methods are very sensitive to the Courant number, as expected. For small Courant num-

bers all methods performed very well, providing accurate results. A simple mass conservation test was also performed and all methods showed excellent behavior.

The usefulness of $RITA_1$ for comparative research in numerical methods and for graduate-level education on hydrodynamics was exemplified in Chapter 4. A sensitivity study examined the optimal value of the parameter G of the wave equation. The results show that the optimal value of G depends on the Courant number, and although the optimal G is often of the order of magnitude of the "characteristic" friction coefficient, it may be significantly higher for small Courant numbers.

A brief comparative interpretation of the different accuracy of each method was done in Section 4.1.2. Non-linear friction is the only term to which a notable gain in accuracy was observed by the use of an alternative method (time extrapolation). This fact may be due to a greater importance of friction, relative to advection and finite amplitude.

The use of time extrapolation techniques for the treatment of non-linear friction was compared with lumping of the momentum equation (Section 4.1.3). The results show that for small Courant numbers the lumping scheme is less accurate than the time-extrapolation, but the lumping scheme is more accurate for larger values of Cu.

The generation of shallow water tides was explored using $RITA_1$ as an educational tool. The theoretical concepts of the transfer of energy by non-linear processes were illustrated and some interesting aspects of the behavior of each non-linear process were detected and interpreted.

We feel the objectives proposed for this thesis were achieved. In particular:

1. In an educational perspective, $RITA_1$ and the associated interface and scientific visualization tools, give the graduate student tools to explore theoretical concepts, and to literally see how they function. This can substantially enhance the learning of both physical processes and numerical methods.
2. The performance of systematic comparisons of alternative schemes is of great interest for the advancement of numerical methods. Due to its characteristics, $RITA_1$ is very well adapted for this type of studies.
3. Preliminary sensitivity analysis of complex multidimensional cases can successfully be performed by $RITA_1$. This practice can be extremely useful on the design of "heavier" studies, by providing information on the dominant processes and on the general behavior of the system being studied towards space and time discretization and numerical strategies.

Areas where $RITA_1$ should be substantially improved in the near future include:

1. Implementation and exploration of Eulerian-Lagrangian Methods, following the formulation described in Chapter 2 or an appropriate alternative;
2. Ability to choose quadratic shape functions;
3. Introduction of numerical solutions involving lumping, such as in ADCIRC[7];
4. Ability to treat moving boundaries.

More than in any specific contribution to hydrodynamic modeling, it is in the concept of an educational, research oriented tool, that is the major interest of this thesis resides. We expect that $RITA_1$ will become the first of a generation of similarly-oriented tools, covering other areas of environmental science and engineering.

REFERENCES

1 Baptista, A.M., J.M. Remédio and C.D. Peterson, "Propagation of Locally-Generated Tsunamis on the Pacific Northwest Coast", in preparation.

2 Goldberg, E.D., The health of the oceans, UNESCO Press, Paris, 1976

3 Haas, Peter M., Saving the Mediterranean : the politics of international environmental cooperation, Columbia University Press, New York, 1990

4 Leendertse, J.J., "Aspects of a Computational Model for Long-Period Water Wave Propagation", Memorandum RM-5294-PR, Rand Corporation, Santa Monica, 1967.

5 Lynch, D. R., "Progress in Hydrodynamic Modeling: Review of U. S. Contributions, 1979-1982", Rev. Geophys. Space Phys., 21, 3, 741-754, 1983.

6 Westerink, J. J., J.J. Connor and K.D. Stolzenbach, "A Frequency-Time Domain Finite Element Model for Tidal Circulation Based on the Least-Squares Harmonic Analysis Method", Int. J. Numer. Methods in Fluids, 8, 813-843, 1988.

7 Luettich, R.A., J.J. Westerink and Scheffner, N.W., ADCIRC: An Advanced Three-Dimensional Circulation Model for Shelves, Coasts and Estuaries. Report 1: Theory and Methodology of ADCIRC-2DDI and ADCIRC-3DL, Coastal Engineering Research Center, Department of the Army, 1991.

8 Nihoul, J.C.J. and B. M. Jamart, Three-Dimensional Models of Marine and Estuarine Dynamics, Elsevier, Amsterdam, 1987

9 Heaps, Norman S., Three-Dimensional Coastal Ocean Models, Coastal and Estuarine Sciences, Christopher N. K. Mooers (Series Editor) , American Geophysical Union, Washington, D.C., 1987

10 Lynch, D.R. and Werner, F.E., "Three-dimensional hydrodynamics on finite elements. Part I: Linearized Harmonic Model, Int. J. Numer. Methods in Fluids, 7, 871-909, 1987.

11 Fortunato, A.B., Three-Dimensional Modelling of Stratified Flow in Tidal Inlets, Ph.D. Thesis, Oregon Graduate Institute of Science and Technology, (in prep).

12 Wood, T. and A.M. Baptista, "A Diagnostic Model for Estuarine Geochemistry", submitted to Water Resources Research (August 1991).

13 Baptista, A.M., "Computational Aspects of the Integrated Analysis of Coastal Watersheds", in Proceedings of the Int. Sem on Water Quality: Assessment and Management, UNESCO-PGIRH/T-WHO, Lisbon, 1989

14 2nd Tidal Flow Forum, Parts I and II, Advances in Water Resources, Vol. 12, pp. 106-222, 1989.

15 Baptista, A.M., J.R. Hurst, P.J. Turner and J.M. Remédio, "ACE_1: An integrated tool for graduate teaching and exploratory research in environmental modeling", CCALMR, SDS#4, (in prep.)

16 Hurst, J., P. Turner and A.M. Baptista, "ACE_1 - User's Manual", Center for Coastal and Land-Margin Research, (in prep.)

17 Hurst, J. and A.M. Baptista, "ELA_1 - User's Manual", Center for Coastal and Land-Margin Research, (in prep.)

18 Center for Coastal and Land-Margin Research, "ACE_{2h} Brochure", October 1991

19 Westerink, J.J., R.A. Luettich, A.M. Baptista, N.W. Scheffner and P. Farrar, "Tide and Storm Surge predictions Using a Finite Element Model", submited to the J. Hydr. Eng., 1992

20 Lynch, D. R., "Finite Element Solution of the Shallow Water Equations", Ph.D. Thesis, Department of Civil Engineering, Princeton University, 1978.

21 Kinnmark, I.P.E. and W.G. Gray, "A Wave Equation Formulation of River Flow", Proc. 6th Intl. Conf. on Finite Element in Water Resources, Springer-Verlag, Berlin, 599-605, 1986.

22 Kinnmark, I.P.E. and W.G. Gray, "A Generalized Wave Equation Formulation of Tidal Circulation", Proc. 4th Intl. Conf. on Numerical Methods on Laminar and Turbulent Flow, Pineridge Press, 1312-1324, 1985.

23 Kinnmark, I.P.E., "The Shallow Water Wave Equations: Formulation, Analysis and Application", Lecture Notes in Engineering, 15, C.A. Brebia and S.A. Orszag [eds.], Springer-Verlag, Berlin, 187p., 1985.

24 Gray, W.G. and I.P.E. Kinnmark, "Evolution of Two-Dimensional FE Wave Equation Models", Proc. 6th Intl. Conf. on Finite Element in Water Resources, Springer-Verlag, Berlin, 29-47, 1986.

25 Westerink, J.J., R.A. Luettich, A.M. Baptista, N.W. Schaeffner, and P. Farrar, "Tide and storm surge prediction in the Gulf of Mexico using a wave-continuity equation finite element model", submited to ASCE J. Hydraulics Division, 1991.

26 Werner, F.E. and D. Lynch, "Field verification of Wave-Equation tidal dynamics in the English Channel and southern North Sea", Adv. Water Resources, 10, 115-130, 1987.

27 Foreman, M.G.G., "An Analysis of the Wave Equation Model for Finite Element Tidal Computations", J. Comput. Phys., 52, 2, 290-312, 1983.

28 Gray, W.G. and I.P.E. Kinnmark, "QUIET: A reduced noise finite element model for tidal circulation", Adv. Eng. Sotfware, 5, 3, 130-136, 1983.

29 Lynch, D. R. and W.G. Gray, "A Wave Equation Model for Finite Element Tidal Computations", Computers and Fluids., 7, 3, 207-228, 1979.

30 Kinnmark, I.P.E. and W.G. Gray, "Time-weighting of the momentum equation in explicit wave equation models of surface water flow", Proc. 4th Intl. Conf. on Finite Element in Water Resources, Springer-Verlag, Berlin, 5.67-5.77, 1982.

31 Kinnmark, I.P.E. and W.G. Gray, "A Two-Dimensional Analysis of the Wave Equation Model for Finite Element Tidal Computations", Int. J. Numer. Methods Eng., 20, 2, 369-383, 1984.

32 Kinnmark, I.P.E. and W.G. Gray, "Stability and Accuracy of Spatial Approximationsfor Wave Equation Tidal Models", J. of Computatinal Physics, 60, 447-466, 1985.

33 Kinnmark, I.P.E. and W.G. Gray, "An Implicit Wave Equation Model for the Shallow Water Equations", Proc. 5th Intl. Conf. on Finite Element in Water Resources, Springer-Verlag, Berlin, 533-543, 1984.

34 Baptista, A. M., Class notes for the course "Dynamics of Estuaries and Coasts - ESE560", Oregon Graduate Institute of Science and Tecnhology, 1991

35 Hwang, L.-S., H.L. Butler and D.J. Divory, "Tsunami model: generation and open-sea characteristics", Bulletin of the Seismological Society of America, 62, 8, 1579-1595, 1972

36 Hauguel, A., "Numerical Modelling of Complex Industrial and Environmental Flows", Proc. Int. Symp. Refined Flow Modelling and Turbulence Measurements, Iowa City, K1-1-K1-25, 1985.

37 Westerink, J.J. and M.E. Cantekin, "Non-Diffusive N+2 Degree Upwinding Methods for the Finite Element Solution of the Time Dependent Transport Equation.", Numerical Methods for Transport and Hydrologic Processes, Computational Methods in Water Resources, 2, Celia et al [eds.], Computational Mechanics Publications, Elsevier, 1988.

38 Hughes, J.R.T., "A Simple Scheme for Developing 'Upwind' Finite Elements", Int. J. Numer. Meths. Eng., 12, 1359-1365, 1978.

39 Kelly, D.W., S. Nakazawa, O.C. Zienkiewicz and J.C. Heinrich, "A Note on Upwinding and Anisotropic Balancing Dissipation in Finite Elemet Approximations to Convective Diffusion Problems", Int. J. Numer. Meths. Eng., 15, 1705-1711, 1980.

40 Heinrich, J.C., P.S. Huyakorn, O.C. Zienkiewicz and A.R. Mitchell, "An 'Upwind' Finite Element Scheme for Two-Dimensional Convective Transport Equation", Int. J. Numer. Meths. Eng., 11, 131-143, 1977.

41 Casulli, V. and Cheng, R.T., "Stability Analysis of Eulerian-Lagrangian Methods for the One-Dimensional Shallow Water Equations", Appl. Math. Modelling, 14, 2, 122-131, 1990.

42 Baptista, A. M., "Solution of Advection-Dominated Transport by Eulerian-Lagrangian Methods Using the Backwards Method of Characteristics", Ph.D. Thesis, Massachusetts Institute of Technology, 1987.

43 Galland, J-C., N. Goutal and J-M. Hervouet, "TELEMAC: A new numerical model for solving shallow water equations", Advances in Water Resources, 14, 138-148, 1991.

44 Lynch, D.R and W.G. Gray, "Analytical solutions for computer flow model testing", J. Hydraulics Division, 14105 - 1427, 1978.

45 Herbst, B.M., S.W. Schoombie, D.F. Griffiths and A.R. Mitchell, "Generalized Petrov-Galerkin Methods for the Numerical Solution of Burgers' Equation", Int. J. Numer. Meths. Eng., 20, 1273-1289, 1984.

46 Dronkers, J.J., Tidal Computations in Rivers and Coastal Waters, North-Holland Publishing Company, Amsterdam, 1964.

TABLES

Table 1. Numerical parameters for the reference linear scheme.

finite amplitude	NO
advection	NO
friction	YES
viscosity	NO
friction type	linear
fin. amp. effect on friction	NO
w_0^1, w_1^1, w_2^1	1.0, -1.0, 0.0
w_0^2, w_1^2, w_2^2	0.35, 0.3, 0.35
w_0^5, w_1^5, w_2^5	0.0, 1.0, 0.0
w_0^6, w_1^6, w_2^6	0.0, 1.0, 0.0
m_0^2, m_1^2	0.5, 0.5
m_0^3, m_1^3	0.0, 1.0

Table 2. Numerical parameters for the Burgers' equation simulations.

	RF	**TE**	**EB**	**UPW**
finite amplitude	NO	NO	NO	NO
advection	YES	YES	YES	YES
friction	NO	NO	NO	NO
viscosity	YES	YES	YES	YES
m_0^1, m_1^1	0.0, 1.0	0.3, 0.7	0.0, 1.0	0.0, 1.0
time extrapolation	NO	YES	NO	NO
element based	NO	NO	YES	NO
upwind	NO	NO	NO	YES
alpha, beta	-	-	-	0.0, 1.2
m_0^4, m_1^4	0.0, 1.0	0.0, 1.0	0.0, 1.0	0.0, 1.0

Table 3. Error norms from the Burgers' equation simulations.

	RF	TE	EB	UPW
L_2 (s^{-1})	0.8203E-02	0.7155E-02	0.5446E-02	0.535E-02

Table 4. Numerical parameters for the finite amplitude simulations.

	RF	TE
finite amplitude	YES	YES
advection	NO	NO
friction	YES	YES
viscosity	NO	NO
friction type	linear	linear
fin. amp. effect on friction	NO	NO
w_0^4, w_1^4, w_2^4	0.0, 1.0	0.3, 0.7
w_0^5, w_1^5, w_2^5	0.0, 1.0	0.0, 1.0
w_0^6, w_1^6, w_2^6	0.0, 0.1	0.0, 1.0
m_0^3, m_1^3	0.0, 1.0	0.0, 1.0

Table 5. Numerical parameters for the non-linear friction simulations.

	RF	TE
finite amplitude	NO	NO
advection	NO	NO
friction	YES	YES
viscosity	NO	NO
friction type	non-linear	non-linear
fin. amp. effect on friction	NO	NO
w_0^5, w_1^5, w_2^5	0.0, 1.0	0.3, 0.7
w_0^6, w_1^6, w_2^6	0.0, 0.1	0.3, 0.7
w_0^7, w_1^7, w_2^7	0.0, 1.0	0.3, 0.7
w_0^8, w_1^8, w_2^8	0.0, 0.1	0.3, 0.7
m_0^3, m_1^3	0.0, 1.0	0.3, 0.7

Table 6. Numerical parameters for the advection simulations.

	RF	TE	EB	UPW
finite amplitude	NO	NO	NO	NO
advection	YES	YES	YES	YES
friction	YES	YES	YES	YES
viscosity	NO	NO	NO	NO
friction type	linear	linear	linear	linear
fin. amp. effect on friction	NO	NO	NO	NO
fin. amp. effect on adv.	NO	NO	NO	NO
w_0^3, w_1^3, w_2^3	.0, 1.0, .0	.3, .7, .0	.0, 1.0, .0	.0, 1.0, .0
element based	NO	NO	YES	NO
w_0^5, w_1^5, w_2^5	.0, 1.0, .0	.0, 1.0, .0	.0, 1.0, .0	.0, 1.0, .0
w_0^6, w_1^6, w_2^6	.0, 1.0, .0	.0, 1.0, .0	.0, 1.0, .0	.0, 1.0, .0
m_0^1, m_1^1	0.0, 1.0	.3, .7	0.0, 1.0	0.0, 1.0
time extrapolation	NO	YES	NO	NO
element based	NO	NO	YES	NO
upwind	NO	NO	NO	YES
alpha, beta	-	-	-	0.0, 1.0
m_0^3, m_1^3	0.0, 1.0	0.0, 1.0	0.0, 1.0	0.0, 1.0

Table 7. Numerical parameters for the fully non-linear simulations.

	RF	**TE**	**EB**	**UPW**
finite amplitude	YES	YES	YES	YES
advection	YES	YES	YES	YES
friction	YES	YES	YES	YES
viscosity	NO	NO	NO	NO
friction type	non-linear	non-linear	non-linear	non-linear
fin. amp. effect on friction	YES	YES	YES	YES
w_0^4, w_1^4, w_2^4	.0, 1.0, .0	.0, 1.0, .0	.0, 1.0, .0	.0, 1.0, .0
fin. amp. effect on adv.	YES	YES	YES	YES
w_0^3, w_1^3, w_2^3	.0, 1.0, .0	.3, .7, .0	.0, 1.0, .0	.0, 1.0, .0
element based	NO	NO	YES	NO
w_0^5, w_1^5, w_2^5	.0, 1.0, .0	.0, 1.0, .0	.0, 1.0, .0	.0, 1.0, .0
w_0^6, w_1^6, w_2^6	.0, 1.0, .0	.0, 1.0, .0	.0, 1.0, .0	.0, 1.0, .0
w_0^7, w_1^7, w_2^7	.0, 1.0, .0	.0, 1.0, .0	.0, 1.0, .0	.0, 1.0, .0
w_0^8, w_1^8, w_2^8	.0, 1.0, .0	.0, 1.0, .0	.0, 1.0, .0	.0, 1.0, .0
m_0^1, m_1^1	0.0, 1.0	.3, .7	0.0, 1.0	0.0, 1.0
time extrapolation	NO	YES	NO	NO
element based	NO	NO	YES	NO
upwind	NO	NO	NO	YES
alpha, beta	-	-	-	0.0, 1.0
m_0^3, m_1^3	0.0, 1.0	0.0, 1.0	0.0, 1.0	0.0, 1.0

Table 8. Time steps and corresponding average Courant numbers.

Δt (s)	30	60	120	240	300	480	600	1200	2400
Cu	.12	.24	.48	.96	1.2	1.92	2.4	4.8	9.6

Table 9. Tidal components of interest.

Component	Frequency (rad.s-1)	Period (h)
S_0	0.0	Inf
O_1	0.6759774260E-04	25.819
$2MS_2$	0.1355936984E-03	12.872
M_2	0.1405188959E-03	12.421
S_2	0.1454441081E-03	12.000
$2SM_2$	0.1503693056E-03	11.607
MO_3	0.2081166458E-03	8.386
SO_3	0.2130418434E-03	8.192
M_4	0.2810377919E-03	6.210
MS_4	0.2859630040E-03	6.103
S_4	0.2908882161E-03	6.000
M_6	0.4215567023E-03	4.140
$2MS_6$	0.4264819145E-03	4.092
$2SM_6$	0.4314070975E-03	4.046
S_6	0.4363323096E-03	4.000
M_8	0.5620755837E-03	3.105

Table 10. Harmonic analysis results. Frictionless linear case. M_2, flat bottom.

Component	Station A			Station B		
	η_0 (m)	χ (%)	ϕ (h)	η_0 (m)	χ (%)	ϕ (h)
S0	.000			.000		
O1	.000	.0	.00	.000	.0	.00
2MS2	.000	.0	.00	.000	.0	.00
M2	2.953	100.0	.00	3.475	100.0	.00
S2	.000	.0	.00	.000	.0	.00
2SM2	.000	.0	.00	.000	.0	.00
MO3	.000	.0	.00	.000	.0	.00
SO3	.000	.0	.00	.000	.0	.00
M4	.000	.0	.00	.000	.0	.00
MS4	.000	.0	.00	.000	.0	.00
S4	.000	.0	.00	.000	.0	.00
M6	.000	.0	.00	.000	.0	.00
2MS6	.000	.0	.00	.000	.0	.00
2SM6	.000	.0	.00	.000	.0	.00
S6	.000	.0	.00	.000	.0	.00
M8	.000	.0	.00	.000	.0	.00

Table 11. Harmonic analysis results. Frictionless linear case. M_2+S_2+O_1, flat bottom.

Component	Station A			Station B		
	η_0 (m)	χ (%)	ϕ (h)	η_0 (m)	χ (%)	ϕ (h)
S_0	.000			.000		
O_1	.422	14.3	.00	.437	12.6	.00
$2MS_2$	.000	.0	.00	.000	.0	.00
M_2	2.953	100.0	.00	3.475	100.0	.00
S_2	1.781	60.3	12.00	2.122	61.1	12.00
$2SM_2$	.000	.0	.00	.000	.0	.00
MO_3	.000	.0	.00	.000	.0	.00
SO_3	.000	.0	.00	.000	.0	.00
M_4	.000	.0	.00	.000	.0	.00
MS_4	.000	.0	.00	.000	.0	.00
S_4	.000	.0	.00	.000	.0	.00
M_6	.000	.0	.00	.000	.0	.00
$2MS_6$	.000	.0	.00	.000	.0	.00
$2SM_6$	.000	.0	.00	.000	.0	.00
S_6	.000	.0	.00	.000	.0	.00
M_8	.000	.0	.00	.000	.0	.00

Table 12. Harmonic analysis results. Frictionless linear case. M_2, inclined bottom.

Component	Station A			Station B		
	η_0 (m)	χ (%)	ϕ (h)	η_0 (m)	χ (%)	ϕ (h)
S0	.000			.000		
O1	.000	.0	.00	.000	.0	.00
2MS2	.000	.0	.00	.000	.0	.00
M2	2.539	100.0	.00	3.124	100.0	.00
S2	.000	.0	.00	.000	.0	.00
2SM2	.000	.0	.00	.000	.0	.00
MO3	.001	.0	2.45	.001	.0	2.45
SO3	.000	.0	.00	.000	.0	.00
M4	.000	.0	.00	.000	.0	.00
MS4	.000	.0	.00	.000	.0	.00
S4	.000	.0	.00	.000	.0	.00
M6	.000	.0	.00	.000	.0	.00
2MS6	.000	.0	.00	.000	.0	.00
2SM6	.000	.0	.00	.000	.0	.00
S6	.000	.0	.00	.000	.0	.00
M8	.000	.0	.00	.000	.0	.00

Table 13. Harmonic analysis results. Frictionless linear case. $M_2+S_2+O_1$, inclined bottom.

Component	Station A			Station B		
	η_0 (m)	χ (%)	ϕ (h)	η_0 (m)	χ (%)	ϕ (h)
S0	.000			.000		
O1	.412	16.2	25.82	.432	13.8	25.82
2MS2	.000	.0	.00	.000	.0	.00
M2	2.539	100.0	.00	3.124	100.0	.00
S2	1.502	59.1	12.00	1.877	60.1	12.00
2SM2	.000	.0	.00	.000	.0	.00
MO3	.001	.0	2.45	.002	.1	2.45
SO3	.000	.0	.00	.000	.0	.00
M4	.000	.0	.00	.000	.0	.00
MS4	.000	.0	.00	.000	.0	.00
S4	.000	.0	.00	.000	.0	.00
M6	.000	.0	.00	.000	.0	.00
2MS6	.000	.0	.00	.000	.0	.00
2SM6	.000	.0	.00	.000	.0	.00
S6	.000	.0	.00	.000	.0	.00
M8	.000	.0	.00	.000	.0	.00

Table 14. Harmonic analysis results. Linear case. M_2, flat bottom.

Component	Station A			Station B		
	η_0 (m)	χ (%)	ϕ (h)	η_0 (m)	χ (%)	ϕ (h)
S0	.000			.000		
O1	.000	.0	.00	.000	.0	.00
2MS2	.000	.0	.00	.000	.0	.00
M2	1.438	100.0	2.01	1.650	100.0	2.60
S2	.000	.0	.00	.000	.0	.00
2SM2	.000	.0	.00	.000	.0	.00
MO3	.000	.0	.00	.000	.0	.00
SO3	.000	.0	.00	.000	.0	.00
M4	.000	.0	.00	.000	.0	.00
MS4	.000	.0	.00	.000	.0	.00
S4	.000	.0	.00	.000	.0	.00
M6	.000	.0	.00	.000	.0	.00
2MS6	.000	.0	.00	.000	.0	.00
2SM6	.000	.0	.00	.000	.0	.00
S6	.000	.0	.00	.000	.0	.00
M8	.000	.0	.00	.000	.0	.00

Table 15. Harmonic analysis results. Linear case. M_2+S_2+O_1, flat bottom.

Component	Station A			Station B		
	η_0 (m)	χ (%)	ϕ (h)	η_0 (m)	χ (%)	ϕ (h)
S0	.000			.000		
O1	.381	26.5	1.77	.393	23.8	2.33
2MS2	.000	.0	.00	.000	.0	.00
M2	1.438	100.0	2.01	1.650	100.0	2.60
S2	.795	55.3	2.02	.921	55.8	2.62
2SM2	.000	.0	.00	.000	.0	.00
MO3	.000	.0	.00	.000	.0	.00
SO3	.000	.0	.00	.000	.0	.00
M4	.000	.0	.00	.000	.0	.00
MS4	.000	.0	.00	.000	.0	.00
S4	.000	.0	.00	.000	.0	.00
M6	.000	.0	.00	.000	.0	.00
2MS6	.000	.0	.00	.000	.0	.00
2SM6	.000	.0	.00	.000	.0	.00
S6	.000	.0	.00	.000	.0	.00
M8	.000	.0	.00	.000	.0	.00

Table 16. Harmonic analysis results. Linear case. M_2, inclined bottom.

Component	Station A			Station B		
	η_0 (m)	χ (%)	ϕ (h)	η_0 (m)	χ (%)	ϕ (h)
S0	.000			.000		
O1	.000	.0	.00	.000	.0	.00
2MS2	.000	.0	.00	.000	.0	.00
M2	1.500	100.0	1.66	1.769	100.0	2.42
S2	.000	.0	.00	.000	.0	.00
2SM2	.000	.0	.00	.000	.0	.00
MO3	.000	.0	.00	.000	.0	.00
SO3	.000	.0	.00	.000	.0	.00
M4	.000	.0	.00	.000	.0	.00
MS4	.000	.0	.00	.000	.0	.00
S4	.000	.0	.00	.000	.0	.00
M6	.000	.0	.00	.000	.0	.00
2MS6	.000	.0	.00	.000	.0	.00
2SM6	.000	.0	.00	.000	.0	.00
S6	.000	.0	.00	.000	.0	.00
M8	.000	.0	.00	.000	.0	.00

Table 17. Harmonic analysis results. Linear case. M_2+S_2+O_1, inclined bottom..

Component	Station A			Station B		
	η_0 (m)	χ (%)	ϕ (h)	η_0 (m)	χ (%)	ϕ (h)
S0	.000			.000		
O1	.383	25.5	1.44	.397	22.5	2.14
2MS2	.000	.0	.00	.000	.0	.00
M2	1.500	100.0	1.66	1.769	100.0	2.42
S2	.833	55.5	1.67	.994	56.2	2.44
2SM2	.000	.0	.00	.000	.0	.00
MO3	.000	.0	.00	.000	.0	.00
SO3	.000	.0	.00	.000	.0	.00
M4	.000	.0	.00	.000	.0	.00
MS4	.000	.0	.00	.000	.0	.00
S4	.000	.0	.00	.000	.0	.00
M6	.000	.0	.00	.000	.0	.00
2MS6	.000	.0	.00	.000	.0	.00
2SM6	.000	.0	.00	.000	.0	.00
S6	.000	.0	.00	.000	.0	.00
M8	.000	.0	.00	.000	.0	.00

Table 18. Finite amplitude generated shallow water tides.

Astronomical Tides	Shallow Water Tides
M_2	S_0, M_4, M_6, M_8, ...
S_2	S_0, S_4, S_6, ...
$M_2 + S_2$	MS_0, MS_4, ...
$M_2 + O_1$	MO_3, MO_2, ...
$S_2 + O_1$	SO_3, SO_2, ...

Table 19. Harmonic analysis results. Linear case + finite amplitude. M_2, flat bottom.

Component	Station A			Station B		
	η_0 (m)	χ (%)	ϕ (h)	η_0 (m)	χ (%)	ϕ (h)
S0	.005			-.010		
O1	.000	.0	.00	.000	.0	.00
2MS2	.000	.0	.00	.000	.0	.00
M2	1.427	100.0	1.98	1.628	100.0	2.58
S2	.000	.0	.00	.000	.0	.00
2SM2	.000	.0	.00	.000	.0	.00
MO3	.000	.0	.00	.000	.0	.00
SO3	.000	.0	.00	.000	.0	.00
M4	.026	1.8	1.62	.078	4.8	1.65
MS4	.000	.0	.00	.000	.0	.00
S4	.000	.0	.00	.000	.0	.00
M6	.003	.2	2.27	.004	.2	.51
2MS6	.000	.0	.00	.000	.0	.00
2SM6	.000	.0	.00	.000	.0	.00
S6	.000	.0	.00	.000	.0	.00
M8	.000	.0	.00	.001	.0	3.00

Table 20. Harmonic analysis results. Linear case + finite amplitude. $M_2+S_2+O_1$, flat bottom.

Component	Station A			Station B		
	η_0 (m)	χ (%)	ϕ (h)	η_0 (m)	χ (%)	ϕ (h)
S0	.007			-.013		
O1	.377	26.5	1.75	.389	23.9	2.31
2MS2	.002	.2	12.12	.001	.1	.31
M2	1.425	100.0	1.97	1.625	100.0	2.58
S2	.787	55.2	1.98	.905	55.7	2.59
2SM2	.001	.1	9.08	.002	.1	7.95
MO3	.022	1.6	1.11	.039	2.4	1.26
SO3	.012	.8	1.06	.020	1.2	1.25
M4	.026	1.8	1.61	.078	4.8	1.65
MS4	.027	1.9	1.63	.086	5.3	1.67
S4	.007	.5	1.63	.024	1.5	1.69
M6	.003	.2	2.30	.004	.2	.49
2MS6	.005	.3	2.32	.006	.4	.52
2SM6	.003	.2	2.35	.003	.2	.53
S6	.001	.0	2.49	.001	.0	.42
M8	.000	.0	.00	.001	.0	2.89

Table 21. Harmonic analysis results. Linear case + finite amplitude. M_2, inclined bottom.

Component	Station A			Station B		
	η_0 (m)	χ (%)	ϕ (h)	η_0 (m)	χ (%)	ϕ (h)
S0	-.001			-.028		
O1	.000	.0	.00	.000	.0	.00
2MS2	.000	.0	.00	.000	.0	.00
M2	1.489	100.0	1.63	1.746	100.0	2.41
S2	.000	.0	.00	.000	.0	.00
2SM2	.000	.0	.00	.000	.0	.00
MO3	.000	.0	.00	.000	.0	.00
SO3	.000	.0	.00	.000	.0	.00
M4	.021	1.4	2.00	.092	5.3	1.41
MS4	.000	.0	.00	.000	.0	.00
S4	.000	.0	.00	.000	.0	.00
M6	.005	.3	1.97	.006	.4	.16
2MS6	.000	.0	.00	.000	.0	.00
2SM6	.000	.0	.00	.000	.0	.00
S6	.000	.0	.00	.000	.0	.00
M8	.001	.1	1.30	.001	.1	2.81

Table 22. Harmonic analysis results. Linear case + finite amplitude. M_2+S_2+O_1, inclined bottom.

Component	Station A			Station B		
	η_0 (m)	χ (%)	ϕ (h)	η_0 (m)	χ (%)	ϕ (h)
S0	-.001			-.038		
O1	.380	25.5	1.42	.395	22.6	2.15
2MS2	.002	.1	11.36	.003	.2	4.49
M2	1.487	100.0	1.63	1.744	100.0	2.41
S2	.825	55.5	1.64	.978	56.1	2.44
2SM2	.001	.1	9.08	.003	.2	6.22
MO3	.017	1.2	1.05	.044	2.5	.95
SO3	.009	.6	.93	.022	1.3	1.00
M4	.020	1.4	2.02	.093	5.3	1.42
MS4	.021	1.4	2.10	.104	6.0	1.44
S4	.005	.3	2.21	.029	1.7	1.46
M6	.004	.3	2.00	.007	.4	.16
2MS6	.008	.5	2.03	.011	.6	.20
2SM6	.004	.3	2.07	.007	.4	.23
S6	.001	.1	2.20	.001	.1	.26
M8	.001	.0	1.18	.001	.1	2.71

Table 23. Non-linear friction generated shallow water tides.

Astronomical Tides	Shallow Water Tides
M_2	M_6, ...
S_2	S_6, ...
$M_2 + S_2$	$2MS_6$, $2SM_6$, $2MS_2$, $2SM_2$, ...

Table 24. Harmonic analysis results. Linear case + non-linear friction. M_2, flat bottom.

Component	Station A			Station B		
	η_0 (m)	χ (%)	ϕ (h)	η_0 (m)	χ (%)	ϕ (h)
S0	.047			.045		
O1	.001	.0	.69	.000	.0	.00
2MS2	.001	.0	.98	.000	.0	.00
M2	1.399	100.0	2.22	1.647	100.0	2.54
S2	.001	.0	1.03	.001	.0	1.25
2SM2	.001	.0	.85	.000	.0	.00
MO3	.000	.0	.00	.000	.0	.00
SO3	.000	.0	.00	.000	.0	.00
M4	.017	1.2	2.76	.057	3.5	2.00
MS4	.000	.0	.00	.000	.0	.00
S4	.000	.0	.00	.000	.0	.00
M6	.022	1.6	1.95	.124	7.5	2.88
2MS6	.000	.0	.00	.000	.0	.00
2SM6	.000	.0	.00	.000	.0	.00
S6	.000	.0	.00	.000	.0	.00
M8	.003	.2	1.72	.011	.7	2.88

Table 25. Harmonic analysis results. Linear case + non-linear friction. $M_2+S_2+O_1$, flat bottom.

Component	Station A			Station B		
	η_0 (m)	χ (%)	ϕ (h)	η_0 (m)	χ (%)	ϕ (h)
S0	.049			.048		
O1	.358	27.4	2.49	.371	24.3	2.85
2MS2	.159	12.2	7.49	.205	13.4	7.53
M2	1.307	100.0	2.26	1.531	100.0	2.60
S2	.613	46.9	2.48	.733	47.9	2.90
2SM2	.041	3.1	7.70	.055	3.6	7.76
MO3	.019	1.5	1.51	.038	2.5	1.41
SO3	.020	1.6	5.13	.026	1.7	5.27
M4	.009	.7	3.14	.038	2.5	2.02
MS4	.008	.6	3.30	.042	2.8	2.02
S4	.002	.2	5.30	.006	.4	1.85
M6	.012	.9	1.92	.052	3.4	3.01
2MS6	.023	1.8	1.89	.109	7.1	2.98
2SM6	.010	.7	1.85	.036	2.4	3.14
S6	.000	.0	.00	.003	.2	.76
M8	.002	.2	2.61	.004	.3	.46

Table 26. Harmonic analysis results. Linear case + non-linear friction. M_2, inclined bottom.

Component	Station A			Station B		
	η_0 (m)	χ (%)	ϕ (h)	η_0 (m)	χ (%)	ϕ (h)
S0	.044			.045		
O1	.001	.0	12.89	.001	.0	12.57
2MS2	.001	.1	7.08	.001	.1	7.10
M2	1.663	100.0	1.51	1.982	100.0	2.23
S2	.001	.1	6.41	.001	.1	6.43
2SM2	.001	.1	6.19	.001	.1	6.24
MO3	.001	.0	4.96	.001	.1	5.14
SO3	.001	.0	4.84	.001	.1	5.02
M4	.016	.9	2.44	.099	5.0	1.71
MS4	.001	.0	3.77	.001	.1	4.08
S4	.001	.0	3.67	.001	.1	4.00
M6	.011	.7	1.54	.121	6.1	2.42
2MS6	.000	.0	.00	.001	.0	3.17
2SM6	.000	.0	.00	.001	.0	3.15
S6	.000	.0	.00	.001	.0	3.13
M8	.007	.4	.54	.019	1.0	2.19

Table 27. Harmonic analysis results. Linear case + non-linear friction. $M_2+S_2+O_1$, inclined bottom.

Component	Station A			Station B		
	η_0 (m)	χ (%)	ϕ (h)	η_0 (m)	χ (%)	ϕ (h)
S0	.052			.056		
O1	.380	24.2	1.55	.395	21.5	2.37
2MS2	.154	9.8	6.57	.257	14.0	6.77
M2	1.567	100.0	1.54	1.836	100.0	2.33
S2	.776	49.5	1.75	.927	50.5	2.71
2SM2	.046	2.9	6.91	.081	4.4	7.17
MO3	.021	1.4	.86	.051	2.8	1.06
SO3	.016	1.0	4.47	.024	1.3	4.61
M4	.007	.4	1.91	.074	4.0	1.82
MS4	.004	.2	1.77	.083	4.5	1.85
S4	.005	.3	.12	.015	.8	2.10
M6	.013	.8	1.33	.055	3.0	2.66
2MS6	.021	1.4	1.31	.113	6.2	2.59
2SM6	.014	.9	1.24	.044	2.4	2.81
S6	.003	.2	1.53	.005	.3	3.98
M8	.003	.2	1.27	.006	.4	2.84

Table 28. Harmonic analysis results. Linear case + finite amplitude and non-linear friction. M_2, flat bottom.

Component	Station A			Station B		
	η_0 (m)	χ (%)	ϕ (h)	η_0 (m)	χ (%)	ϕ (h)
S0	.055			.031		
O1	.000	.0	.00	.000	.0	.00
2MS2	.000	.0	.00	.000	.0	.00
M2	1.396	100.0	2.20	1.643	100.0	2.53
S2	.000	.0	.00	.000	.0	.00
2SM2	.000	.0	.00	.000	.0	.00
MO3	.000	.0	.00	.000	.0	.00
SO3	.000	.0	.00	.000	.0	.00
M4	.046	3.3	1.97	.137	8.4	1.82
MS4	.000	.0	.00	.000	.0	.00
S4	.000	.0	.00	.000	.0	.00
M6	.026	1.9	2.12	.113	6.9	2.88
2MS6	.000	.0	.00	.000	.0	.00
2SM6	.000	.0	.00	.000	.0	.00
S6	.000	.0	.00	.000	.0	.00
M8	.011	.8	.71	.025	1.5	2.34

Table 31. Harmonic analysis results. Linear case + finite amplitude and non-linear friction. M_2+S_2+O_1, inclined bottom.

Component	Station A			Station B		
	η_0 (m)	χ (%)	ϕ (h)	η_0 (m)	χ (%)	ϕ (h)
S0	.052			-.039		
O1	.378	24.1	1.44	.396	21.7	2.31
2MS2	.146	9.3	6.59	.257	14.1	6.79
M2	1.570	100.0	1.52	1.822	100.0	2.35
S2	.779	49.6	1.70	.916	50.3	2.74
2SM2	.043	2.7	6.95	.082	4.5	7.25
MO3	.034	2.2	1.07	.103	5.7	1.16
SO3	.011	.7	3.99	.021	1.2	3.09
M4	.010	.6	3.10	.178	9.8	1.72
MS4	.012	.7	3.79	.200	11.0	1.75
S4	.010	.7	5.45	.051	2.8	2.04
M6	.011	.7	2.06	.035	1.9	2.54
2MS6	.021	1.3	2.00	.079	4.3	2.53
2SM6	.008	.5	1.98	.023	1.3	2.71
S6	.001	.0	2.78	.004	.2	.70
M8	.003	.2	.49	.008	.4	2.43

Table 32. Harmonic analysis results. Linear case + advection. M_2, flat bottom.

Component	Station A			Station B		
	η_0 (m)	χ (%)	ϕ (h)	η_0 (m)	χ (%)	ϕ (h)
S0	.071			.108		
O1	.001	.0	14.03	.001	.1	13.97
2MS2	.001	.0	7.86	.001	.1	7.79
M2	1.446	100.0	1.97	1.649	100.0	2.56
S2	.001	.0	7.17	.001	.1	7.04
2SM2	.001	.0	6.92	.001	.1	6.81
MO3	.001	.0	5.41	.001	.0	5.29
SO3	.000	.0	.00	.001	.0	5.14
M4	.023	1.6	.60	.071	4.3	.52
MS4	.000	.0	.00	.000	.0	.00
S4	.000	.0	.00	.000	.0	.00
M6	.001	.1	.25	.005	.3	.78
2MS6	.000	.0	.00	.000	.0	.00
2SM6	.000	.0	.00	.000	.0	.00
S6	.000	.0	.00	.000	.0	.00
M8	.002	.1	1.23	.002	.1	2.58

Table 33. Harmonic analysis results. Linear case + advection. M_2+S_2+O_1, flat bottom.

Component	Station A			Station B		
	η_0 (m)	χ (%)	ϕ (h)	η_0 (m)	χ (%)	ϕ (h)
S0	.089			.139		
O1	.384	26.4	1.72	.398	23.9	2.29
2MS2	.010	.7	1.09	.010	.6	1.97
M2	1.458	100.0	1.96	1.663	100.0	2.56
S2	.813	55.7	1.97	.935	56.3	2.57
2SM2	.004	.3	1.62	.005	.3	2.74
MO3	.011	.8	7.80	.022	1.3	7.82
SO3	.007	.5	7.89	.012	.7	7.71
M4	.021	1.4	.63	.069	4.2	.47
MS4	.022	1.5	.70	.078	4.7	.51
S4	.005	.3	.84	.021	1.2	.47
M6	.001	.1	4.12	.005	.3	.78
2MS6	.002	.1	.07	.008	.5	.81
2SM6	.001	.1	3.92	.004	.3	.86
S6	.001	.0	3.11	.001	.0	1.45
M8	.001	.1	1.13	.001	.1	2.34

Table 34. Harmonic analysis results. Linear case + advection. M_2, inclined bottom.

Component	Station A			Station B		
	η_0 (m)	χ (%)	ϕ (h)	η_0 (m)	χ (%)	ϕ (h)
S0	.037			.092		
O1	.000	.0	.00	.001	.0	13.64
2MS2	.000	.0	.00	.001	.0	7.55
M2	1.495	100.0	1.63	1.751	100.0	2.40
S2	.000	.0	.00	.001	.0	6.72
2SM2	.000	.0	.00	.001	.0	6.52
MO3	.000	.0	.00	.001	.0	5.09
SO3	.000	.0	.00	.001	.0	4.95
M4	.013	.8	1.06	.069	4.0	.17
MS4	.000	.0	.00	.000	.0	.00
S4	.000	.0	.00	.000	.0	.00
M6	.001	.1	1.73	.003	.2	.28
2MS6	.000	.0	.00	.000	.0	.00
2SM6	.000	.0	.00	.000	.0	.00
S6	.000	.0	.00	.000	.0	.00
M8	.001	.0	.93	.001	.1	2.34

Table 35. Harmonic analysis results. Linear case + advection. M_2+S_2+O_1, inclined bottom.

Component	Station A			Station B		
	η_0 (m)	χ (%)	ϕ (h)	η_0 (m)	χ (%)	ϕ (h)
S0	.048			.120		
O1	.383	25.5	1.42	.400	22.8	2.15
2MS2	.003	.2	.70	.004	.2	3.45
M2	1.499	100.0	1.63	1.756	100.0	2.40
S2	.834	55.7	1.64	.988	56.3	2.42
2SM2	.001	.1	1.66	.003	.2	4.21
MO3	.007	.5	7.72	.020	1.1	7.46
SO3	.004	.3	7.74	.011	.6	7.23
M4	.013	.8	1.08	.068	3.9	.14
MS4	.014	.9	1.22	.078	4.4	.19
S4	.004	.2	1.41	.021	1.2	.19
M6	.001	.0	1.97	.002	.1	.35
2MS6	.001	.1	1.91	.004	.3	.37
2SM6	.001	.1	2.12	.002	.1	.45
S6	.000	.0	.00	.000	.0	.00
M8	.000	.0	.00	.001	.1	2.10

Table 36. Harmonic analysis results. Fully non-linear case. M_2, flat bottom.

Component	Station A			Station B		
	η_0 (m)	χ (%)	ϕ (h)	η_0 (m)	χ (%)	ϕ (h)
S0	.120			.123		
O1	.000	.0	.00	.000	.0	.00
2MS2	.000	.0	.00	.001	.0	7.54
M2	1.399	100.0	2.18	1.645	100.0	2.50
S2	.000	.0	.00	.000	.0	.00
2SM2	.000	.0	.00	.000	.0	.00
MO3	.000	.0	.00	.000	.0	.00
SO3	.000	.0	.00	.000	.0	.00
M4	.063	4.5	1.58	.174	10.6	1.42
MS4	.000	.0	.00	.000	.0	.00
S4	.000	.0	.00	.000	.0	.00
M6	.035	2.5	2.07	.100	6.1	2.91
2MS6	.000	.0	.00	.000	.0	.00
2SM6	.000	.0	.00	.000	.0	.00
S6	.000	.0	.00	.000	.0	.00
M8	.015	1.1	.70	.040	2.5	2.20

Table 37. Harmonic analysis results. Fully non-linear case. $M_2+S_2+O_1$, flat bottom.

Component	Station A			Station B		
	η_0 (m)	χ (%)	ϕ (h)	η_0 (m)	χ (%)	ϕ (h)
S0	.154			.155		
O1	.356	27.1	2.33	.370	24.1	2.70
2MS2	.147	11.2	7.53	.190	12.4	7.57
M2	1.313	100.0	2.20	1.533	100.0	2.54
S2	.617	47.0	2.40	.732	47.8	2.81
2SM2	.038	2.9	7.81	.052	3.4	7.85
MO3	.051	3.9	1.20	.083	5.4	1.23
SO3	.005	.3	4.36	.006	.4	3.96
M4	.048	3.7	1.50	.143	9.3	1.51
MS4	.048	3.7	1.53	.159	10.4	1.57
S4	.008	.6	1.21	.035	2.3	1.80
M6	.017	1.3	2.23	.035	2.3	2.99
2MS6	.034	2.6	2.18	.076	4.9	3.00
2SM6	.014	1.1	2.32	.019	1.2	3.21
S6	.002	.1	3.37	.004	.3	1.10
M8	.003	.2	1.09	.006	.4	2.49

Table 38. Harmonic analysis results. Fully non-linear case. M_2, inclined bottom.

Component	Station A			Station B		
	η_0 (m)	χ (%)	ϕ (h)	η_0 (m)	χ (%)	ϕ (h)
S0	.077			.078		
O1	.001	.1	12.86	.001	.1	12.79
2MS2	.001	.1	7.11	.002	.1	7.10
M2	1.655	100.0	1.48	1.955	100.0	2.22
S2	.001	.1	6.47	.002	.1	6.46
2SM2	.001	.1	6.24	.002	.1	6.24
MO3	.001	.1	5.04	.002	.1	5.00
SO3	.001	.1	4.93	.002	.1	4.82
M4	.033	2.0	2.15	.243	12.4	1.14
MS4	.001	.1	3.97	.001	.1	3.86
S4	.001	.0	3.89	.001	.1	3.79
M6	.043	2.6	1.89	.077	3.9	2.60
2MS6	.000	.0	.00	.001	.0	2.93
2SM6	.000	.0	.00	.001	.0	2.89
S6	.000	.0	.00	.001	.0	2.84
M8	.013	.8	3.06	.042	2.1	1.80

Table 39. Harmonic analysis results.Fully non-linear case. $M_2+S_2+O_1$, inclined bottom.

Component	Station A			Station B		
	η_0 (m)	χ (%)	ϕ (h)	η_0 (m)	χ (%)	ϕ (h)
S0	.107			.106		
O1	.376	24.0	1.46	.390	21.6	2.29
2MS2	.146	9.3	6.61	.245	13.6	6.87
M2	1.564	100.0	1.51	1.804	100.0	2.30
S2	.776	49.6	1.70	.900	49.9	2.66
2SM2	.043	2.8	6.92	.077	4.3	7.35
MO3	.036	2.3	.74	.106	5.9	.87
SO3	.008	.5	4.26	.012	.7	2.58
M4	.009	.6	1.52	.205	11.4	1.33
MS4	.002	.1	2.55	.232	12.9	1.39
S4	.011	.7	5.34	.057	3.1	1.76
M6	.024	1.5	2.12	.017	.9	2.76
2MS6	.045	2.9	2.05	.046	2.6	2.72
2SM6	.020	1.3	2.20	.009	.5	3.38
S6	.003	.2	2.98	.007	.4	.87
M8	.002	.1	.56	.009	.5	2.43

FIGURES

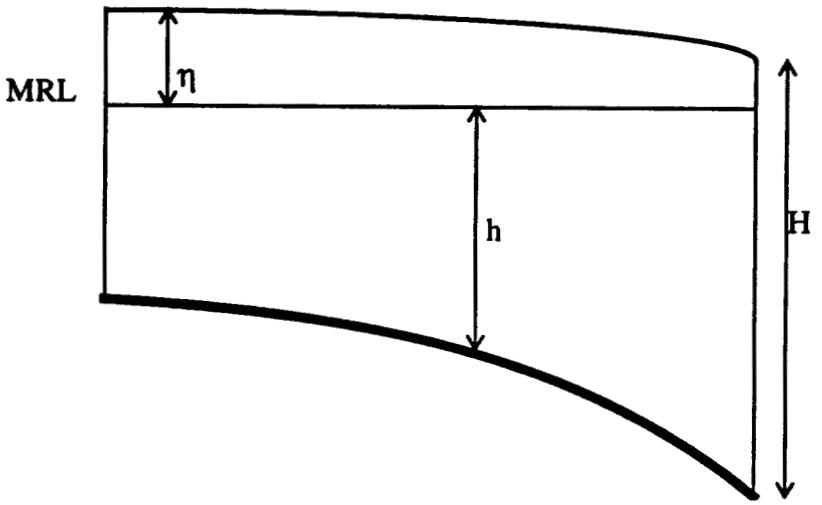

Fig. 1. Geometry of the problem (MRL- Mean Reference Level; H - total water depth; h - depth; η - elevation).

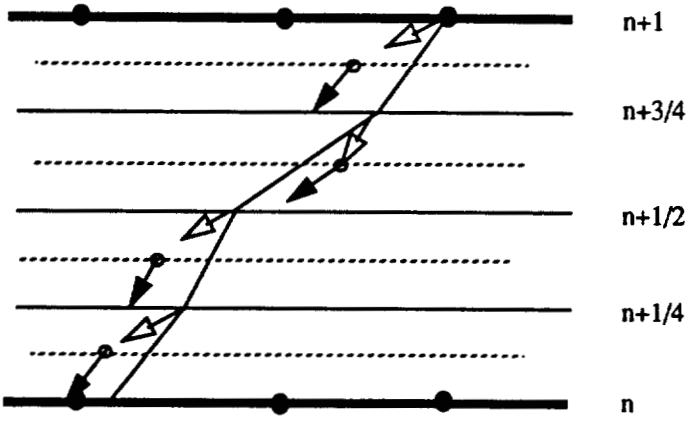

Fig. 2. Four-step 2nd order Runge-Kutta tracking scheme: tracking from time n+1 to time n.

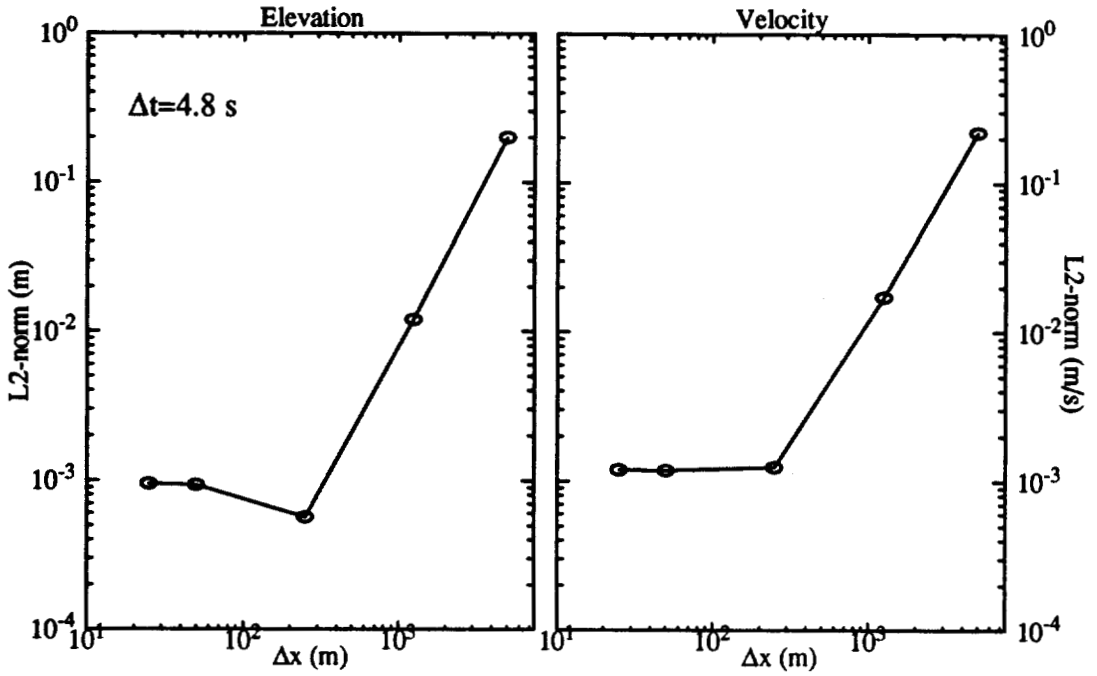

Fig. 3. Sensitivity to space discretization. L_2-norm as function of Δx; linear case.

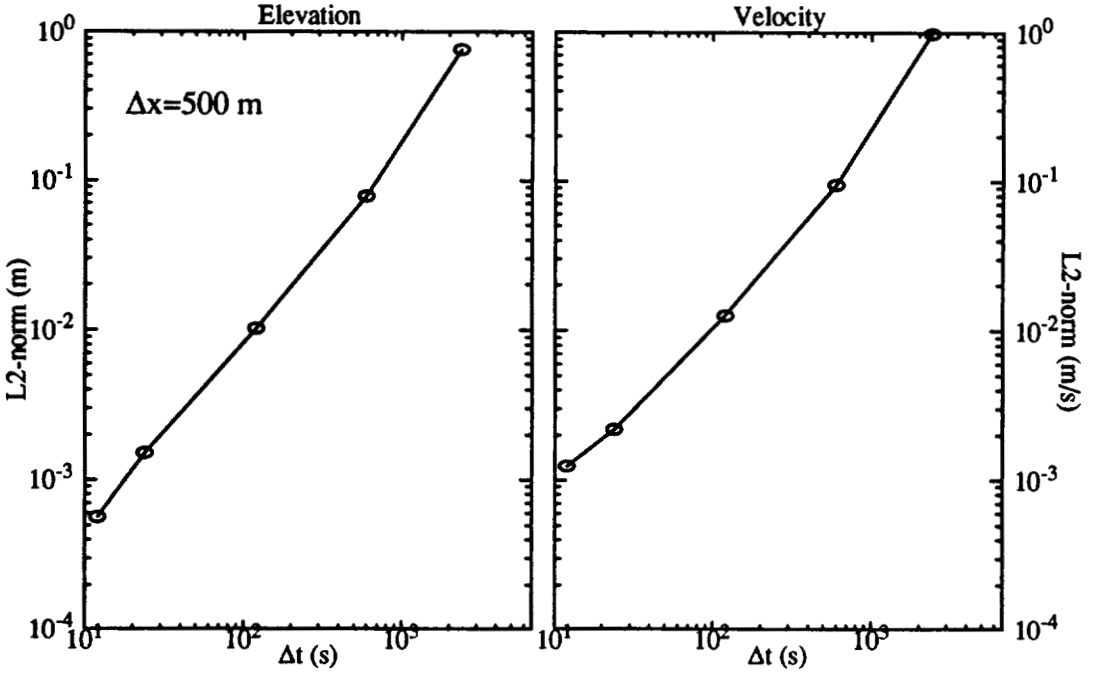

Fig. 4. Sensitivity to time discretization. L_2-norm as function of Δt; linear case.

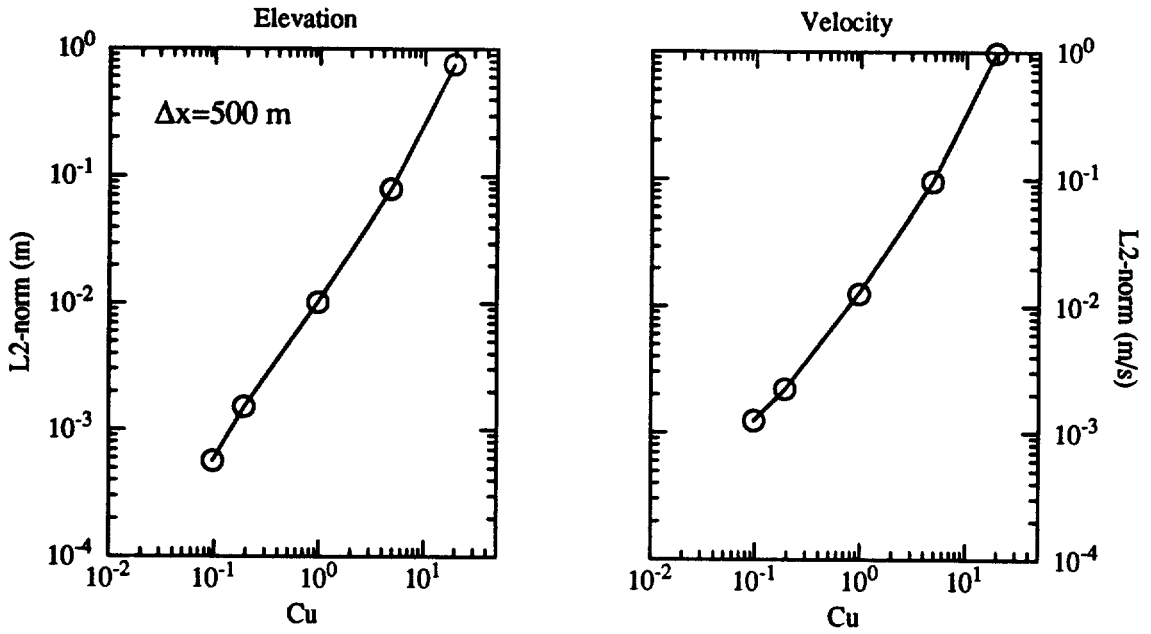

Fig. 5. Sensitivity to Courant number. L_2-norm as function of Cu; linear case.

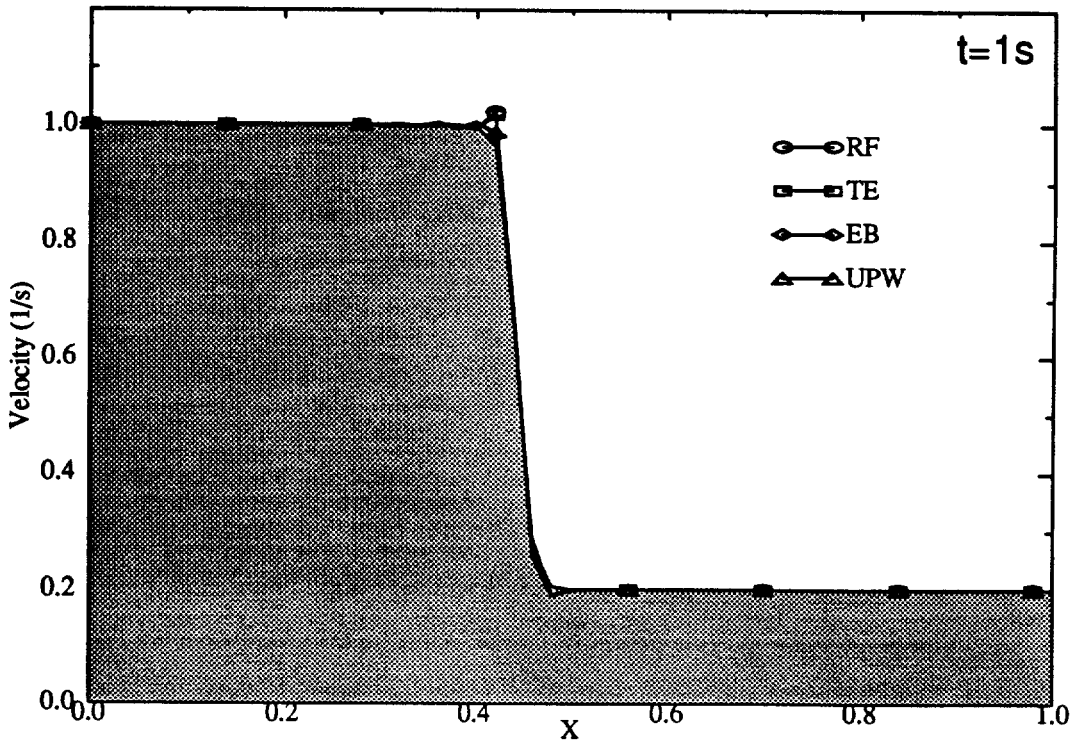

Fig. 6. Numerical and analytical (shadow area) solution of the Burgers' equation. Snapshot of velocities for various methods.

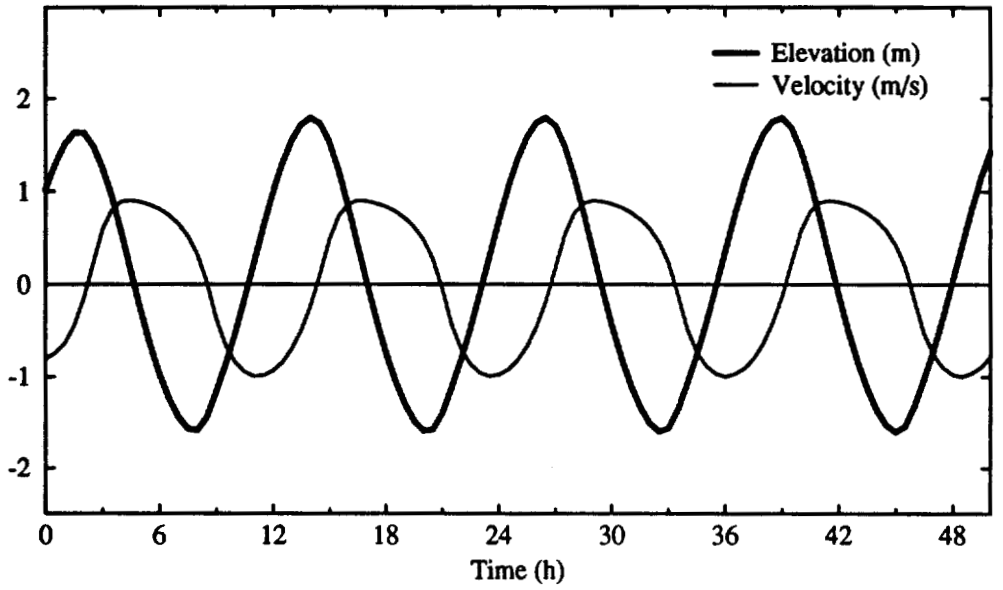

Fig. 7. Time series of "refined" elevations and velocities at the middle of the channel (fully non-linear case).

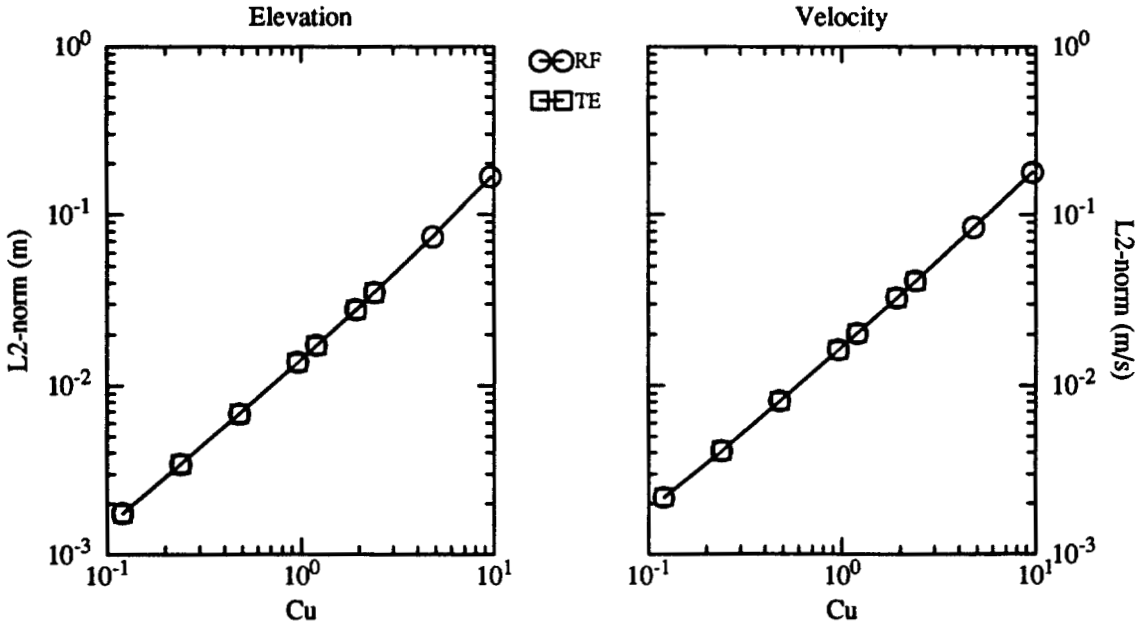

Fig. 8. Linear case + finite amplitude. L_2-norms as function of the Courant number.

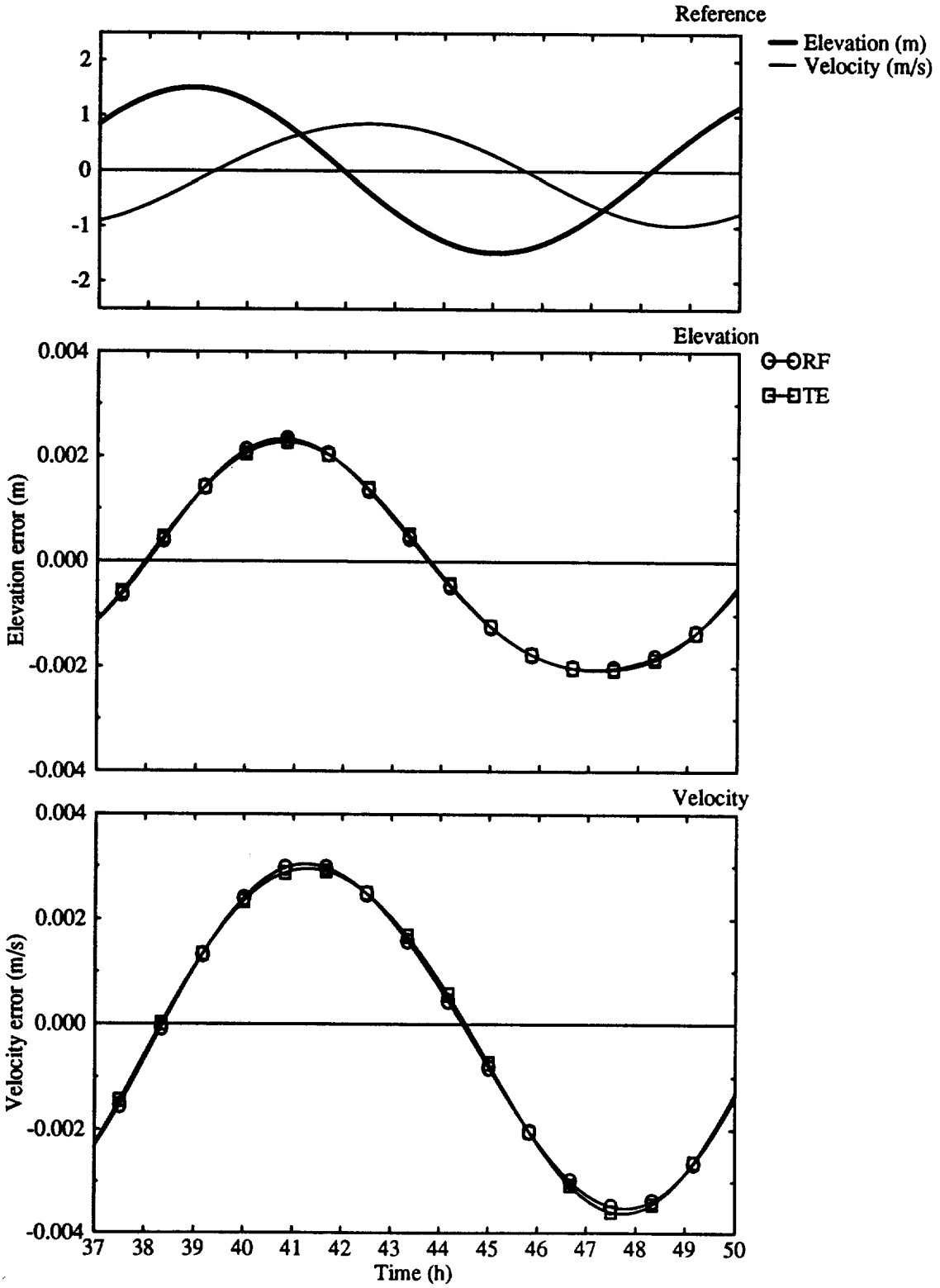

Fig. 9. Linear case + finite amplitude. Time series of errors in elevation and velocity. Cu=0.12.

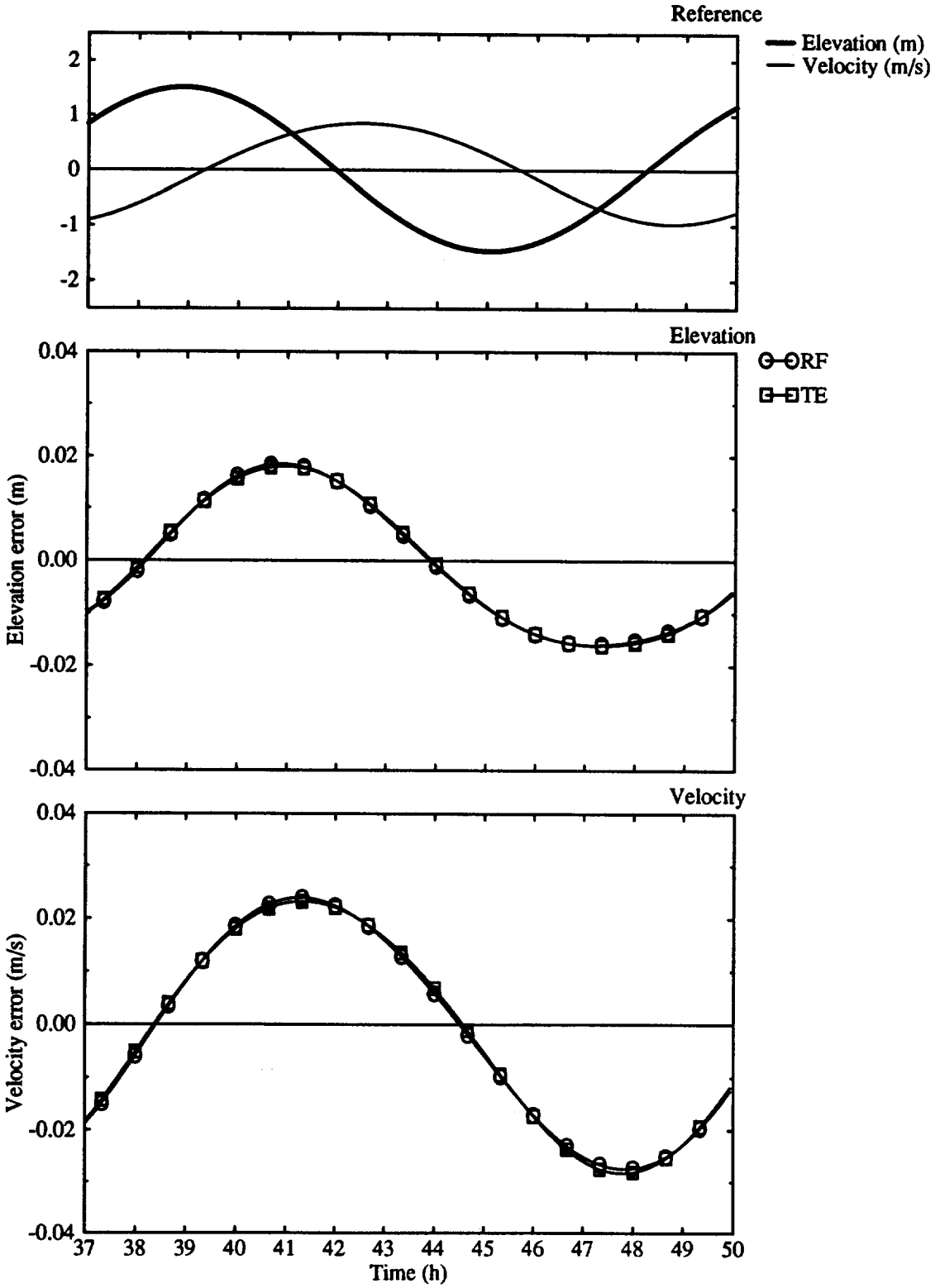

Fig. 10. Linear case + finite amplitude. Time series of errors in elevation and velocity. Cu=0.96.

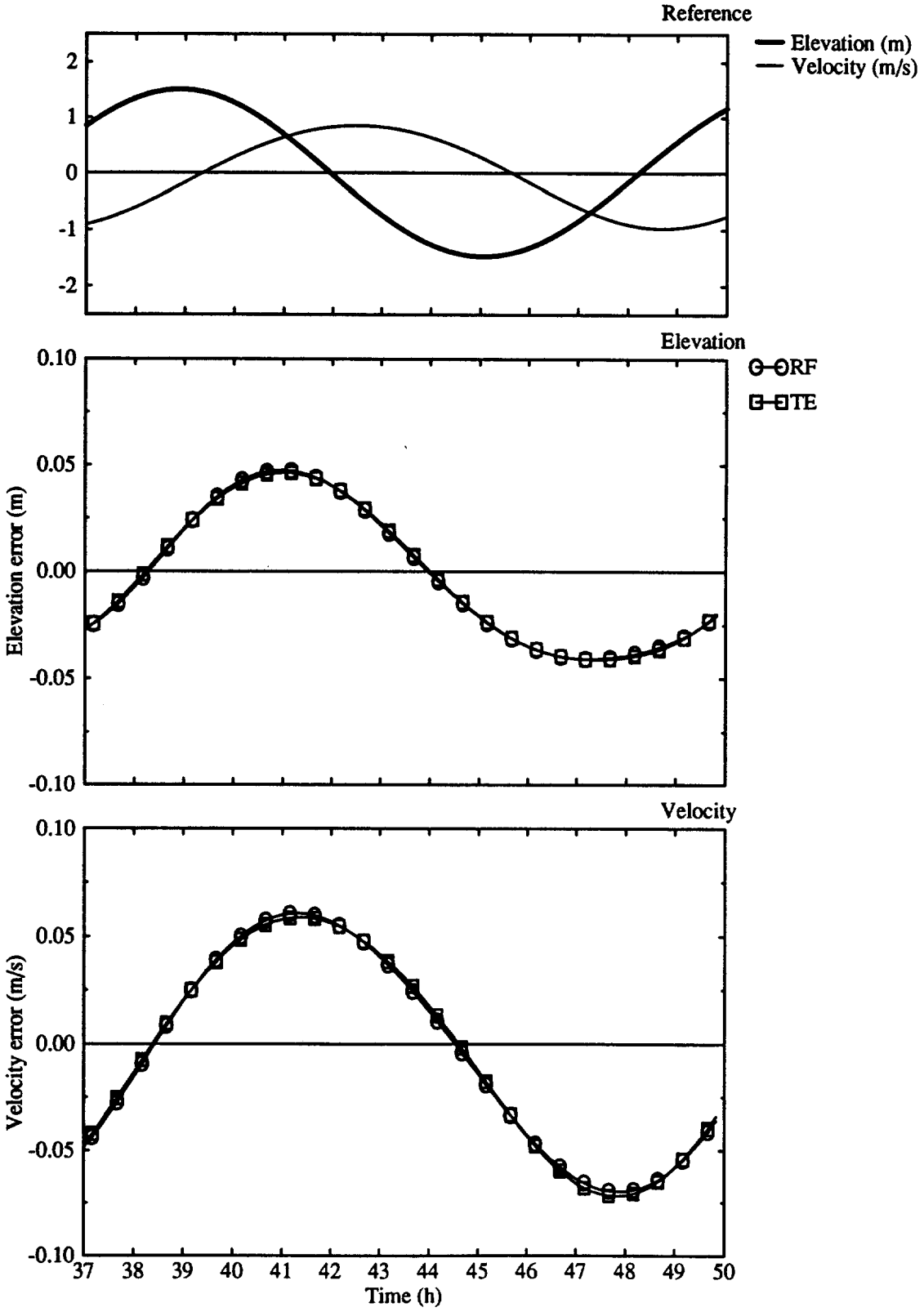

Fig. 11. Linear case + finite amplitude. Time series of errors in elevation and velocity. Cu=2.4.

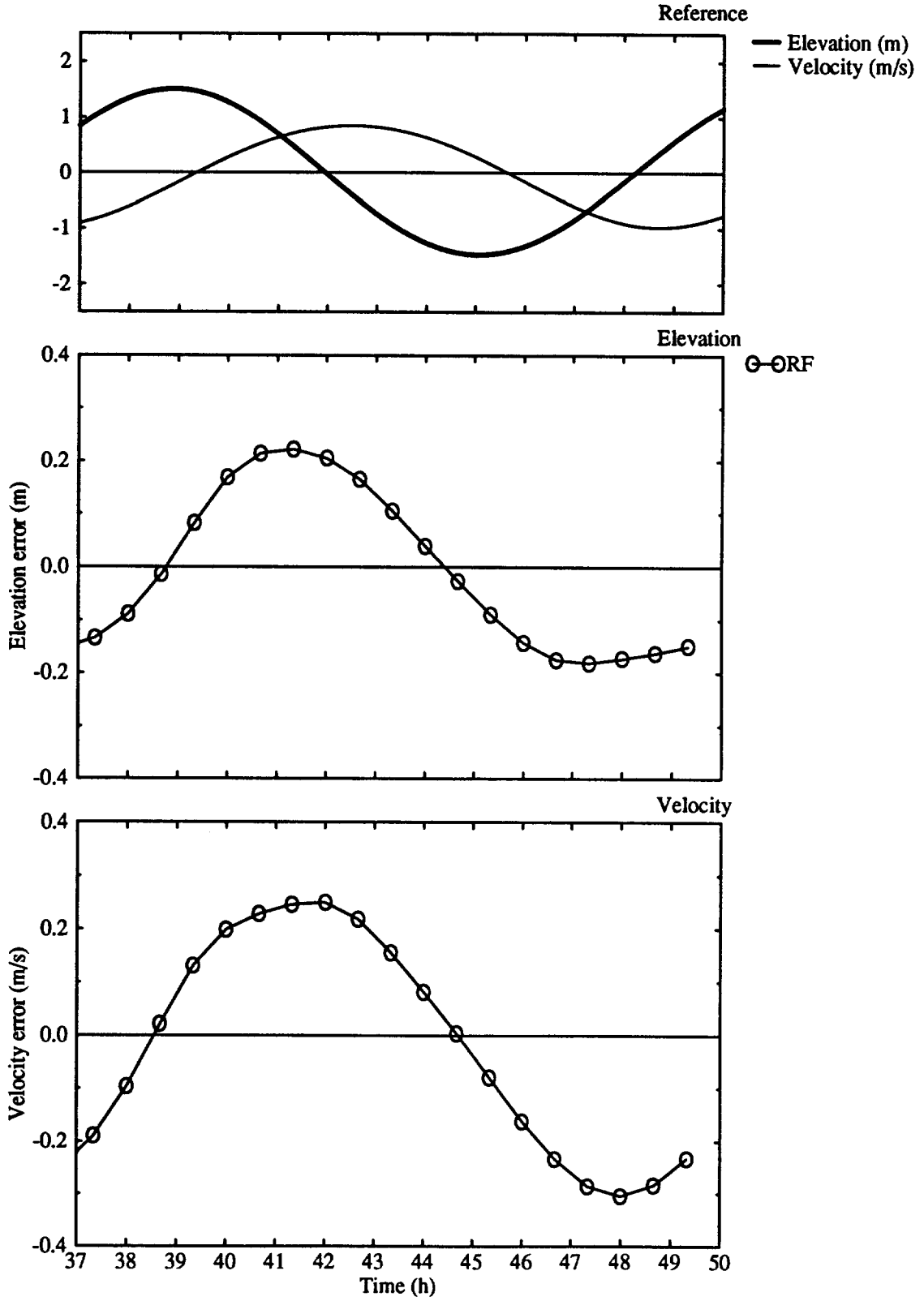

Fig. 12. Linear case + finite amplitude. Time series of errors in elevation and velocity. Cu=9.6.

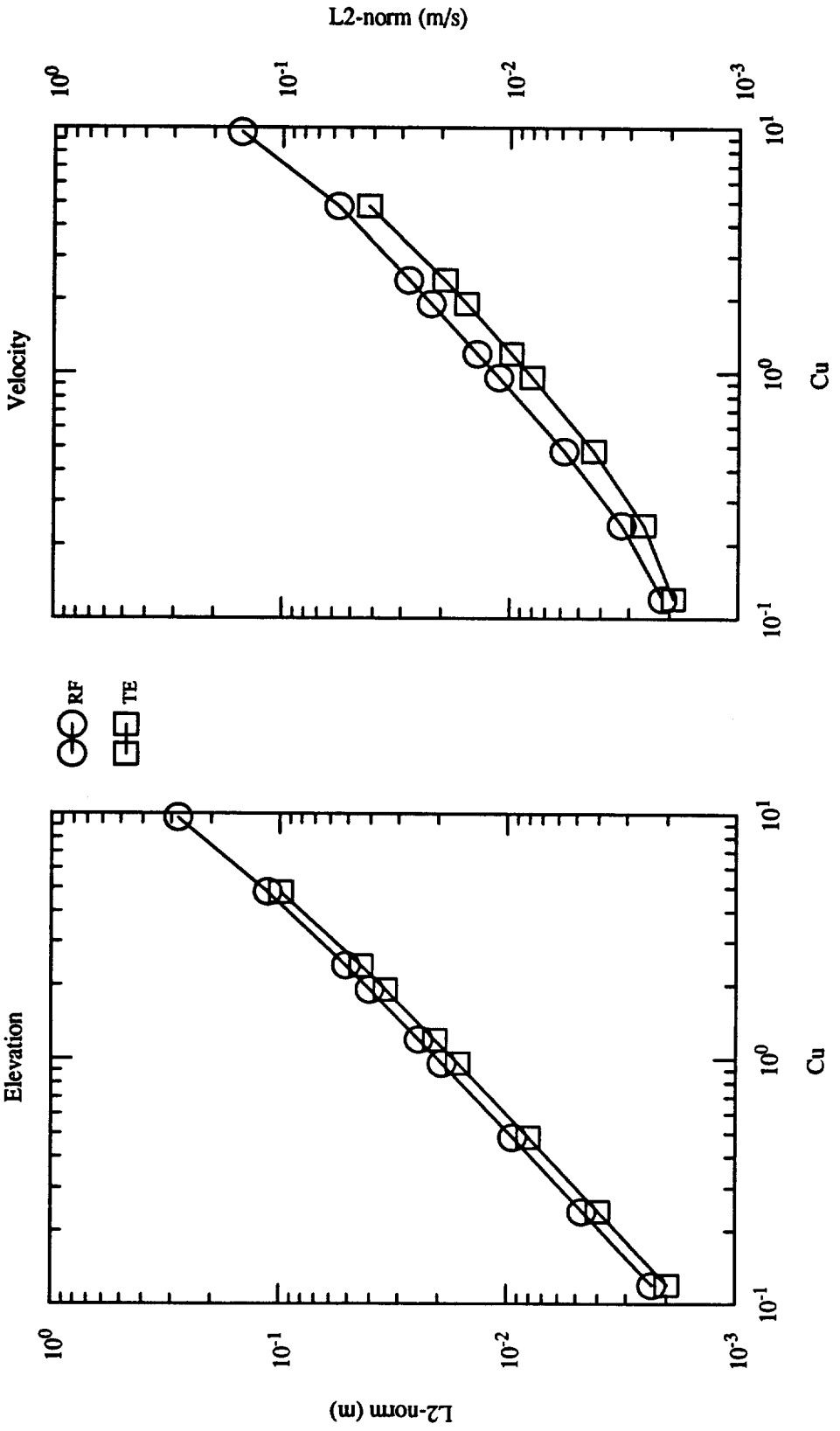

Fig. 13. Linear case + non-linear friction. L_2-norms as function of Cu.

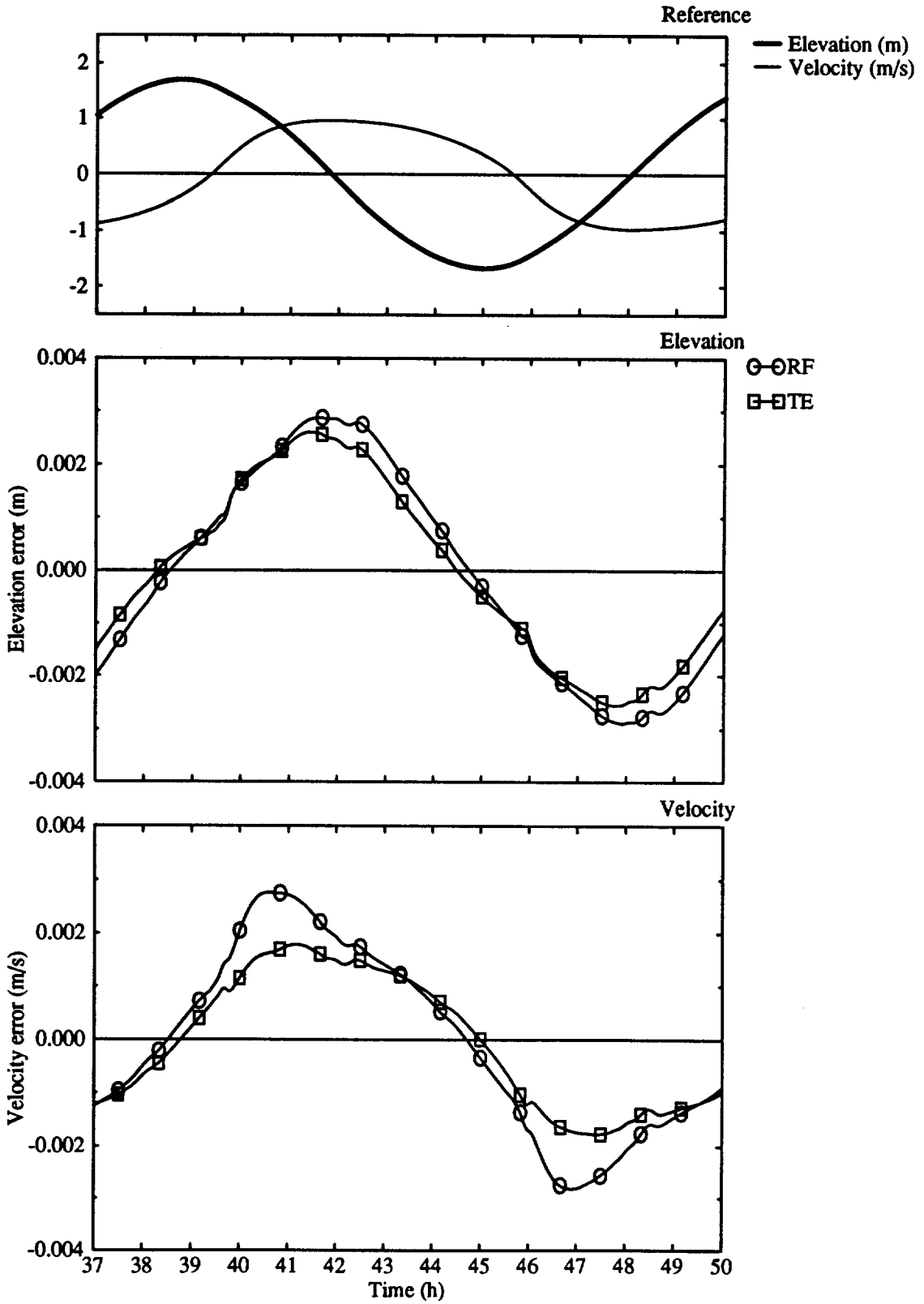

Fig. 14. Linear case + non-linear friction. Time series of errors in elevation and velocity. Cu=0.12.

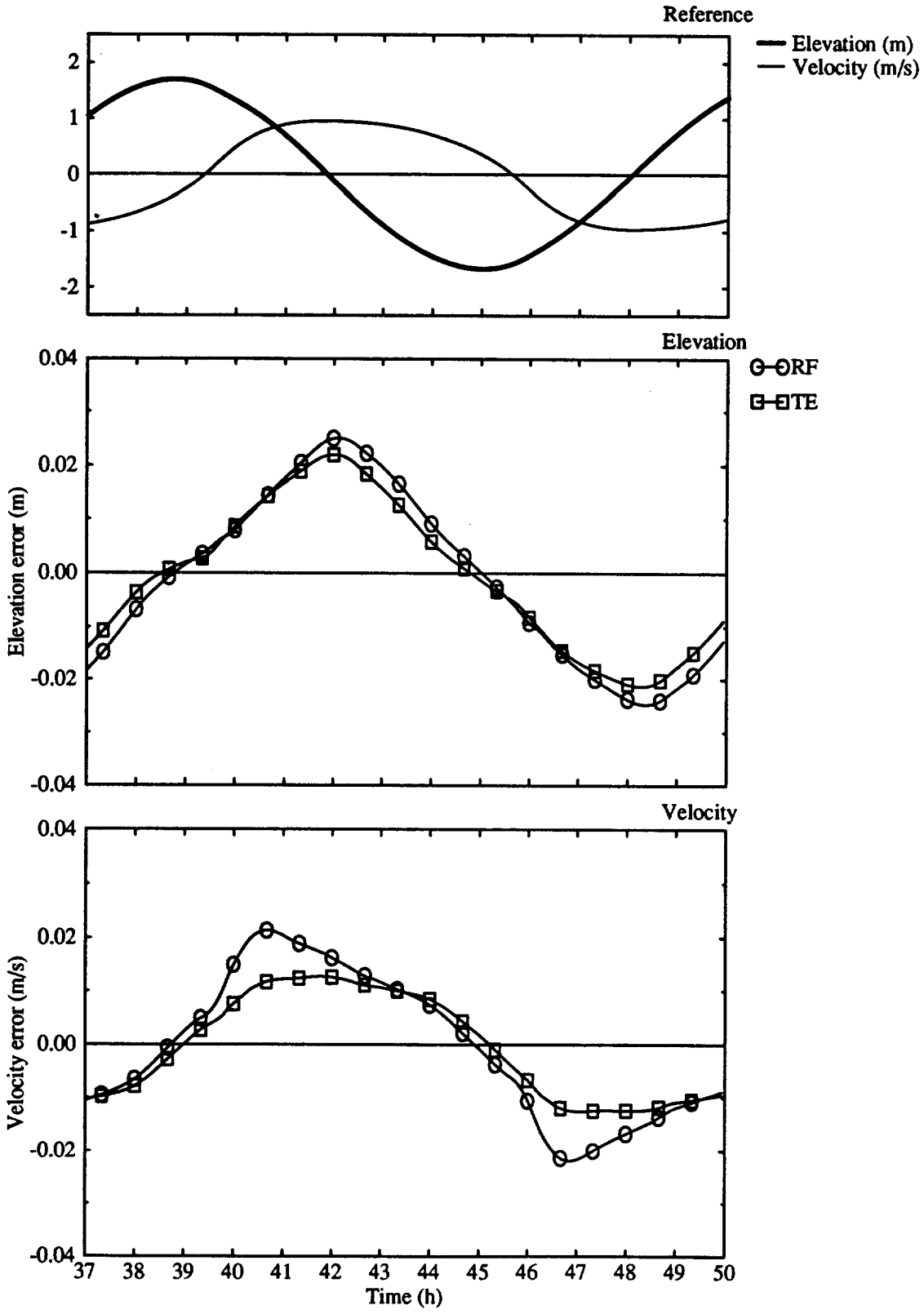

Fig. 15. Linear case + non-linear friction. Time series of errors in elevation and velocity. Cu=0.96.

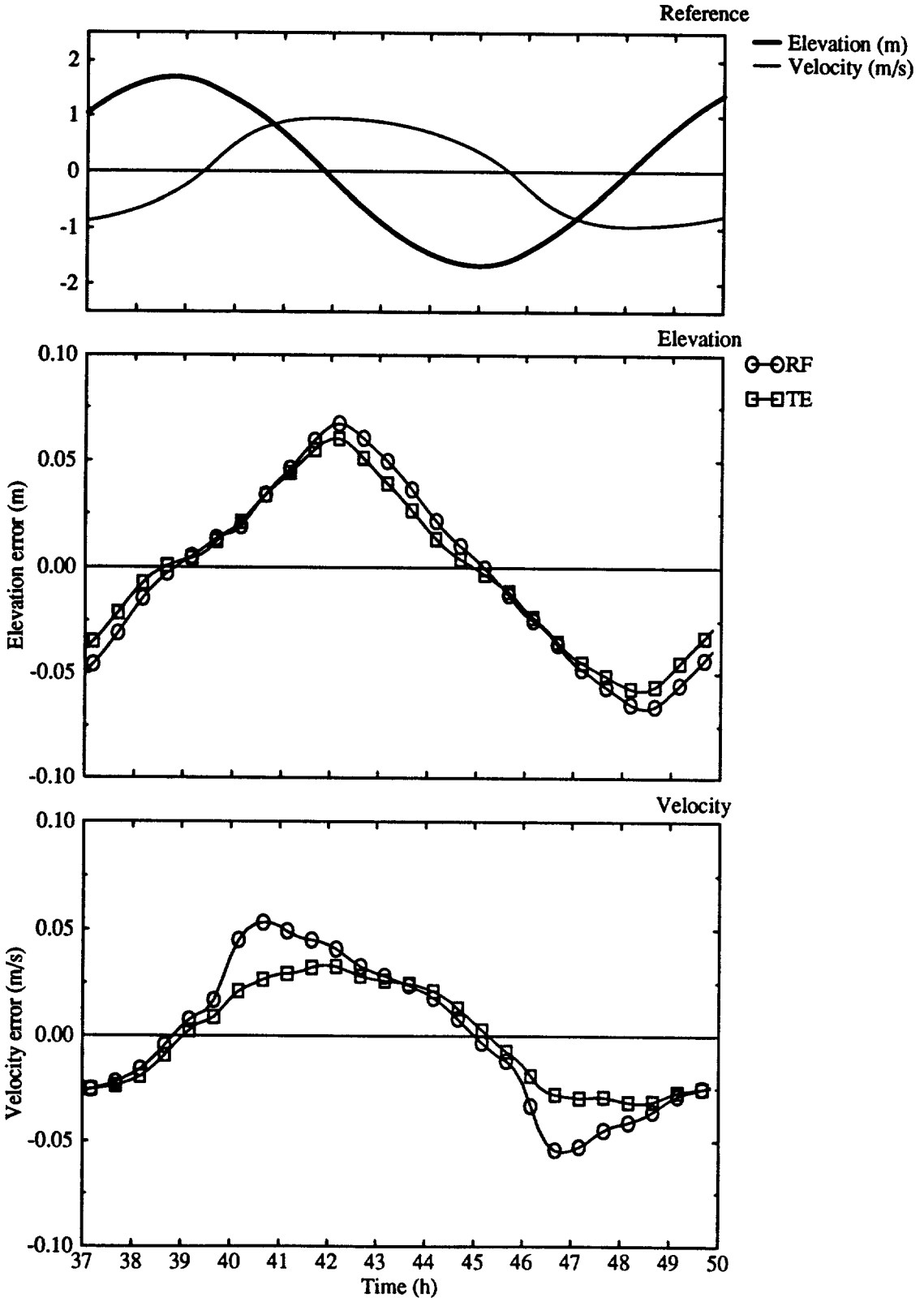

Fig. 16. Linear case + non-linear friction. Time series of errors in elevation and velocity. Cu=2.4.

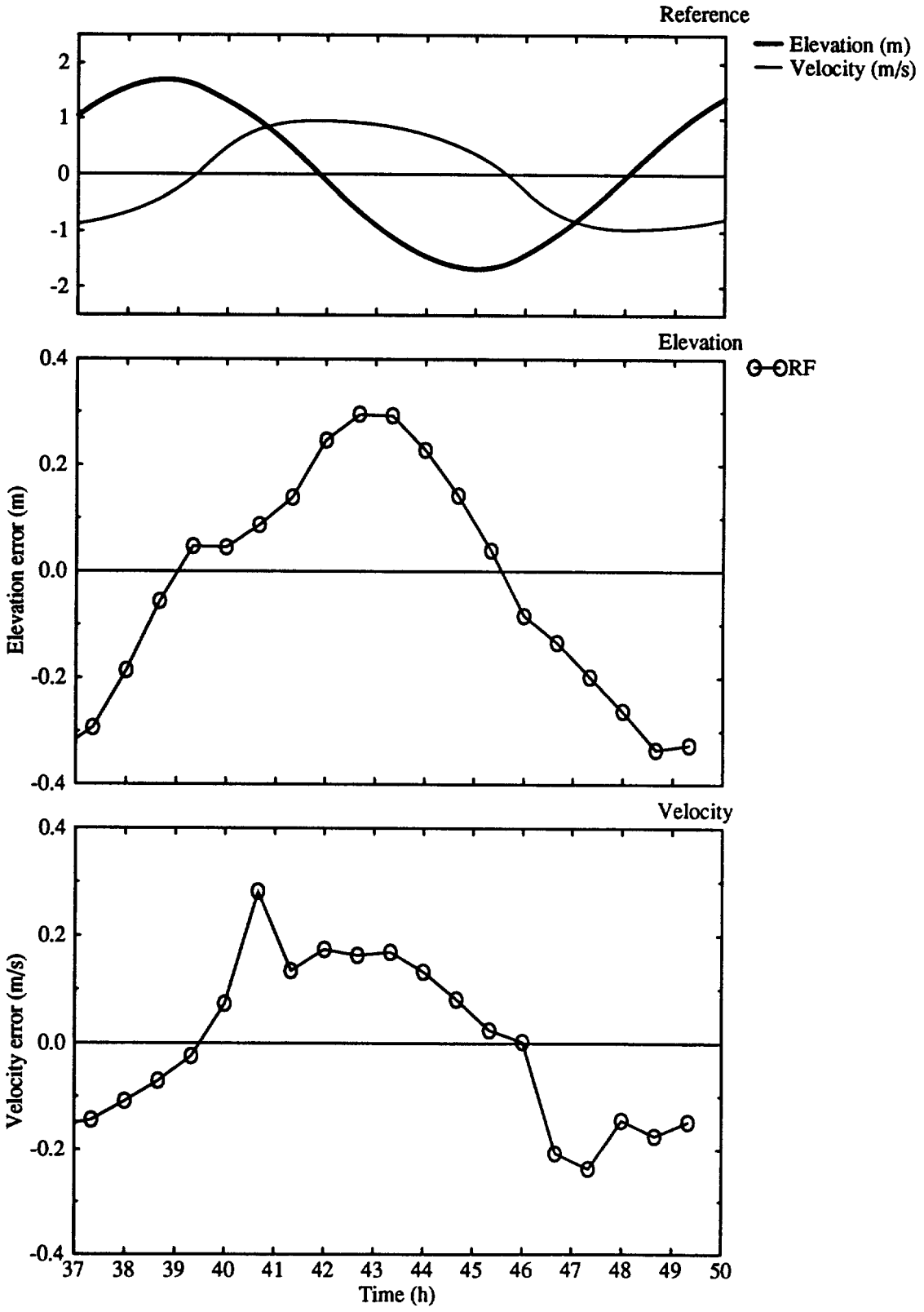

Fig. 17. Linear case + non-linear friction. Time series of errors in elevation and velocity. Cu=9.6.

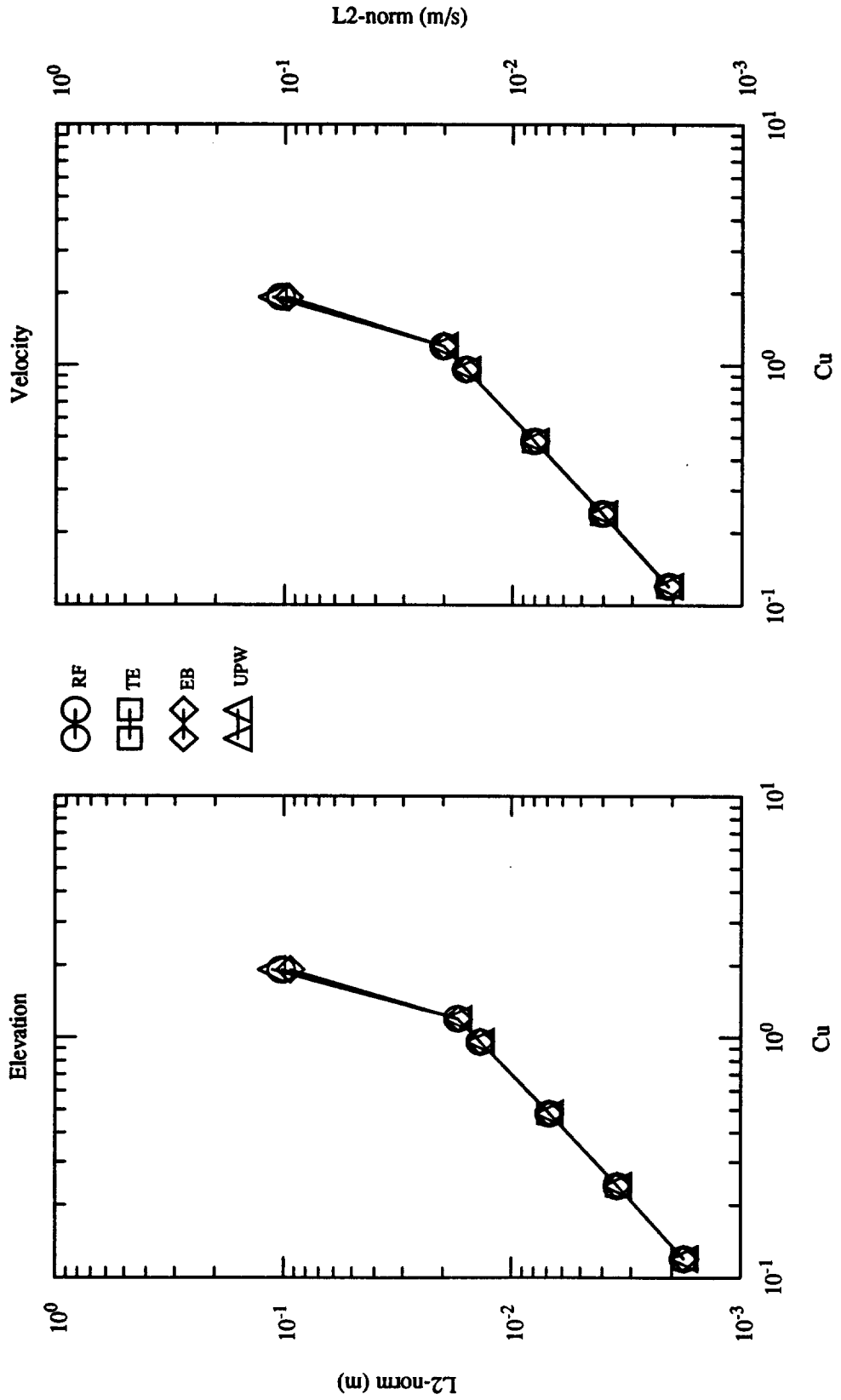

Fig. 18. Linear case + advection. L_2-norms as function of Cu.

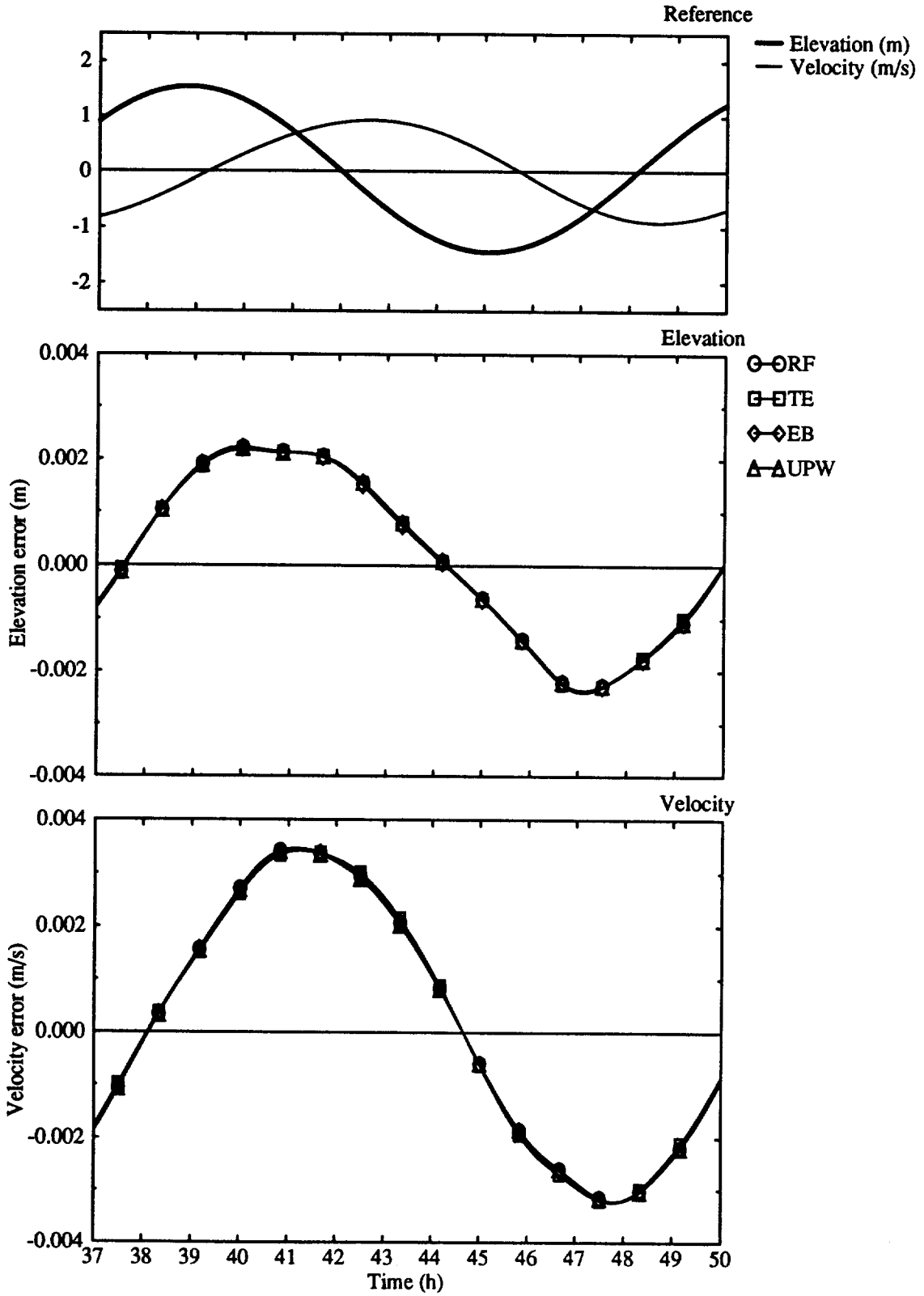

Fig. 19. Linear case + advection. Time series of errors in elevation and velocity. Cu=0.12.

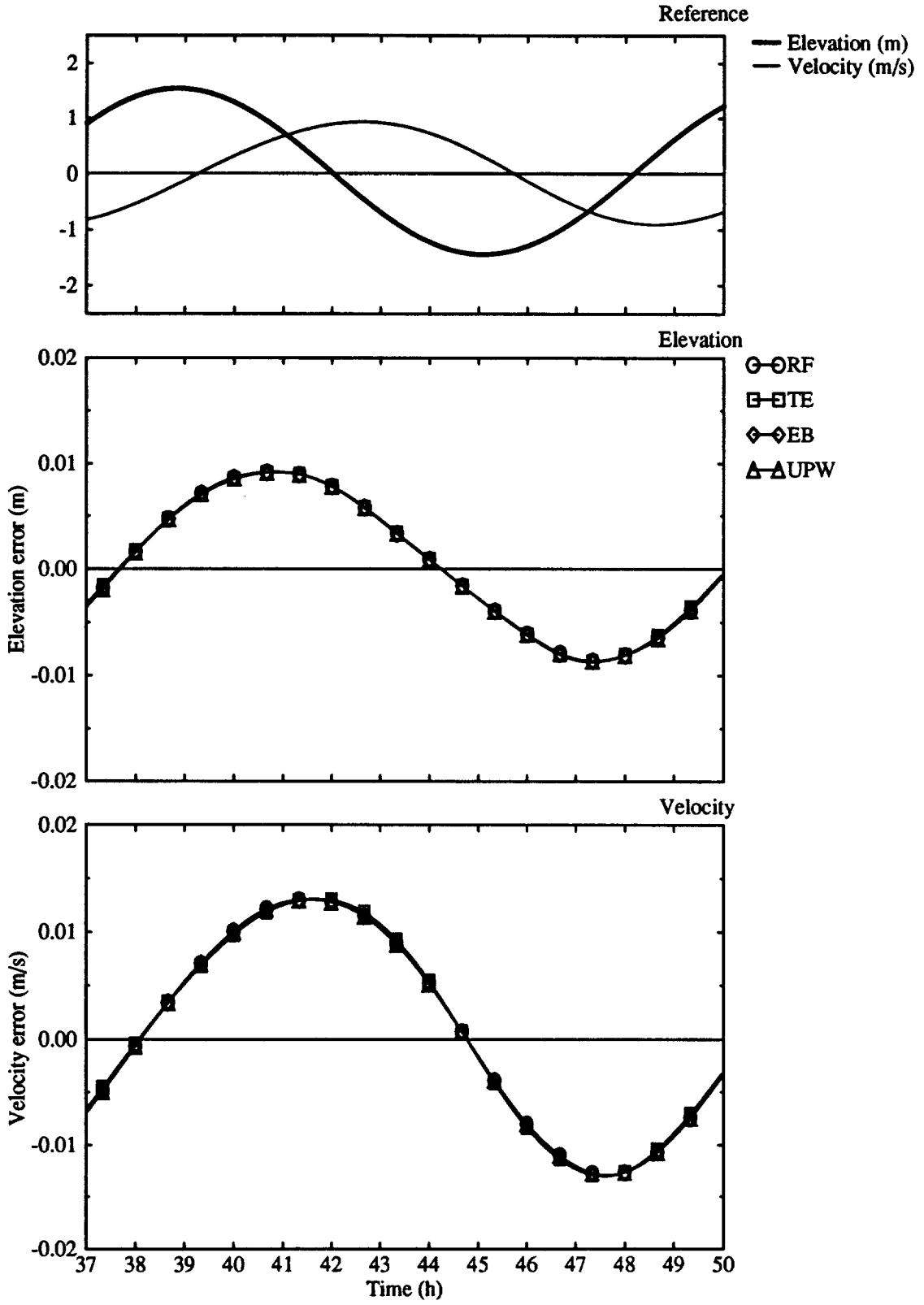

Fig. 20. Linear case + advection. Time series of errors in elevation and velocity. Cu=0.48.

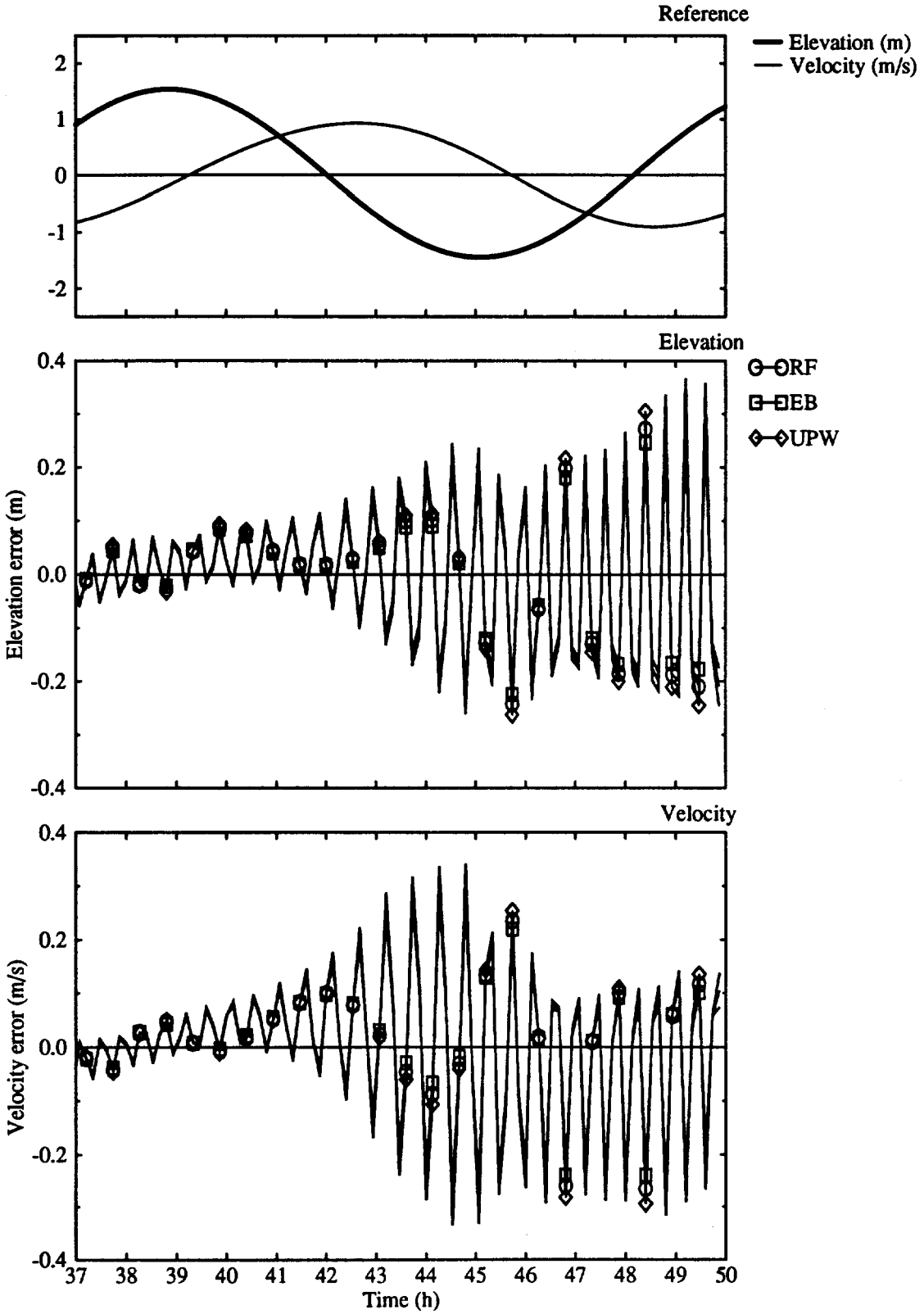

Fig. 21. Linear case + advection. Time series of errors in elevation and velocity. Cu=1.92.

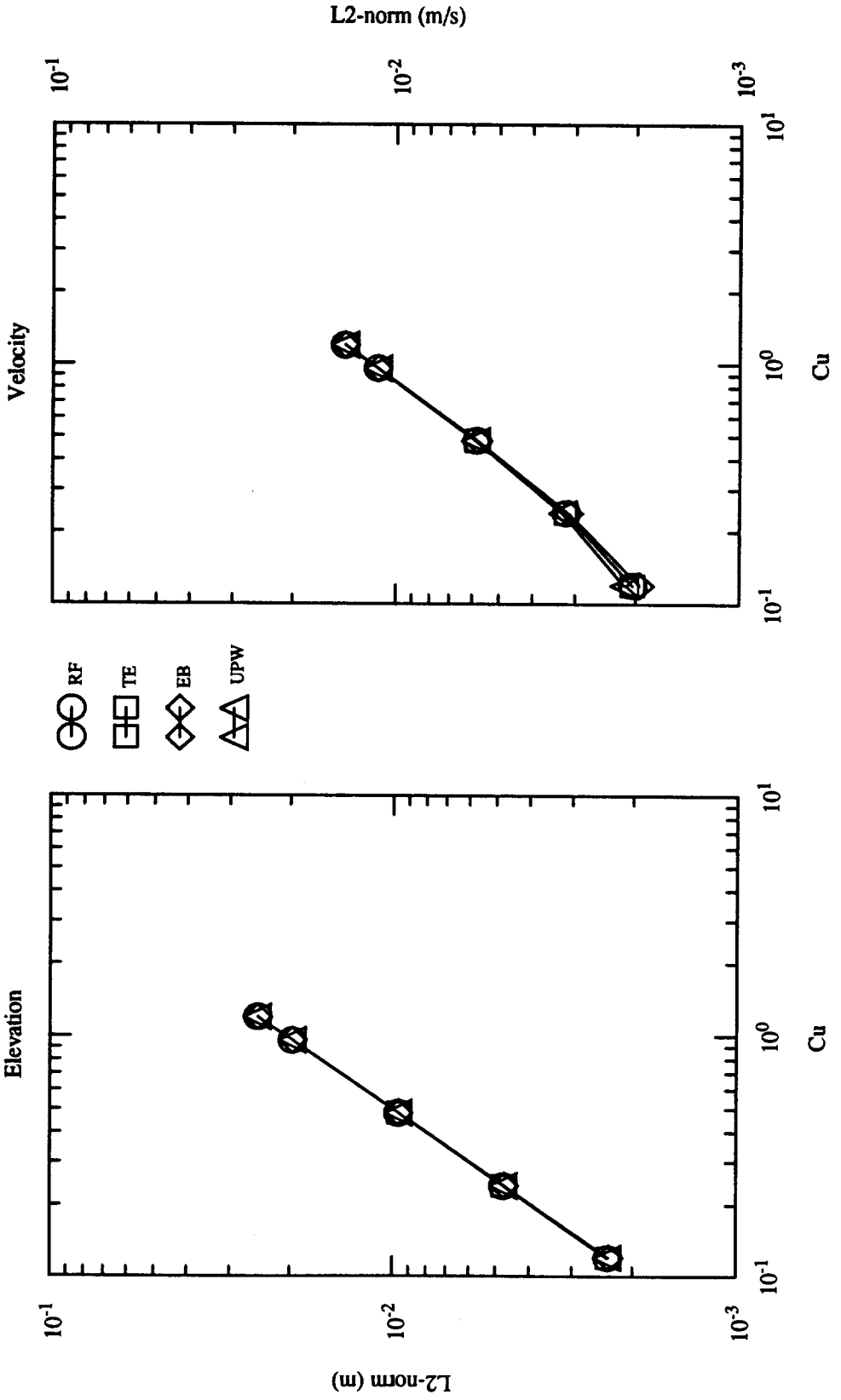

Fig. 22. Fully non-linear case. L_2-norms as function of Cu.

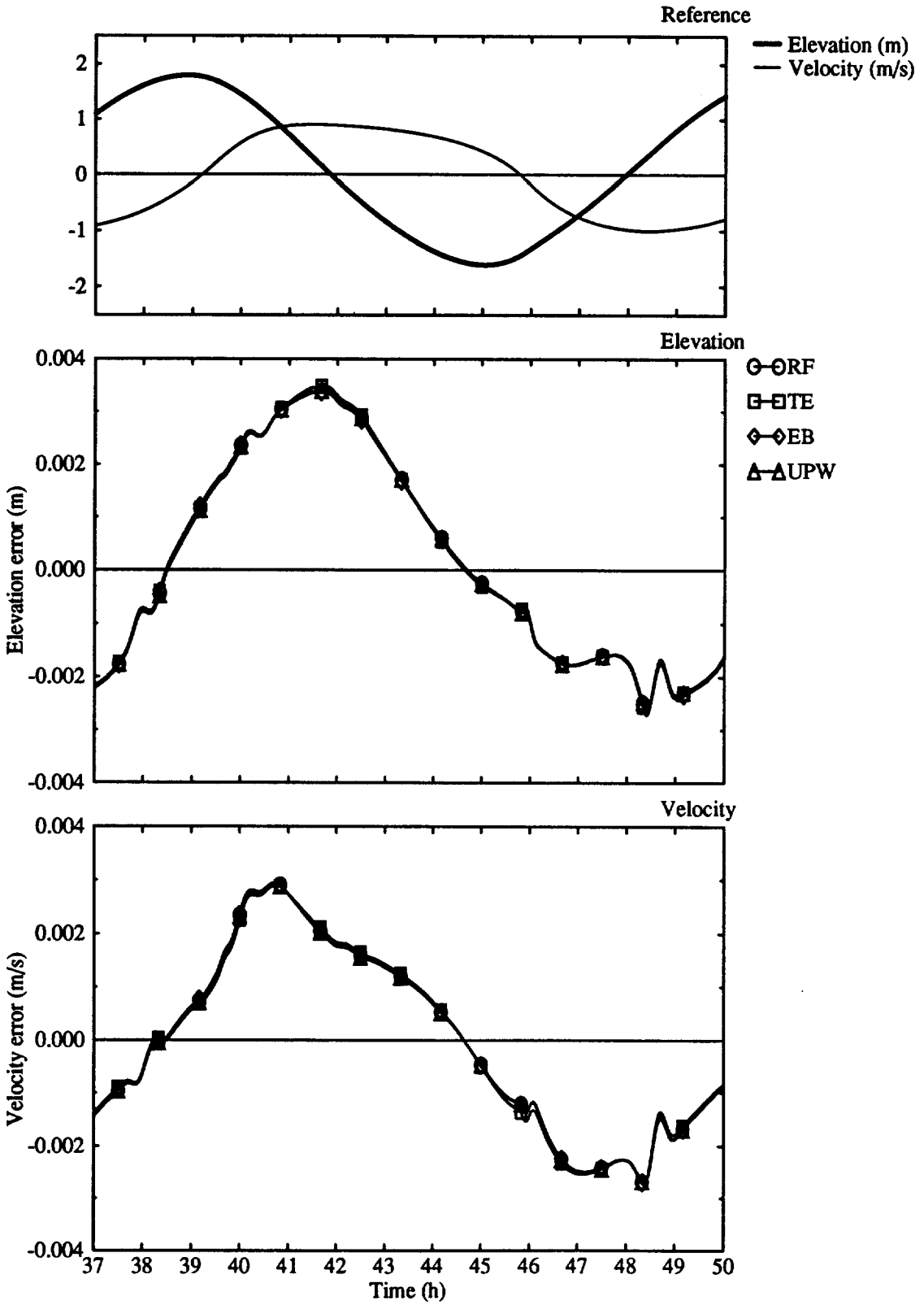

Fig. 23. Fully non-linear case. Time series of errors in elevation and velocity. Cu=0.12.

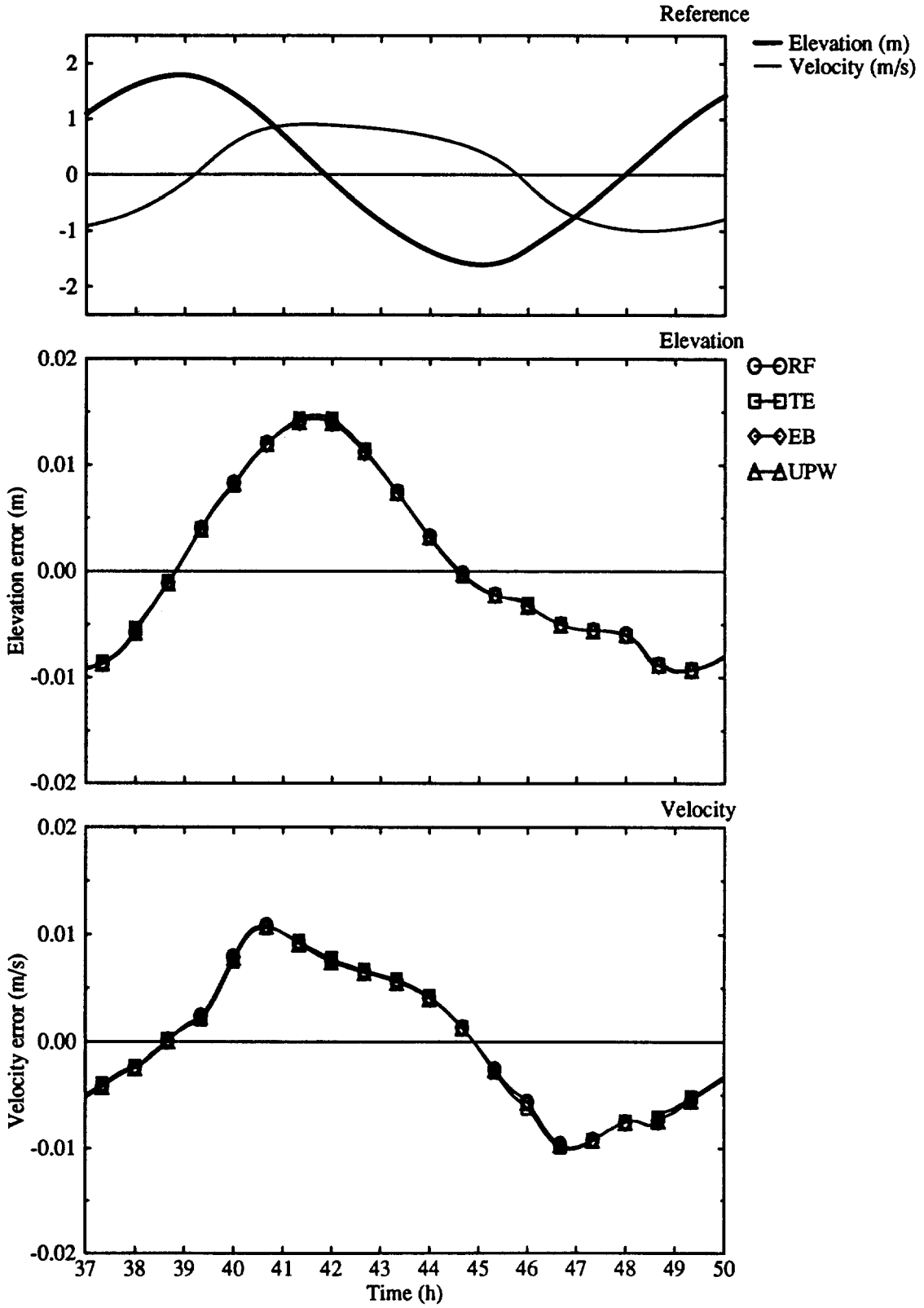

Fig. 24. Fully non-linear case. Time series of errors in elevation and velocity. Cu=0.48.

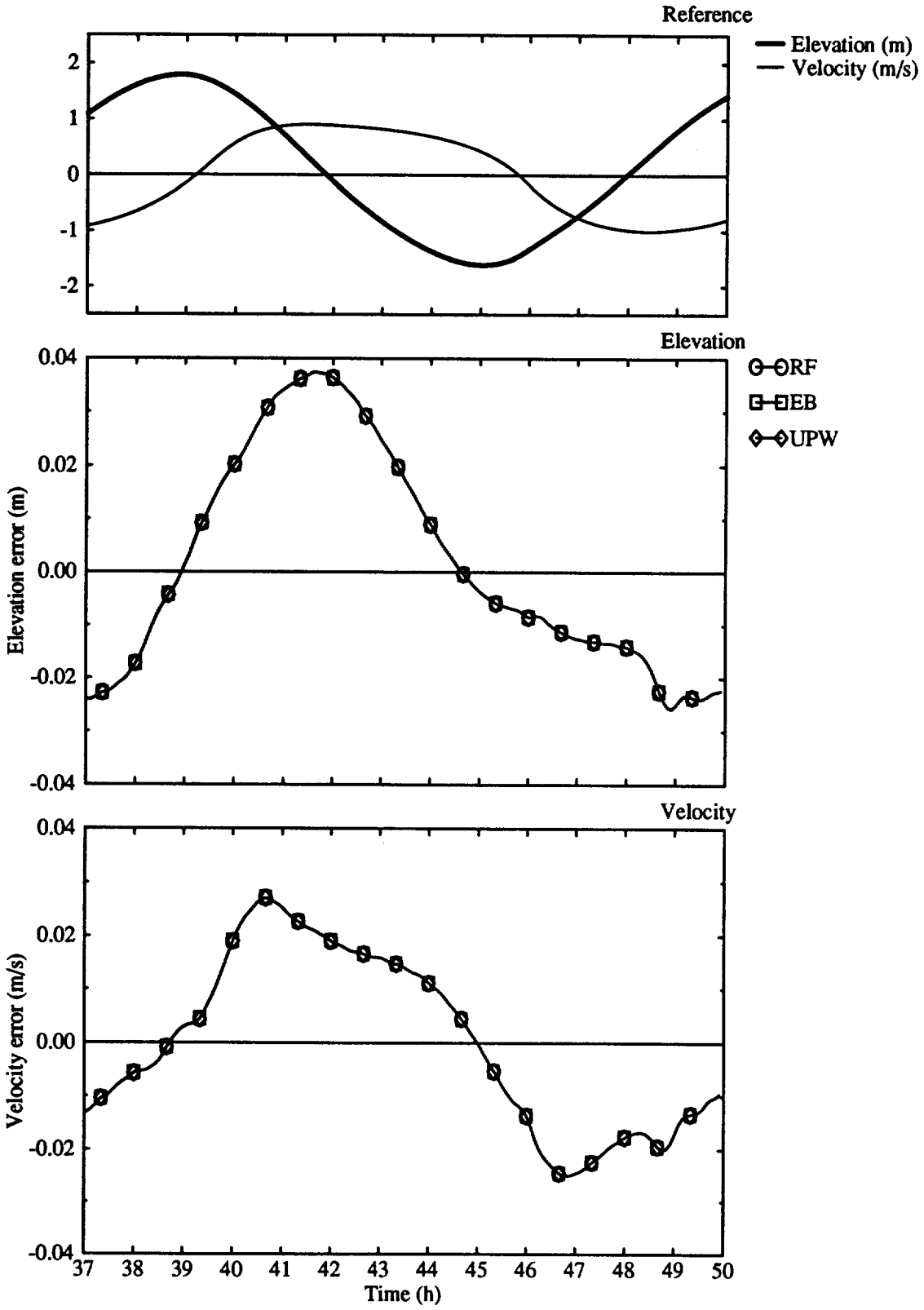

Fig. 25. Fully non-linear case. Time series of errors in elevation and velocity. Cu=1.2.

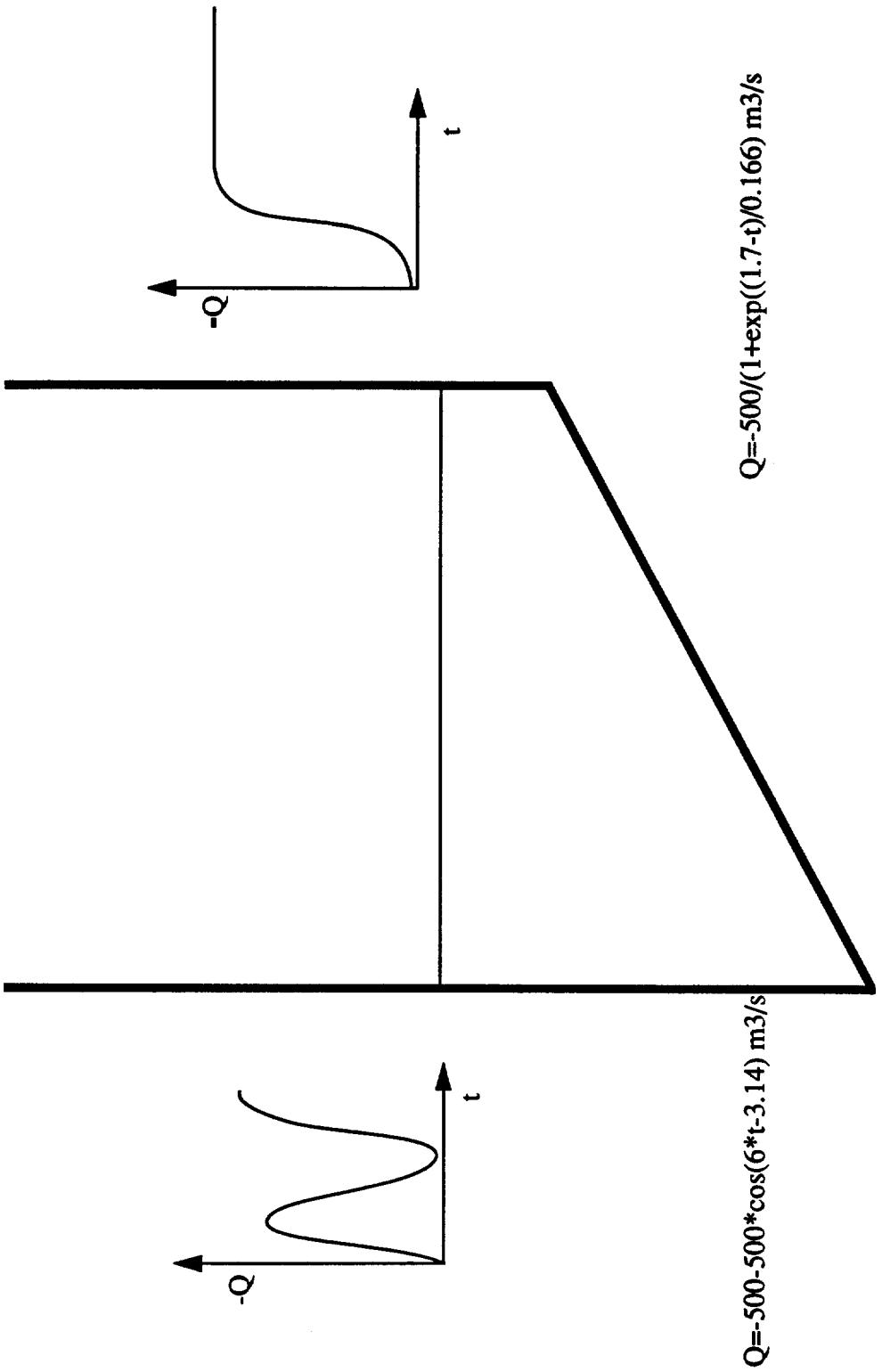

Fig. 26. Test case for mass conservation.

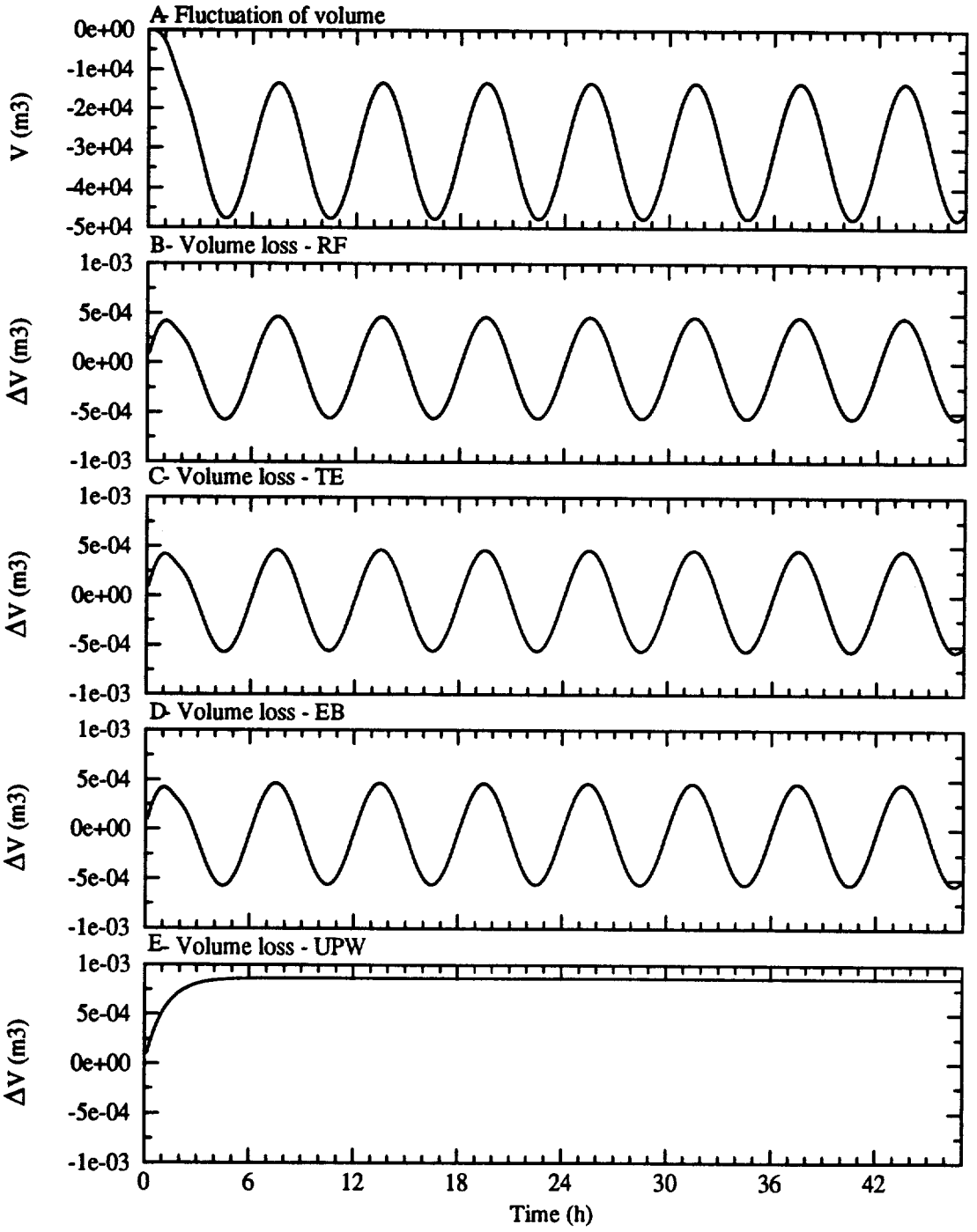

Fig. 27. Volume loss for the four main numerical methods.

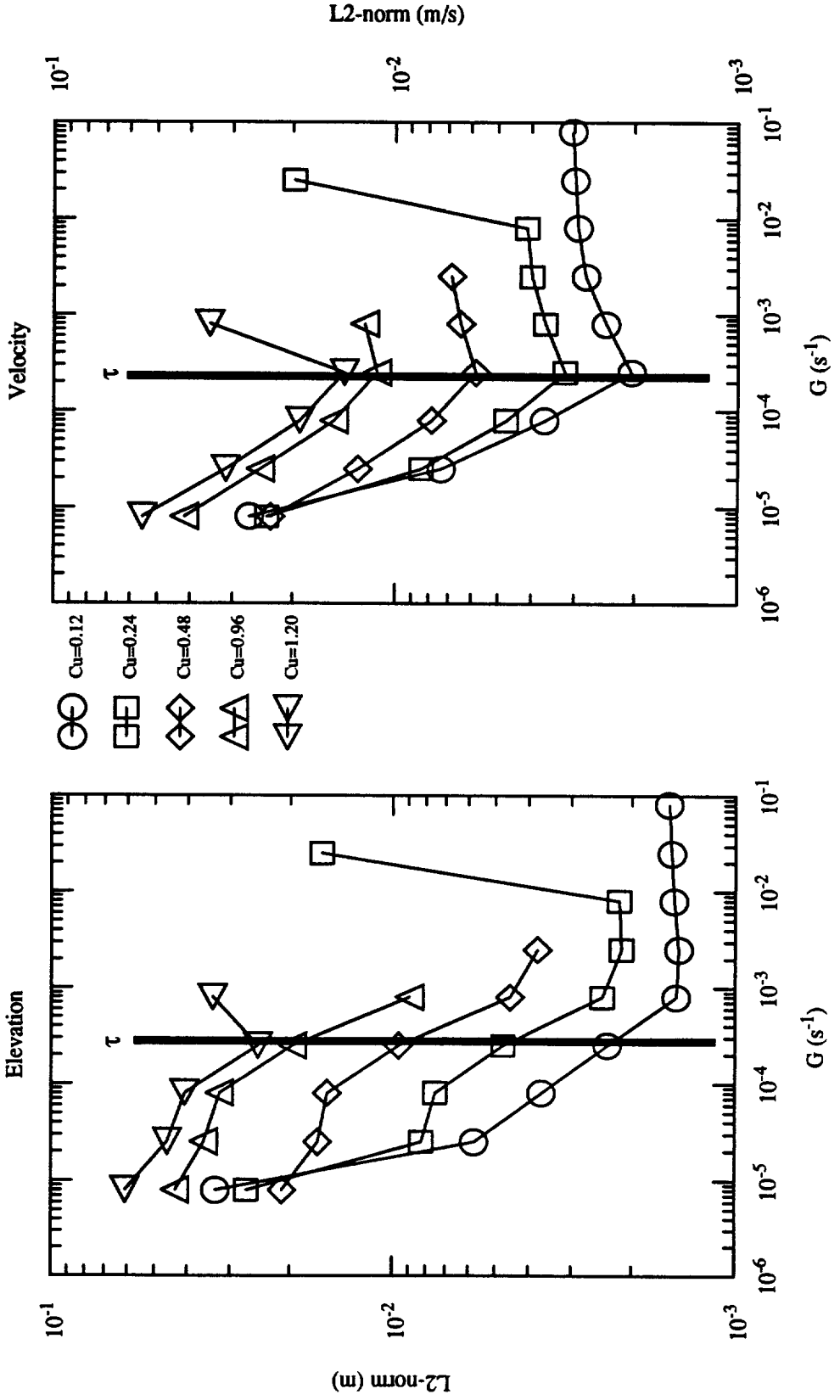

Fig. 28. L2-norms for elevation and velocity, versus the value of G, for a set of average Courant numbers.

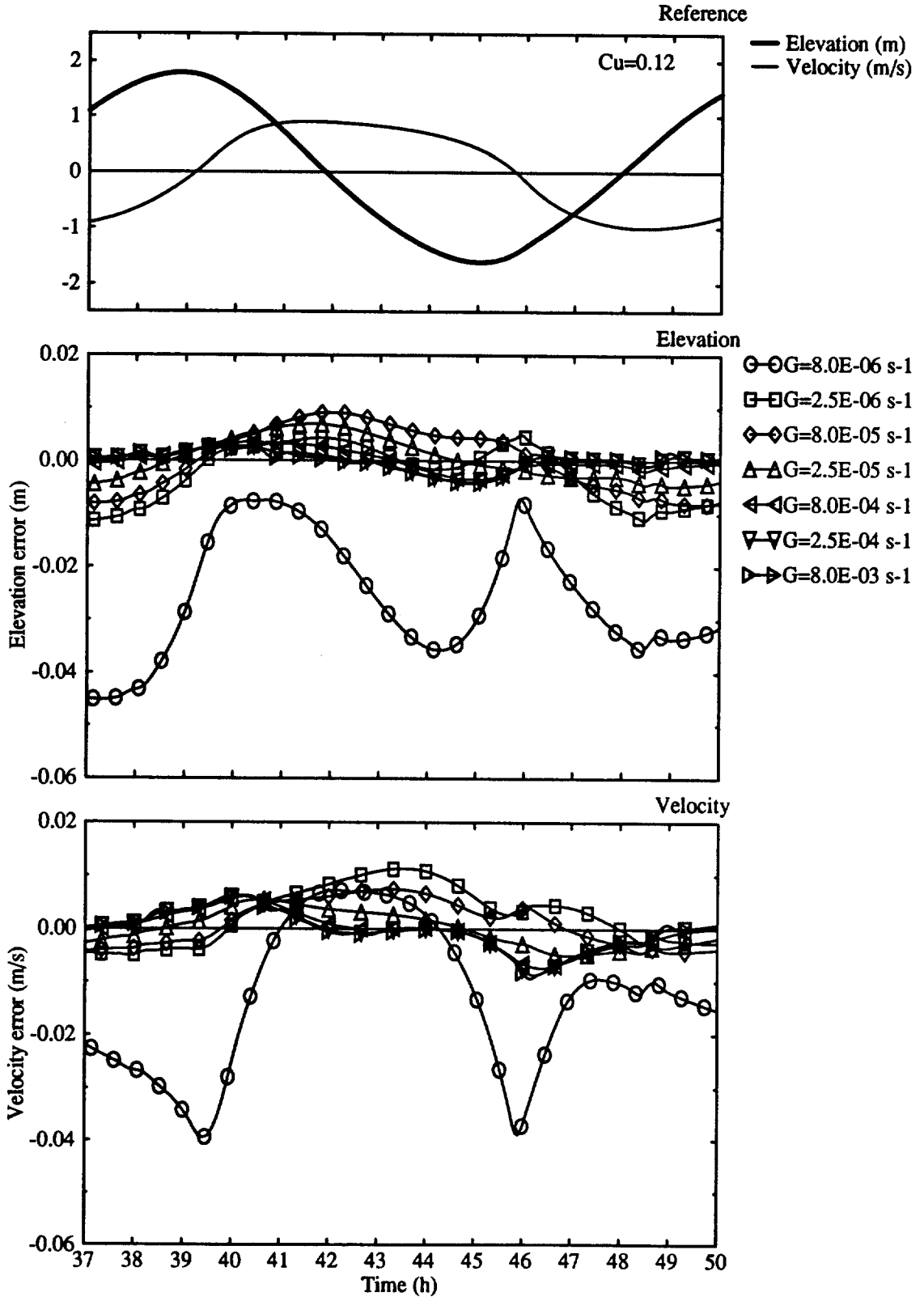

Fig. 29. Time series of errors in elevation and velocity, for a set of values of G.

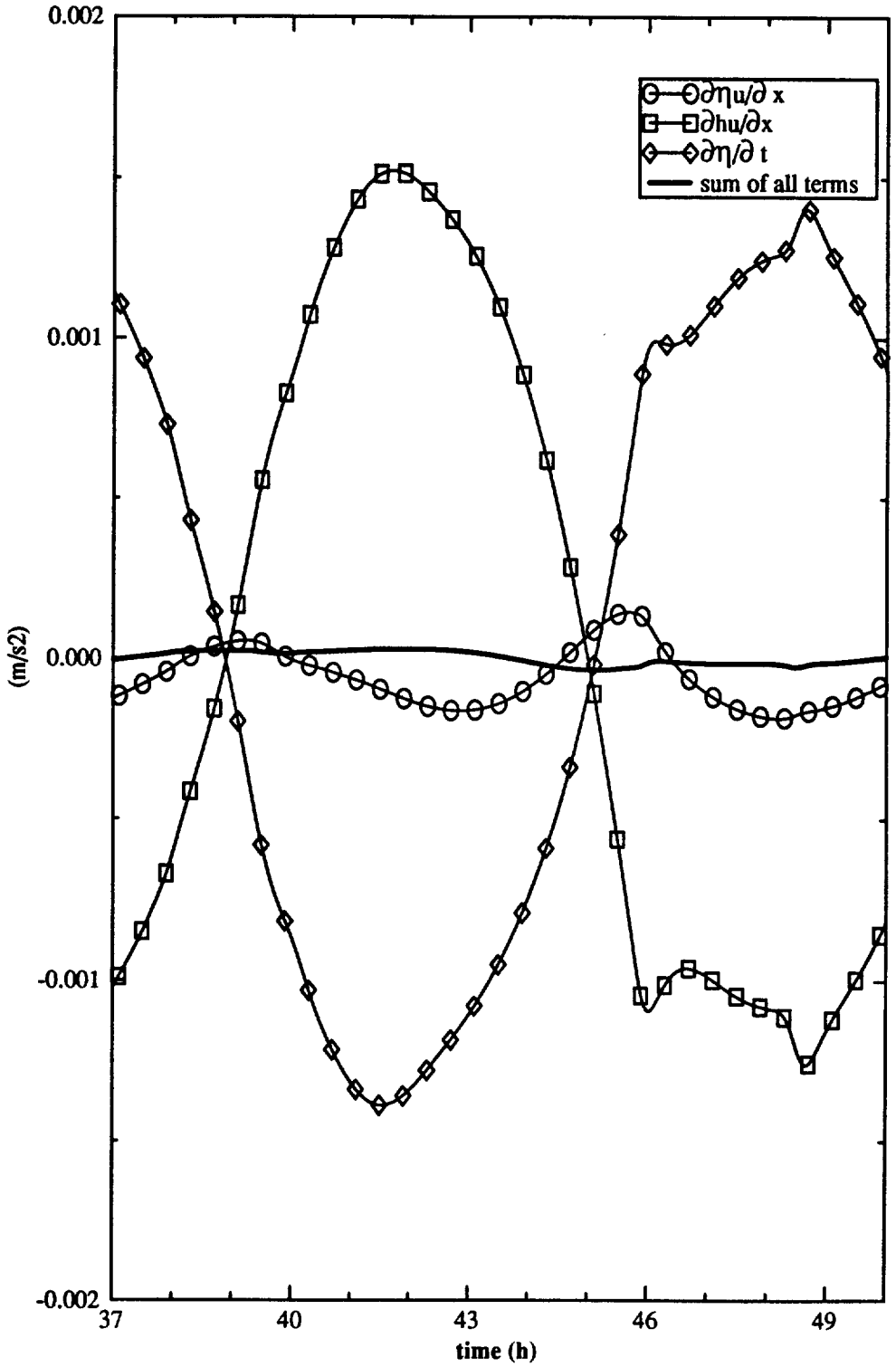

Fig. 30. Values of terms in the continuity equation, and error.

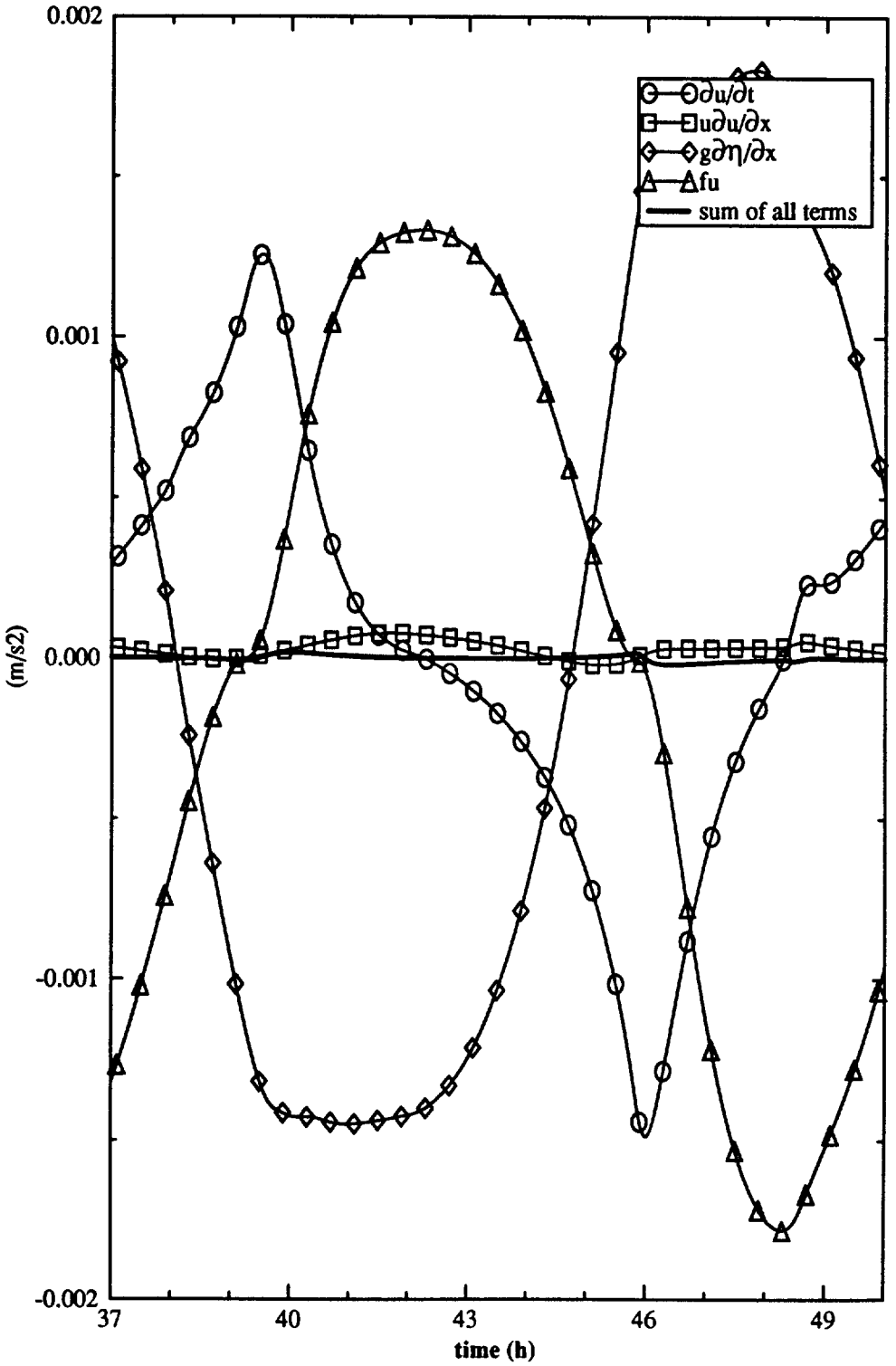

Fig. 31. Values of terms in the momentum equation, and error.

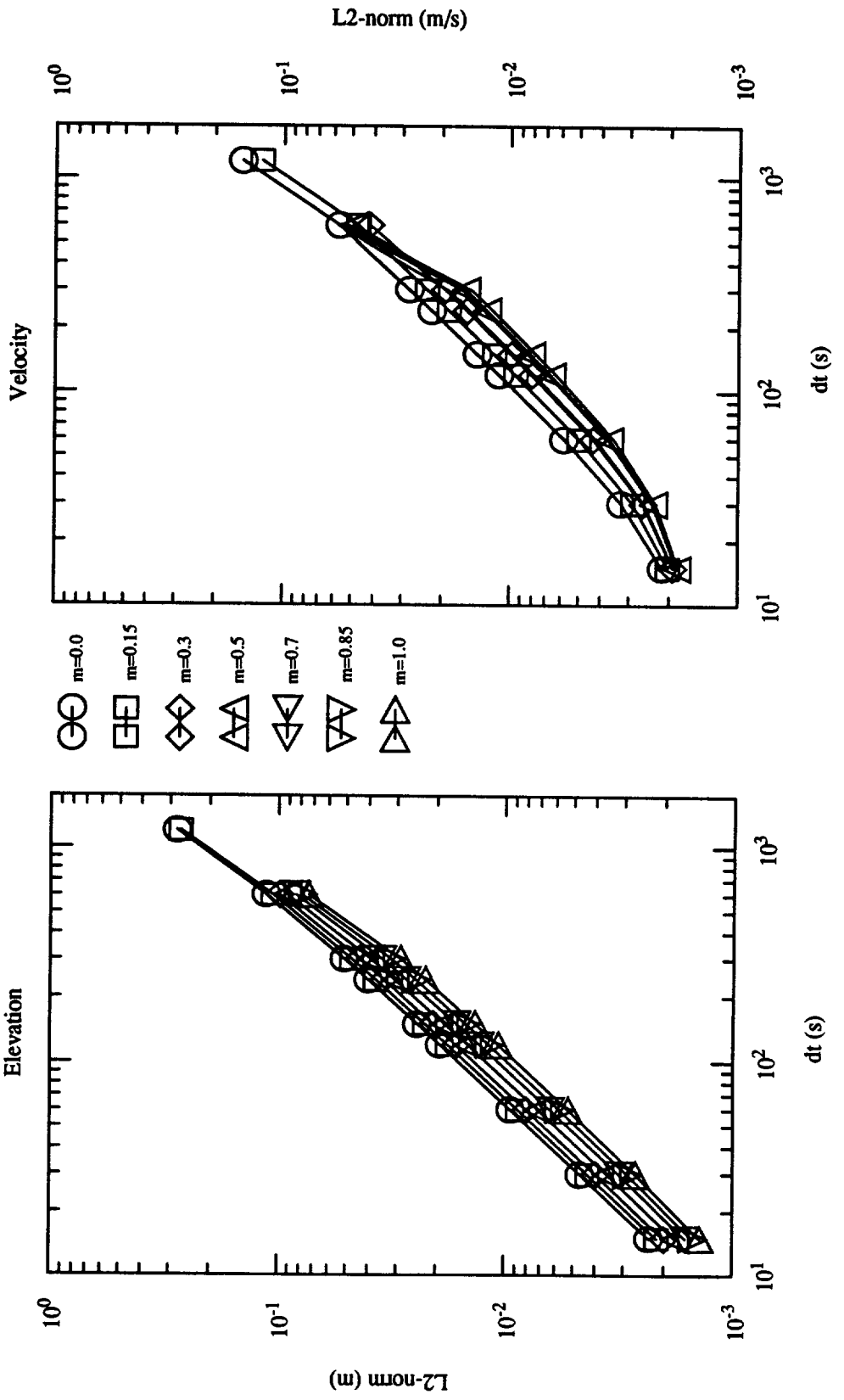

Fig. 32. Time extrapolation - error norms.

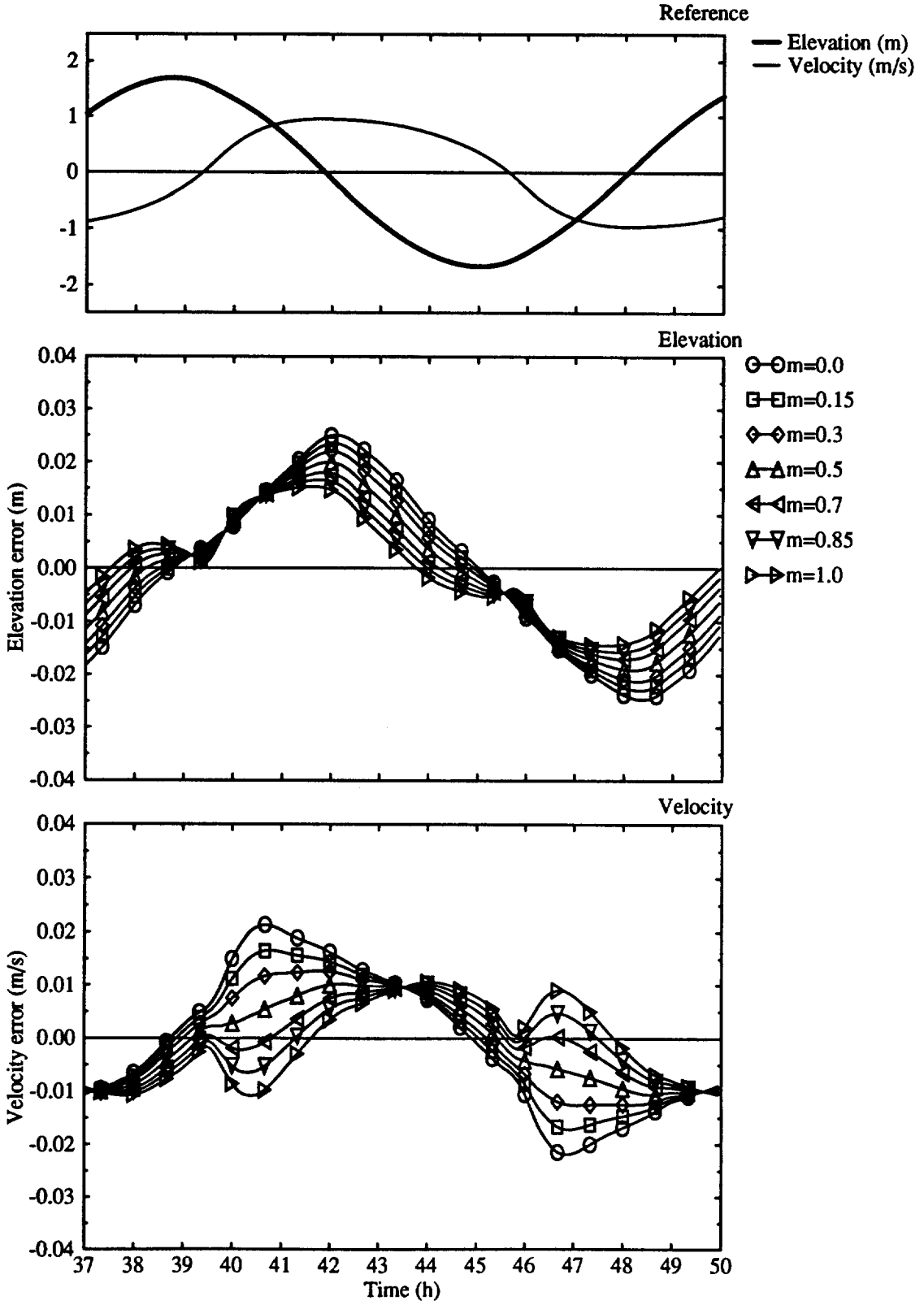

Fig. 33. Time extrapolation results: error noms as function of time for Cu=0.96.

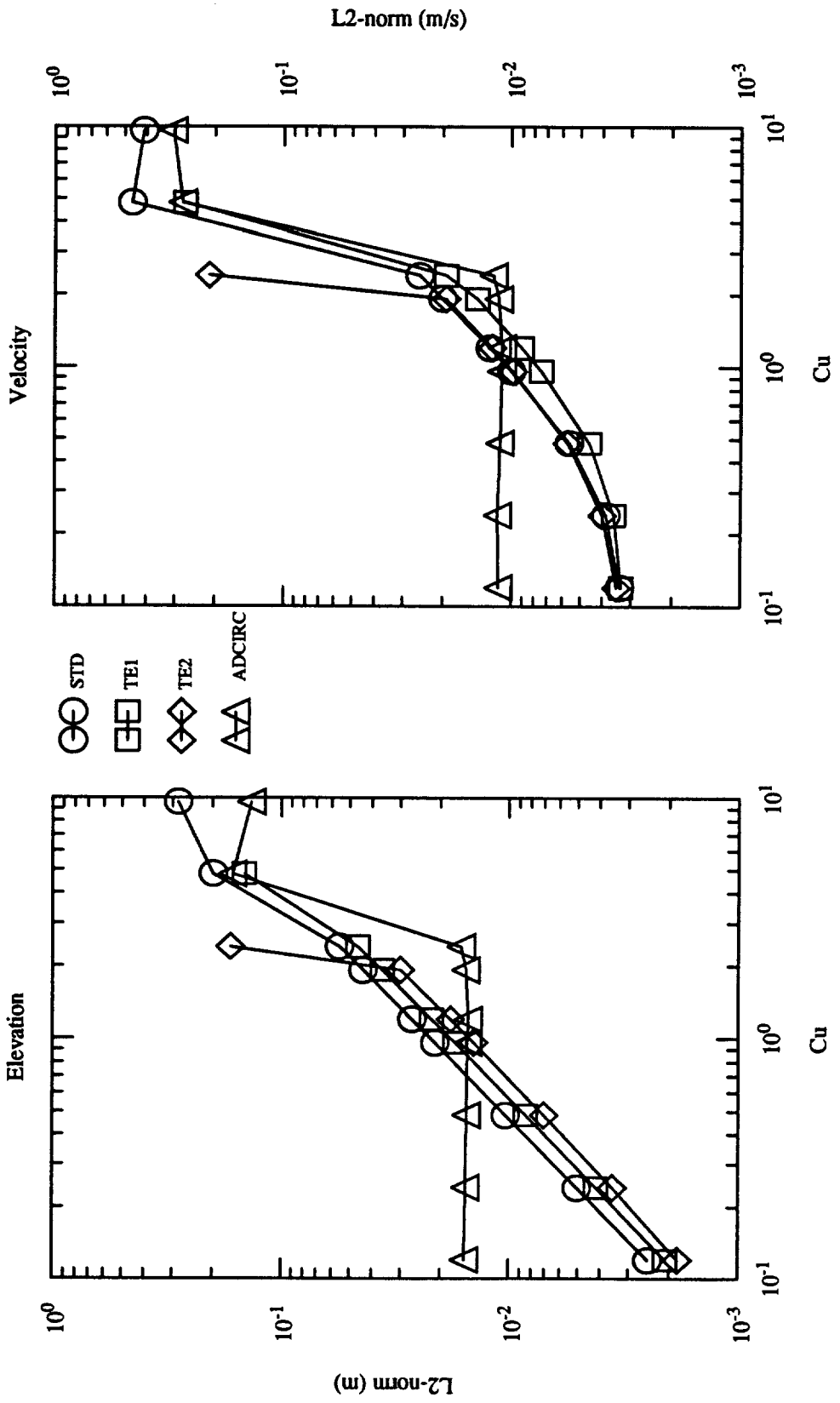

Fig. 34. L_2-norms as function of the Courant number. Comparison between RF, TE and a lumping method (ADCIRC).

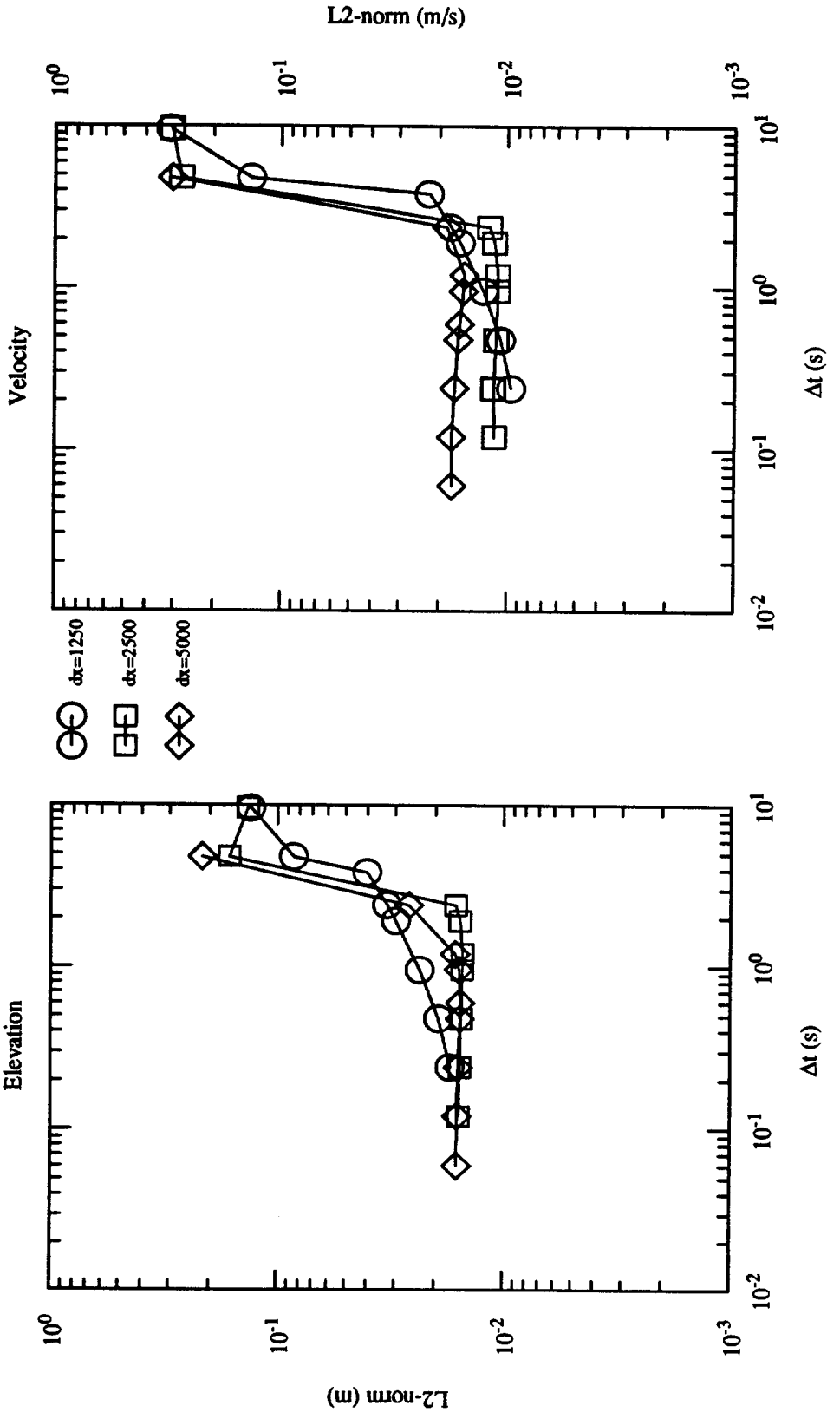

Fig. 35. ADCIRC - Error-norms as function of Δt for three different Δx.

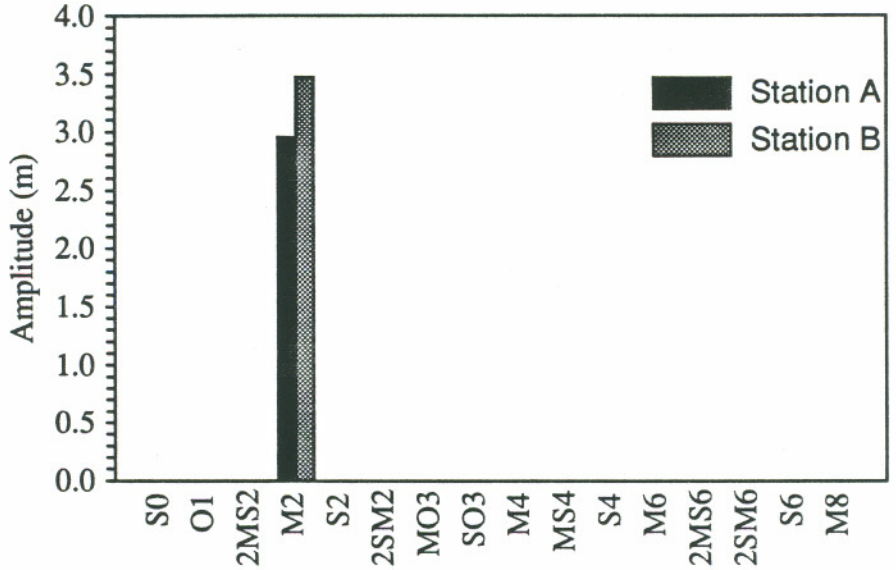

Fig. 36. Harmonic analysis results. Frictionless linear case. M_2, flat bottom.

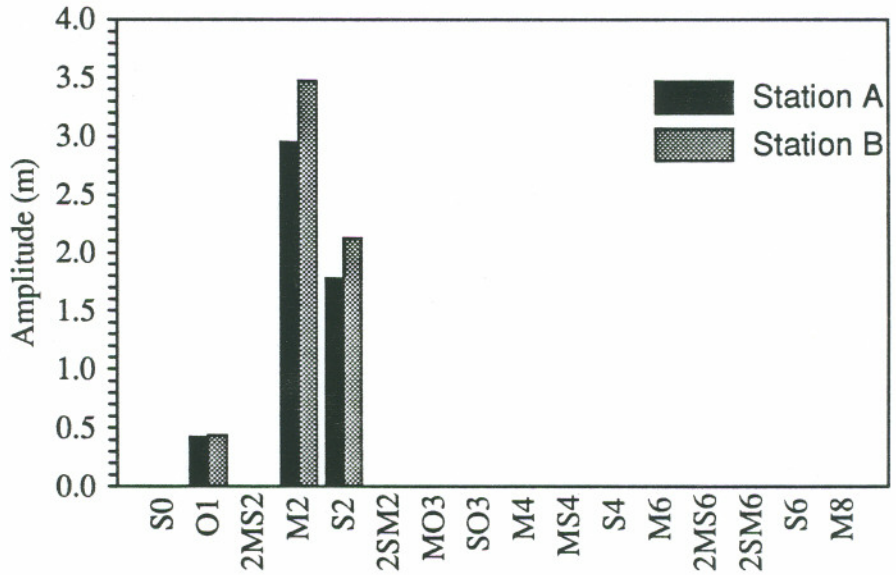

Fig. 37. Harmonic analysis results. Frictionless linear case. M_2+S_2+O_1, flat bottom.

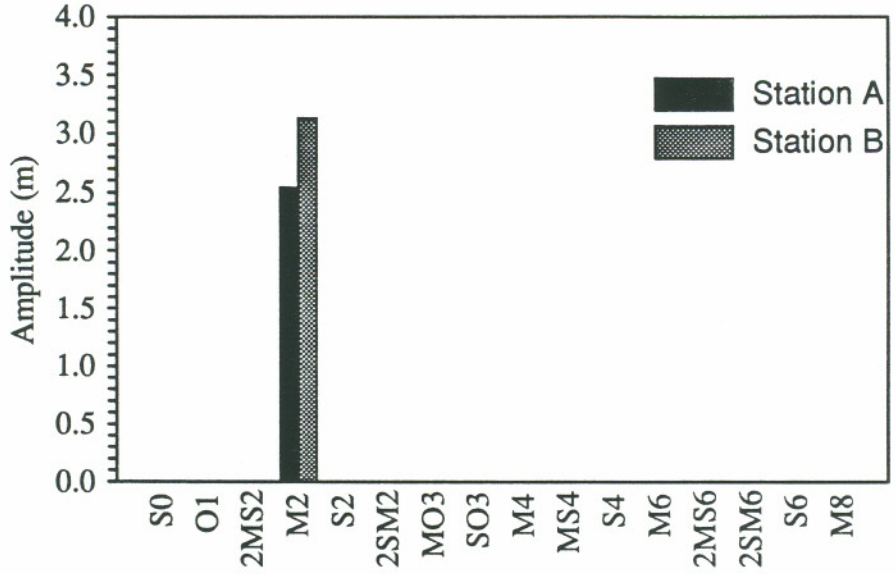

Fig. 38. Harmonic analysis results. Frictionless linear case. M_2, inclined bottom.

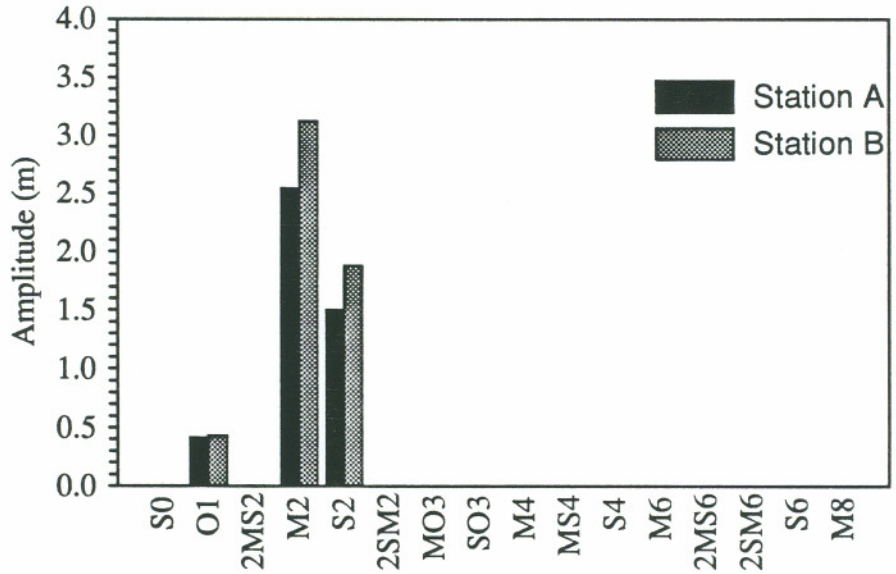

Fig. 39. Harmonic analysis results. Frictionless linear case. $M_2+S_2+O_1$, inclined bottom.

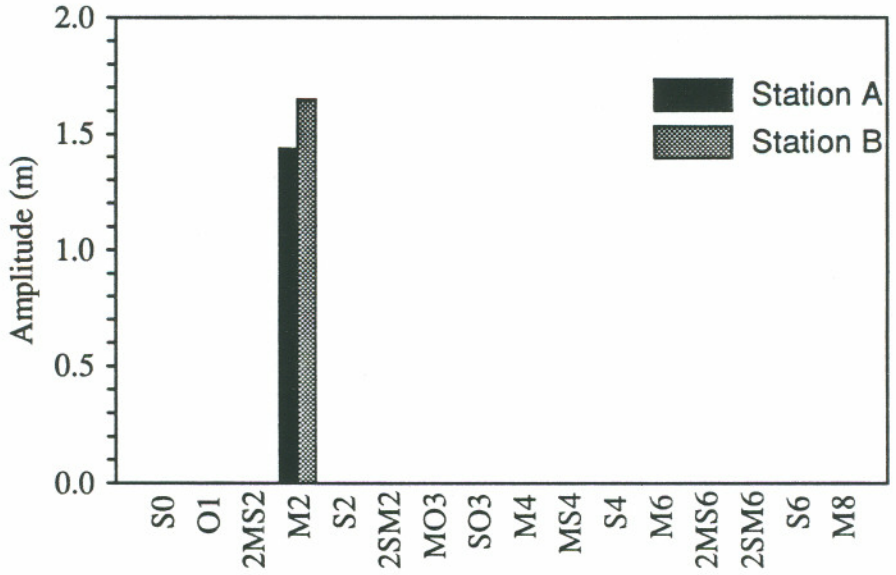

Fig. 40. Harmonic analysis results. Linear case. M_2, flat bottom.

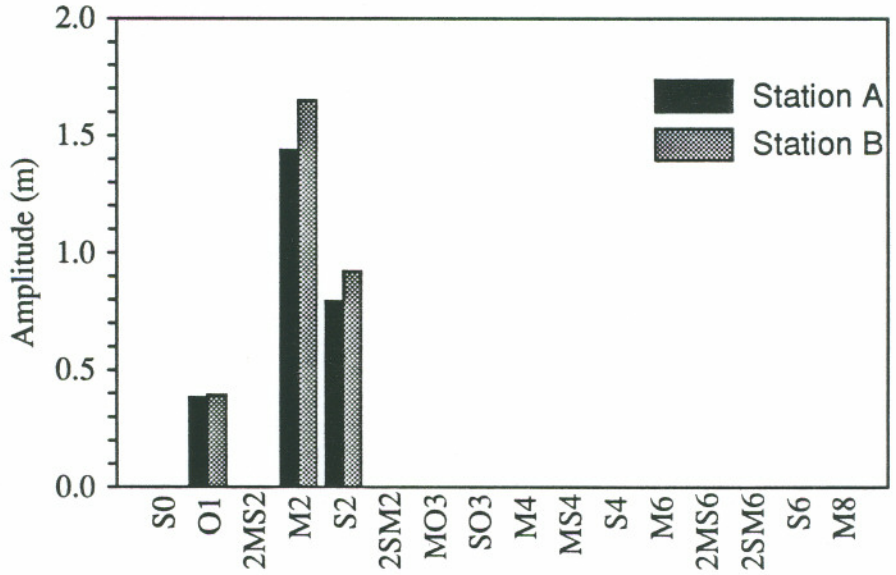

Fig. 41. Harmonic analysis results. Linear case. M_2+S_2+O_1, flat bottom.

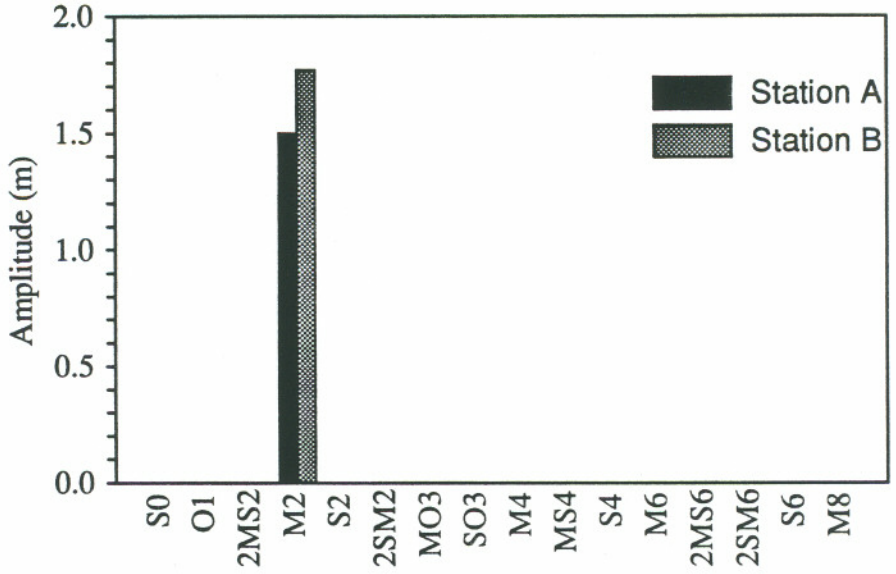

Fig. 42. Harmonic analysis results. Linear case. M_2+S_2+O_1, inclined bottom.

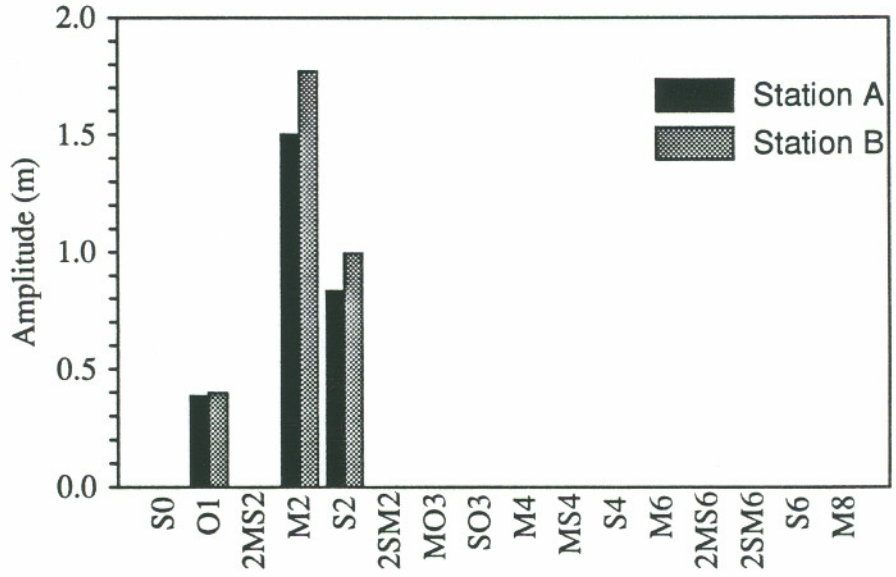

Fig. 43. Harmonic analysis results. Linear case. M_2+S_2+O_1, inclined bottom.

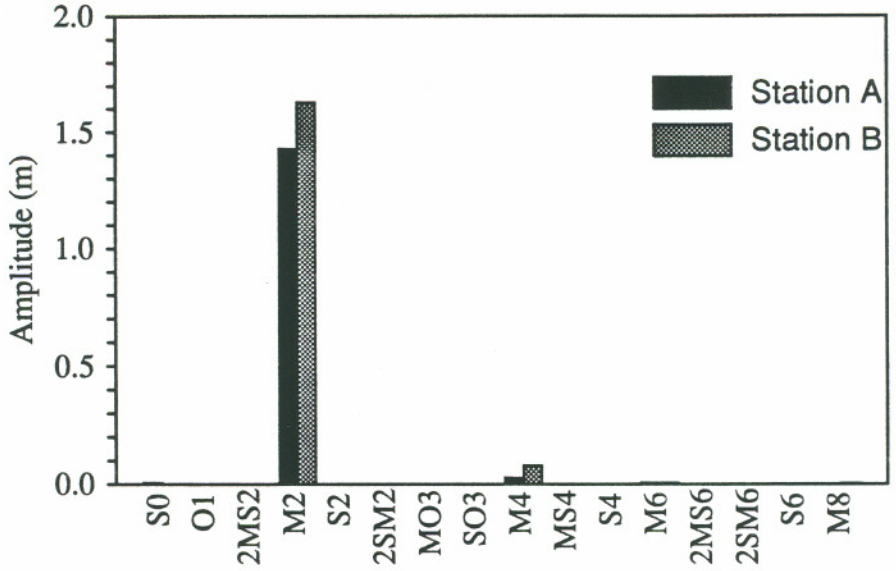

Fig. 44. Harmonic analysis results. Linear case + finite amplitude. M_2, flat bottom.

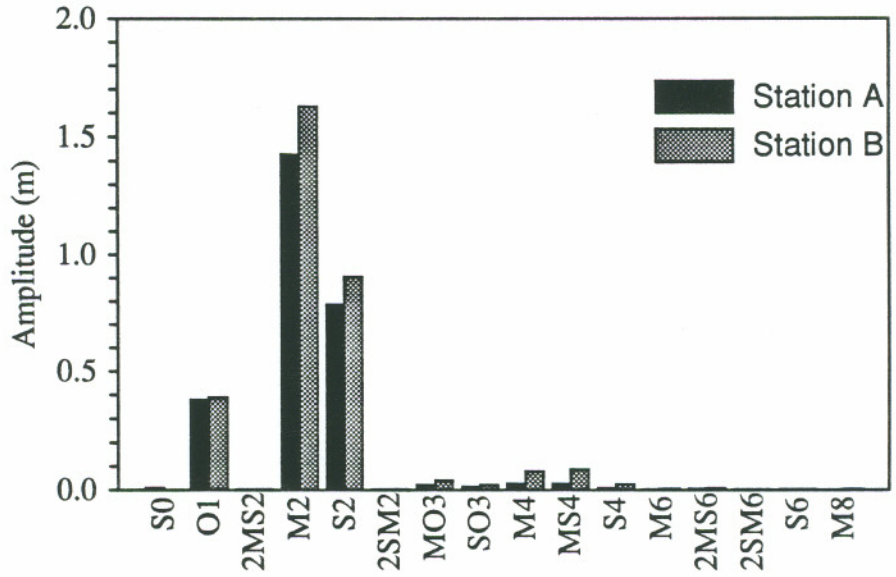

Fig. 45. Harmonic analysis results. Linear case + finite amplitude. $M_2+S_2+O_1$, flat bottom.

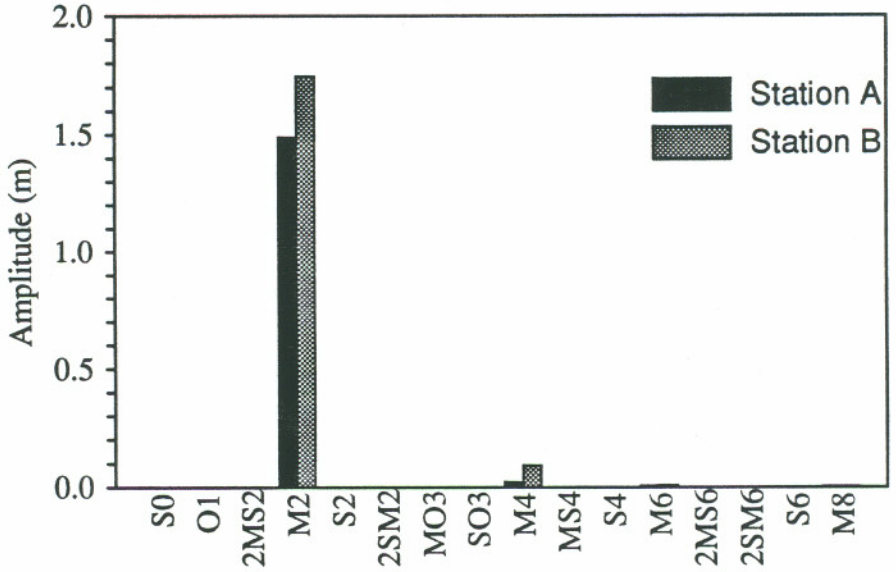

Fig. 46. Harmonic analysis results. Linear case + finite amplitude. M_2, inclined bottom.

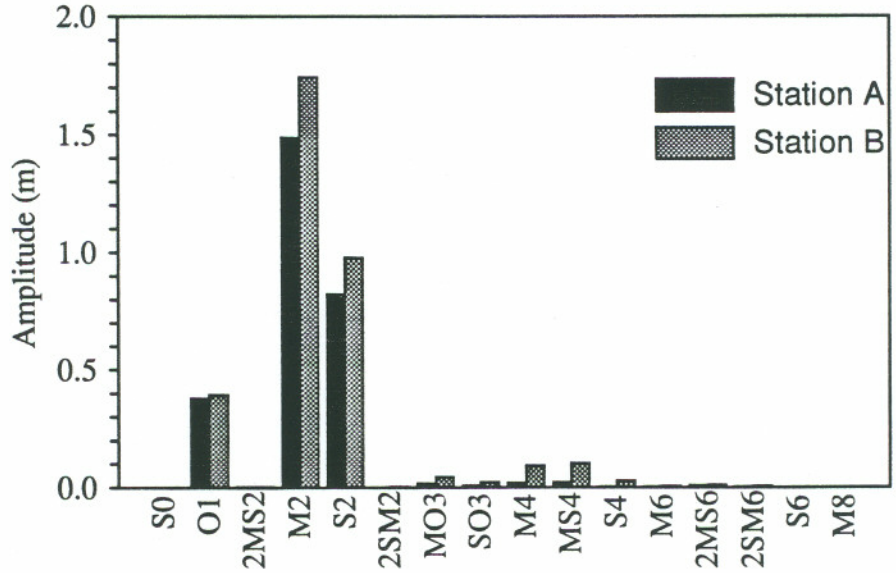

Fig. 47. Harmonic analysis results. Linear case + finite amplitude. M_2+S_2+O_1, inclined bottom.

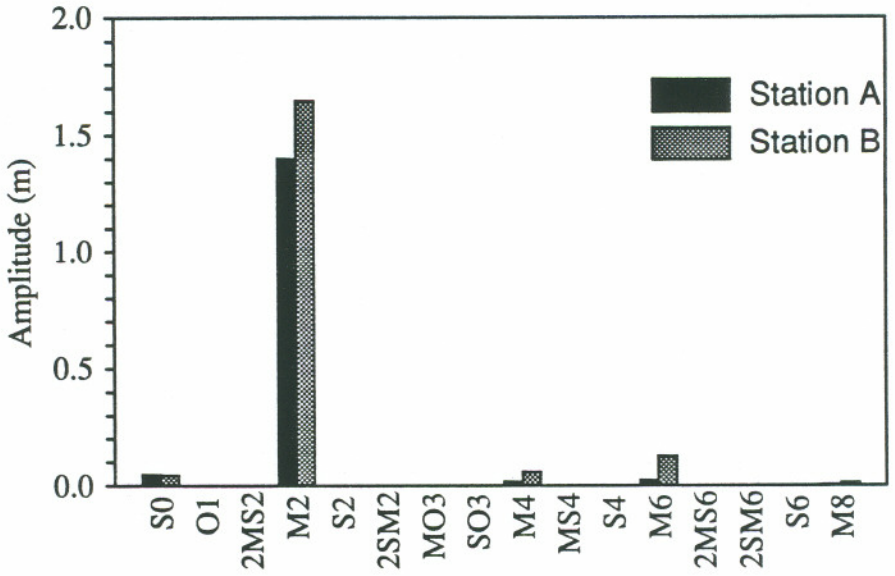

Fig. 48. Harmonic analysis results. Linear case + non-linear friction. M_2, flat bottom.

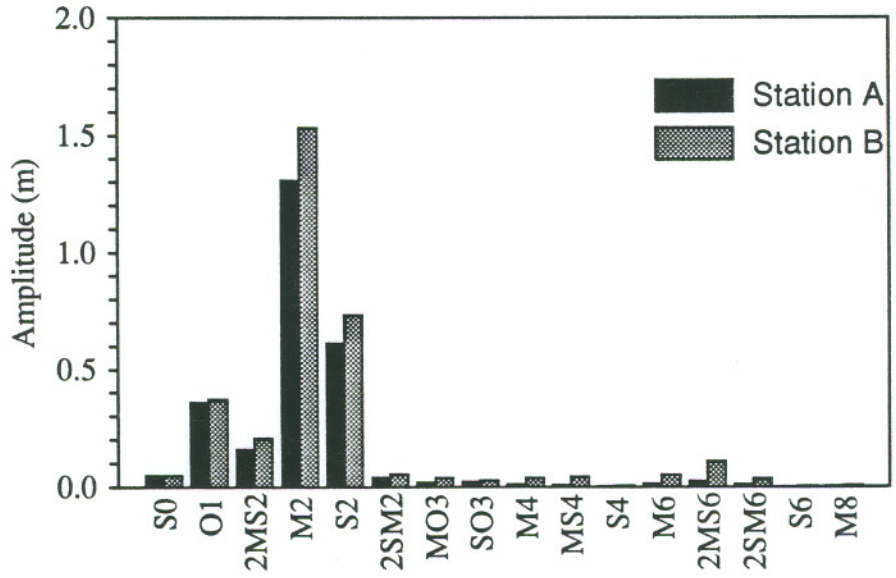

Fig. 49. Harmonic analysis results. Linear case + non-linear friction. M_2+S_2+O_1, flat bottom.

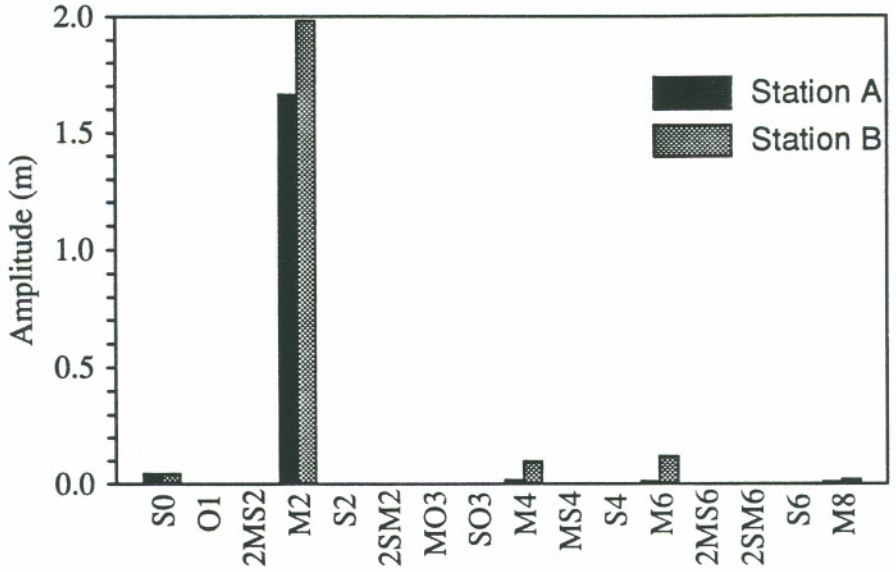

Fig. 50. Harmonic analysis results. Linear case + non-linear friction. M_2, inclined bottom.

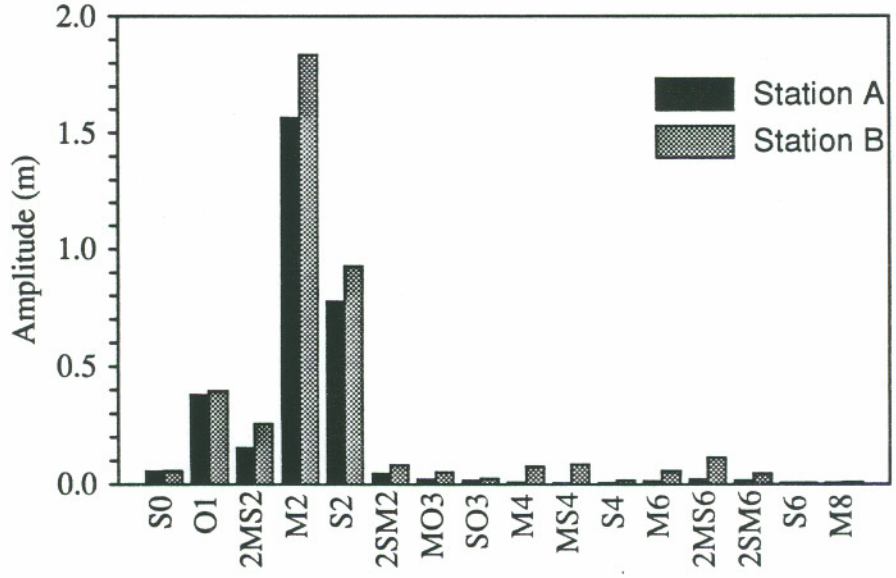

Fig. 51. Harmonic analysis results. Linear case + non-linear friction. $M_2+S_2+O_1$, inclined bottom.

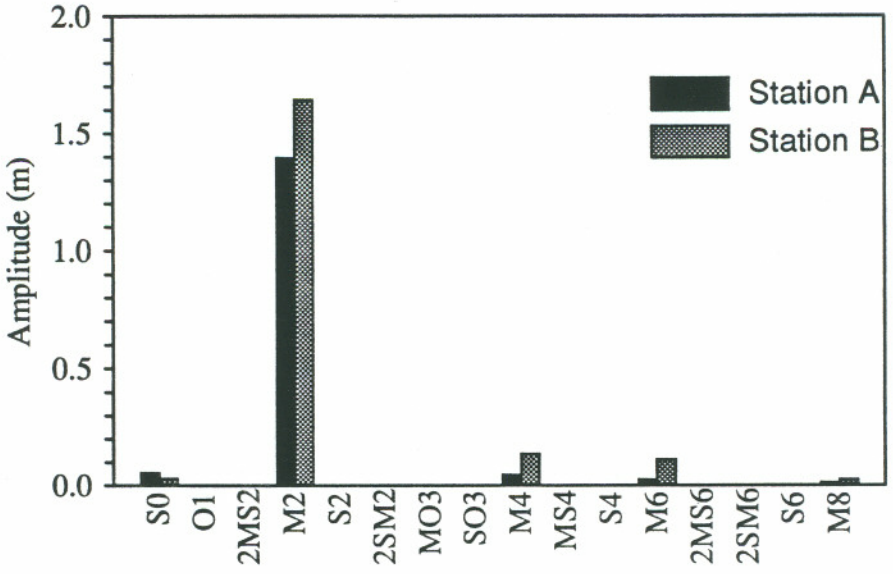

Fig. 52. Harmonic analysis results. Linear case + finite amplitude and non-linear friction. M_2, flat bottom.

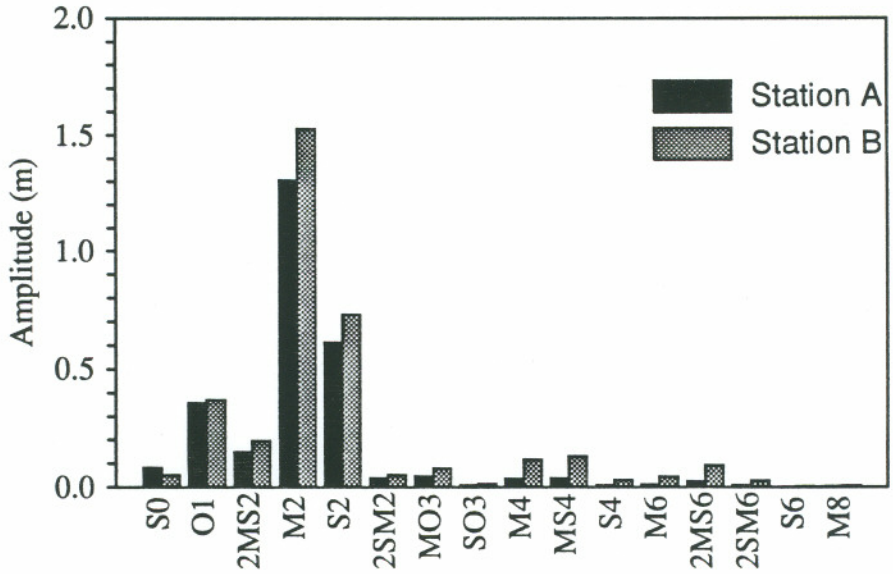

Fig. 53. Harmonic analysis results. Linear case + finite amplitude and non-linear friction. $M_2+S_2+O_1$, flat bottom.

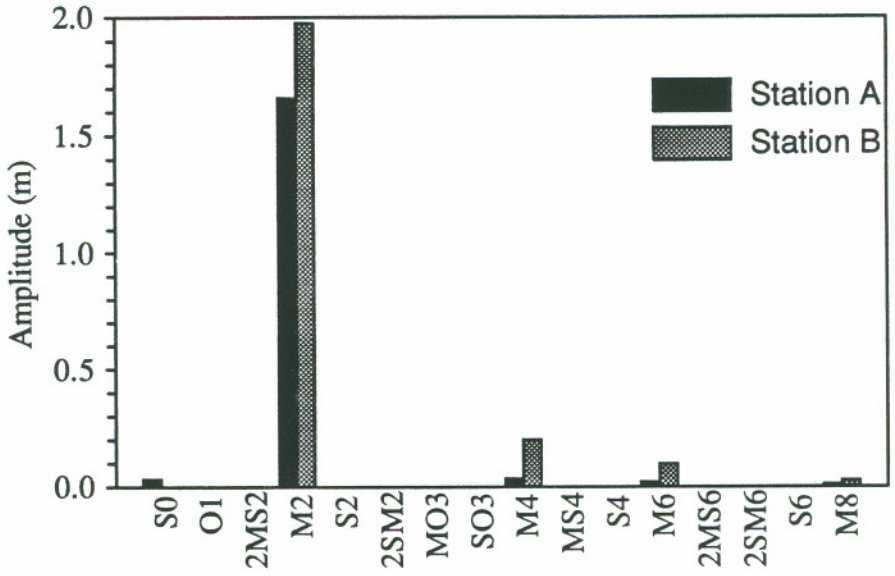

Fig. 54. Harmonic analysis results. Linear case + finite amplitude and non-linear friction. M_2, inclined bottom.

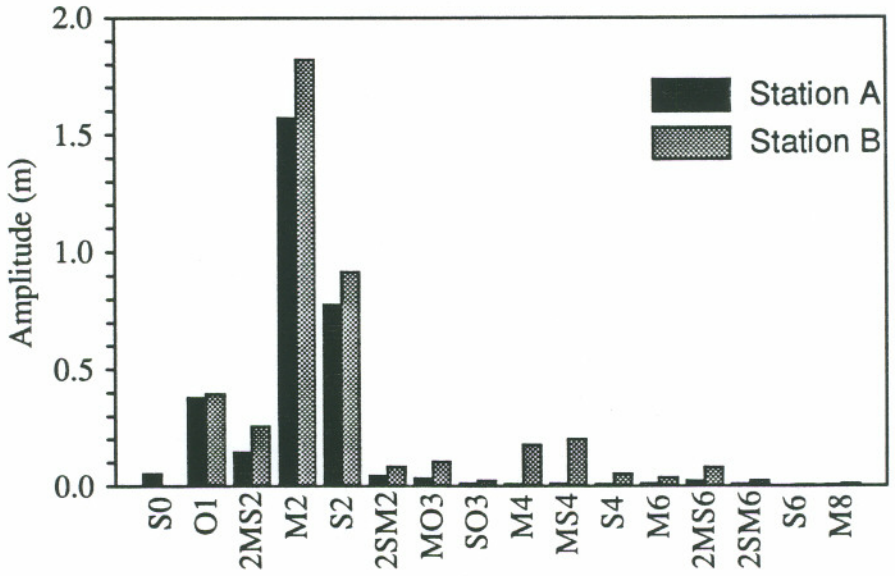

Fig. 55. Harmonic analysis results. Linear case + finite amplitude and non-linear friction. $M_2+S_2+O_1$, inclined bottom.

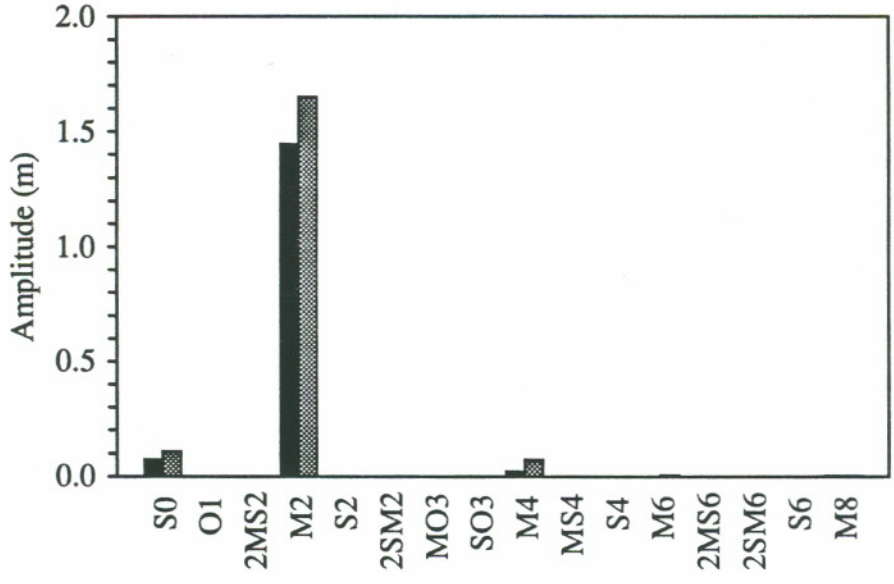

Fig. 56. Harmonic analysis results. Linear case + advection. M_2, flat bottom.

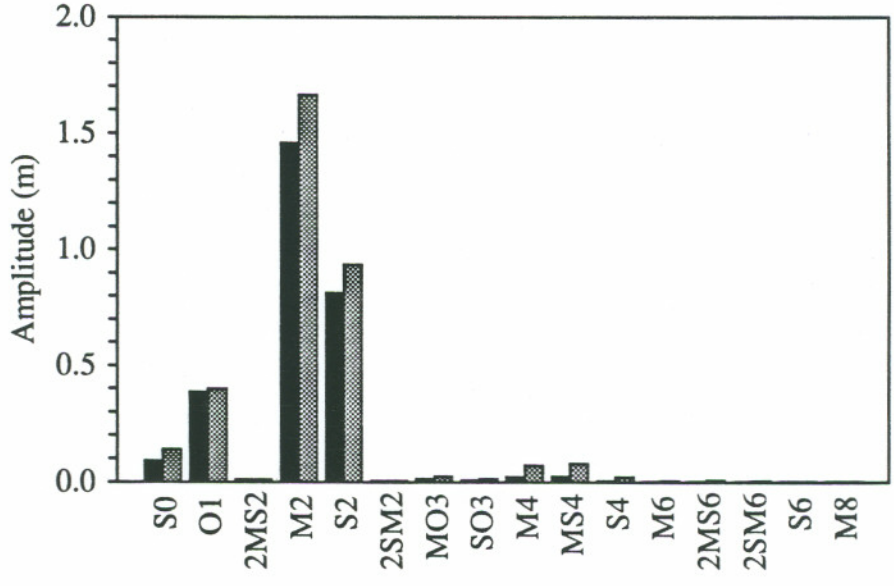

Fig. 57. Harmonic analysis results. Linear case + advection. M_2+S_2+O_1, flat bottom.

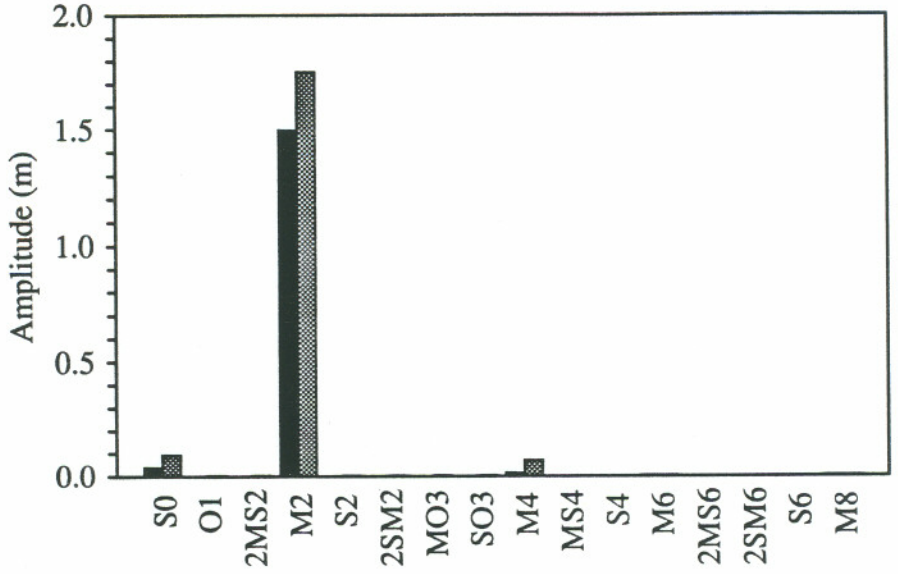

Fig. 58. Harmonic analysis results. Linear case + advection. M_2, inclined bottom.

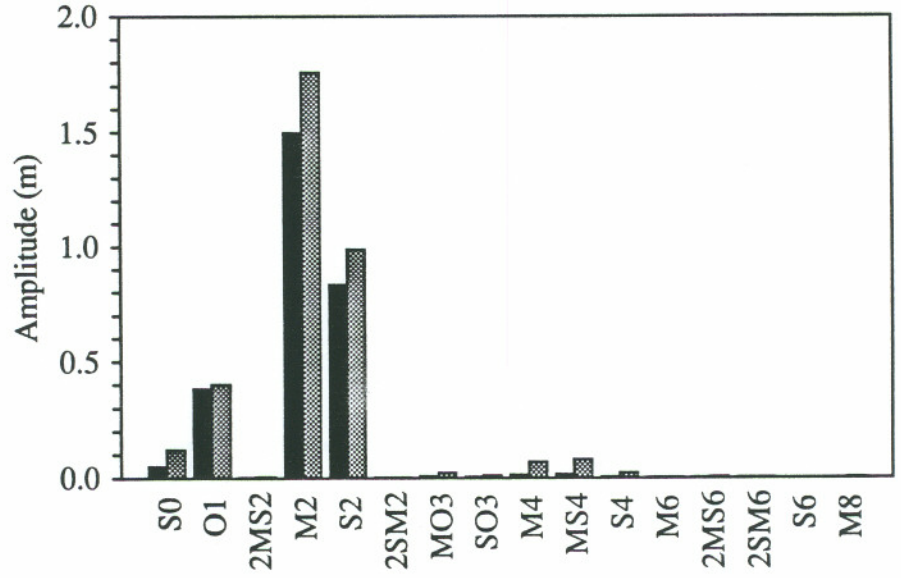

Fig. 59. Harmonic analysis results. Linear case + advection. $M_2+S_2+O_1$, inclined bottom.

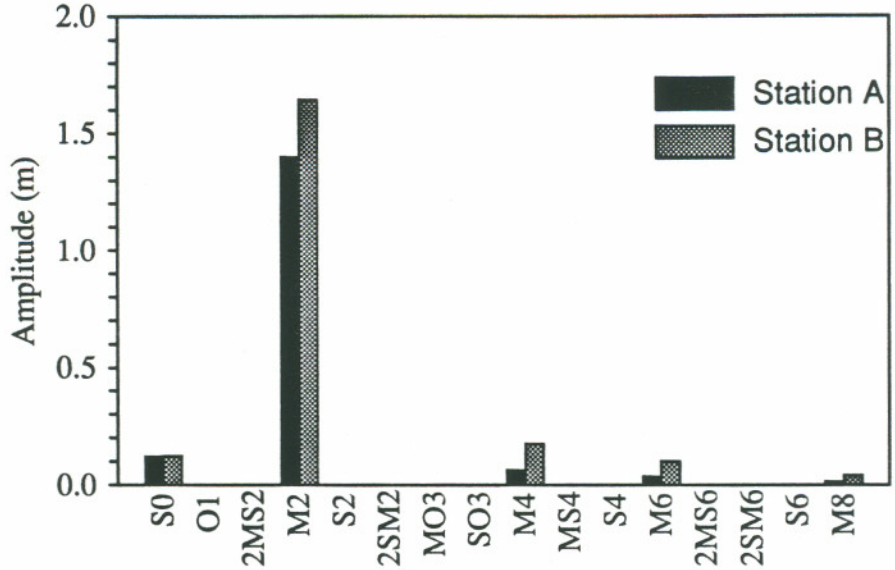

Fig. 60. Harmonic analysis results. Fully non-linear case. M_2, flat bottom.

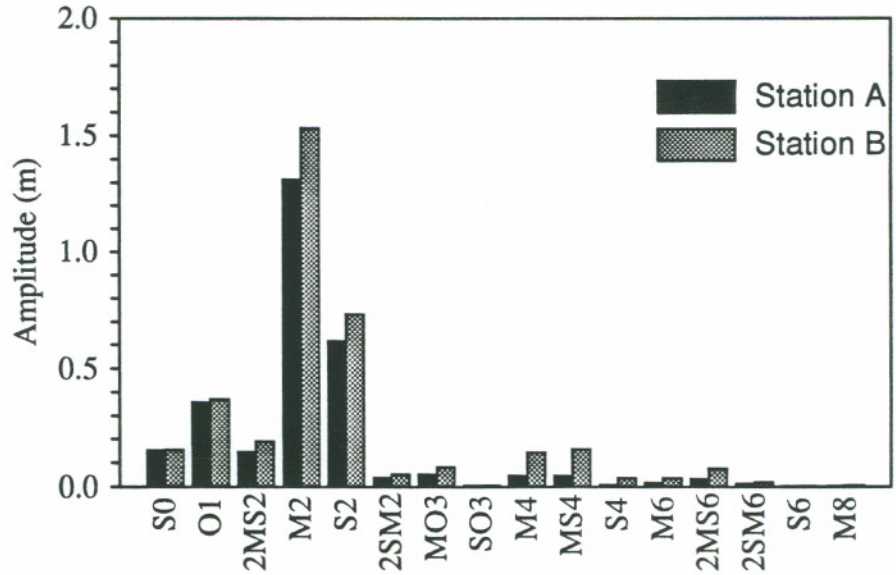

Fig. 61. Harmonic analysis results. Fully non-linear case. $M_2+S_2+O_1$, flat bottom.

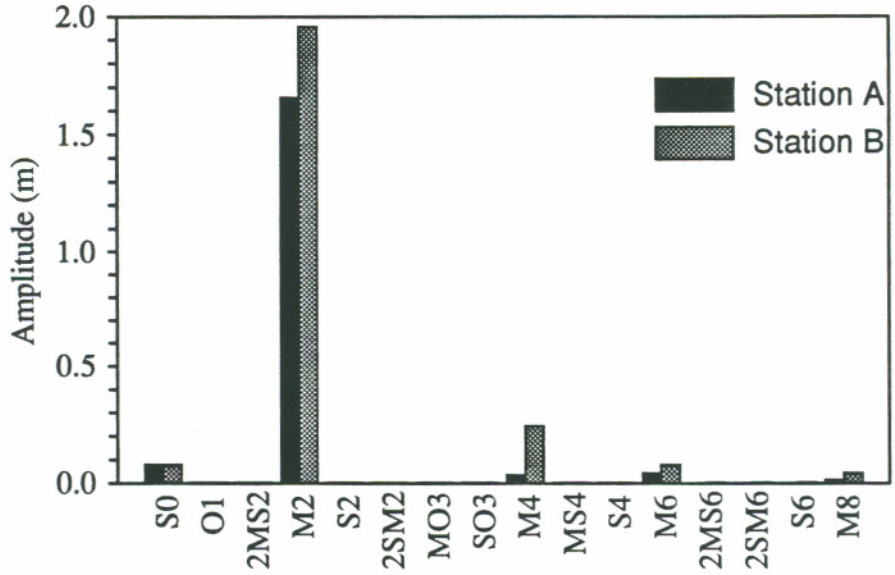

Fig. 62. Harmonic analysis results. Fully non-linear case. M_2, inclined bottom.

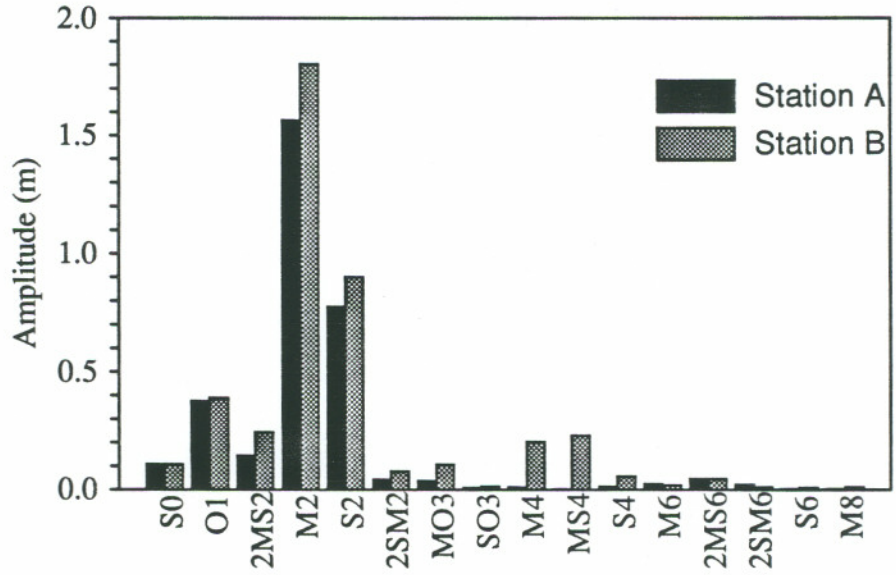

Fig. 63. Harmonic analysis results. Fully non-linear case. $M_2+S_2+O_1$, inclined bottom.

APPENDIX A

Analytical Solutions

A.1. Tidal channel

Lynch and Gray[1] present a set of solution of the linearized 1-D shallow waters equations:

$$\frac{\partial \eta}{\partial t} + h\frac{\partial u}{\partial x} = 0 \qquad [A.1]$$

$$\frac{\partial u}{\partial t} + g\frac{\partial \eta}{\partial x} + \lambda u + \frac{W}{h} = 0 \qquad [A.2]$$

for several geometries and forcings.

From the work of Lynch and Gray, we will review here the analytical solutions that are used in Chapter 3 to partially validate $RITA_1$. Problems of interest in our case involve a no-flux boundary condition at one end of the channel, and a sinusoidal variation of the free surface at the other end, e.g.:

$$\begin{aligned} u &= 0 \quad @ \quad x = 0 \\ \eta &= A\cos(\omega t) \quad @ \quad x = L \end{aligned} \qquad [A.3]$$

The bathymetry is of the form:

$$h(x) = h_0 x^n \qquad [A.4]$$

h_0 and n are constants. Lynch and Gray let n take the values 0, 1, or 2, but we will consider here only the first two cases.

For tidal forcings alone (see Lynch and Gray for wind forcing) the surface elevation and the velocity due to tidal forcing can be written as:

n = 0:

$$\eta_t = \mathrm{Re}\left(A\frac{\cos[\beta(x-x_1)]}{\cos[\beta(x_2-x_1)]}e^{i\omega t}\right) \qquad [A.5]$$

$$u = \mathrm{Re}\left(\left(-\frac{iA\omega}{\beta h_0}\right)\frac{\sin[\beta(x-x_1)]}{\cos[\beta(x_2-x_1)]}e^{i\omega t}\right) \qquad [A.6]$$

n = 1:

$$\eta_t = \mathrm{Re}\left([aJ_0(2\beta\sqrt{x}) + bY_0(2\beta\sqrt{x})]\,e^{i\omega t}\right) \qquad [A.7]$$

$$u = \mathrm{Re}\left(\frac{-i\omega}{\beta h_0 \sqrt{x}}\left[aJ_1(2\beta\sqrt{x}) + bY_1(2\beta\sqrt{x})\right]e^{i\omega t}\right) \qquad [A.8]$$

with:

$$\beta^2 = \frac{(\omega^2 - i\omega\lambda)}{gh_0} \qquad [A.9]$$

$$a = \frac{A\left(Y_1(2\beta\sqrt{x_1})\right)}{\left(J_0(2\beta\sqrt{x_2})\right)\left(Y_1(2\beta\sqrt{x_1})\right) - \left(Y_0(2\beta\sqrt{x_2})\right)\left(J_1(2\beta\sqrt{x_1})\right)}$$

$$b = -\frac{A\left(J_1(2\beta\sqrt{x_1})\right)}{\left(J_0(2\beta\sqrt{x_2})\right)\left(Y_1(2\beta\sqrt{x_1})\right) - \left(Y_0(2\beta\sqrt{x_2})\right)\left(J_1(2\beta\sqrt{x_1})\right)} \qquad [A.10]$$

where x_1 and x_2 are the coordinates of the closed and open end of the channel, respectively, and J and Y are Bessel functions.

A.2. Burgers equation

The Burgers' equation has the form:

$$\frac{\partial u}{\partial t} = \nu\frac{\partial^2 u}{\partial x^2} - u\frac{\partial u}{\partial x} \qquad [A.11]$$

Herbst et al.[2] present the following particular solution:

$$u(x, t) = f(x - ct - \beta) \qquad [A.12]$$

with:

$$f(y) = \frac{\left(c + \alpha + (c - \alpha)\exp\left(\alpha\frac{y}{\nu}\right)\right)}{1 + \exp\left(\alpha\frac{y}{\nu}\right)} \qquad [A.13]$$

This solution represents a wave front initially at $x \equiv \beta$, travelling at a speed c and such that $u(x, t) \rightarrow c \pm \alpha$ if $x \rightarrow \pm\alpha$ for any value of t. The initial and boundary conditions that should be used with the Burgers equation, in a [0,1] domain, in order to obtain [A.12] are given by:

$$u(x, 0) = f(x - \beta) \qquad [A.14]$$

$$u(0, t) = f(-ct - \beta) \qquad [A.15]$$

$$u(1, t) = f(1 - ct - \beta) \qquad [A.16]$$

References:

1 Lynch, D.R and W.G. Gray, "Analytical solutions for computer flow model testing", J. Hydraulics Division, 1415 - 1427, 1978.

2 Herbst, B.M., S.W. Schoombie, D.F. Griffiths and A.R. Mitchell, "Generalized Petrov-Galerkin Methods for the Numerical Solution of Burgers' Equation", Int. J. Numer. Meths. Eng., 20, 1273-1289, 1984.

APPENDIX B

$\underline{\text{RITA}_1}$: Brief User's Manual

B.1. File structure

The primary input files for RITA_1 are the grid file (*caseN*.gr3 - *caseN* being an arbitrary name of the test case (5 characters) and "gr3" a mandatory suffix) and two parameter files: one with the specifications of the numerical scheme (*scheme*.sch - *scheme* being an arbitrary name of the numerical scheme and "sch" a mandatory suffix) and the other with the initial and boundary conditions of the study case, as well as with the definition of the output files to be generated (*caseNnn*.ibo - *caseN* as the meaning explained above, *nn* are two digits that specify the run and "ibo" is a mandatory suffix). The structure for each one of the files is given below (Tables B.1, B.2 and B.3). Additional files may be required, namely files with initial conditions and/or tsunami data (Tables B.4 and B.5).

The output files are specified by the user and they can be:

- *caseNxnn*.res (where *x* is the 5th character of *scheme* and *caseN* and *nn* haves the meaning explained above) - nodal elevations and velocities regularly spaced in space and time (Table B.7);
- *caseNxnn*.cpz (where *x* is the 5th character of *scheme* and *caseN* and *nn* haves the meaning explained above) - time series of elevations at selected nodes (Table B.6);
- *caseNxnn*.cpf (where *x* is the 5th character of *scheme* and *caseN* and *nn* haves the meaning explained above) - time series of flows at selected nodes (Table B.6);
- *caseNxnn*.cpv (where *x* is the 5th character of *scheme* and *caseN* and *nn* haves the meaning explained above) -time series of velocities at selected nodes (Table B.6).

In the tables below the variable name is the name of the variable in the code, the variable type specifies the number of values read and its nature (alpha=alphanumeric, int=integer*2 and real=real*8).

Table B.1. Structure of grid file - caseN.gr3.

variable name	variable type	meaning
case	alpha	name of the case
nnd	int	number of nodes
xnode(i), znode(i) [i=1,nnd]	2real	distance from the origin, depth
width	real	width of the channel

Table B.2. Structure of parameter file #1 - scheme.sch.

variable name	variable type	meaning
alpha	alpha	comments
gwe	real	wave equation's G factor (s^{-1})
kfa, kad, kfr, kvis	4int	flags for finite amplitude, advection, friction and viscosity
lfr, kfaaf	2int	flag for linearized friction, finite amplitude in friction
w10, w11, w12	3real	time discretization factors - time derivative in GCWE
w20, w21, w22	3real	time discretization factors - gravity/GCWE
w40, w41, w42	3real	time discretization factors - finite amplitude/GCWE
kfaaw	int	flag for finite amplitude in advection/GCWE
w30, w31, w32	3real	time discretization factors - advection/GCWE
kcw, keb	2int	flags for continuity and element based - advection /GCWE
w50, w51, w52	3real	time discretization factors - linear friction/GCWE
w60, w61, w62	3real	time discretization factors - linear G/GCWE
w70, w71, w72	3real	time discretization factors - non-linear friction /GCWE
w80, w81, w82	3real	time discretization factors - non-linear G/GCWE
klum	int	flag for lumping of the ME
pm10, pm11	2real	time discretization factors - advection/ME
knup, alph, bet	int, 2real	code for upwind/element based and parameters for upwind - advection/ME
pm20, pm21	2real	time discretization factors - gravity/ME
pm30, pm31	2real	time discretization factors - friction/ME
kfaav	int	flag for finite amplitude - viscosity/ME
pm40, pm41	2real	time discretization factors - viscosity/ME
kelm, nit, crit	2int,real	flag for ELM, max no. of iterations, convergence criteria

Table B.3. Structure of parameter file #2 - caseNxx.ibo.

	name	type	meaning
	alpha	alpha	case
	alpha	alpha	comments
	tau, visc	2real	friction coefficient, viscosity coefficient if lfr=0 - manning coefficient if lfr=1 - linear friction parameter
	grv	real	acceleration of gravity
	dt, nti	real, int	time step, no. of time steps
	kic	int	type of initial conditions
if kic=0	zinit, finit, tinit	3real	initial elevation, flow and time
if kic=1	inft	int	no of times in fileinit
if kic=1	fileinit	alpha	file with initial conditions
	kresf, tpinit, ntip	int, real, int	flag for result file (.res)
	kocpz, ntsoz, nmcpoz	3int	flag for output of elevation, initial time step, no. of nodes
if kocpz=1	ncpoz(i),i=1,nmcpoz	(nmcpoz)int	nodes for elevation output
	kocpf, ntsof, nmcpof	3int	flag for output of flow, initial time step, no. of nodes
if kocpf=1	ncpof(i),i=1,nmcpof	(nmcpof)int	nodes for flow output
	kocpv, ntsov, nmcpov	3int	flag for output of velocity, initial time step, no. of nodes
if kocpv=1	ncpov(i),i=1,nmcpov	(nmcpov)int	nodes for velocity output
	kbcd	int	type of downstream boundary condition
if kbcd=1,4	bccd	real	if kbcd=1 - constant elevation if kbcd=4 - constant flow
if kbcd=2,3	ntcd	int	no. of components
if kbcd=2,3	bcvphd,bcvamd,bcvfrd	3real	phase, amplitude, period (h)
if kbcd=6	bcvphd,bcvamd,bcvfrd, bcvrdd	4real	phase, amplitude, period (h), reference
if kbcu=7	bcvamd,bcvfrd, bcvrdd	3real	amplitude, offset, shape factor
	kbcu	int	type of upstream boundary condition
if kbcu=1,4	bccu	real	if kbcu=1 - constant elevation if kbcu=4 - constant flow
if kbcu=2,3	ntcu	int	no. of components
if kbcu=2,3	bcvphu(j), bcvamu(j), bcvfru(j)	3real	phase, amplitude, period (h)
if kbcu=6	bcvphu,bcvamu,bcvfru, bcvrdu	4real	phase, amplitude, period (h), reference
if kbcu=7	bcvamu,bcvfru, bcvrdu	3real	amplitude, offset, shape factor
	kci,nskci	2int	flag for integral, nts skip for printing
	ktsu	int	flag for tsunamis
if ktsu=1	tsufil	alpha	file with tsunami conditions
if ktsu=1	ntsu, nttsu	2int	initial t. step for tsunami release, no. of t.steps

Table B.4. Structure of initial conditions data file.

variable name	variable type	meaning
[j=1,inft]		
a(i), u(i) [i=1,nnd]	2real	elevation, velocity

Table B.5. Structure of tsunami data file.

variable name	variable type	meaning
xnode(i), znode(i) [i=1,nnd]	2real	distance from the origin, depth

Table B.6. Structure of general output file - caseNxnn.res.

variable name	variable type	meaning
[j=T,nti,,ntip]		(T - time step after tpinit)
"&", t	alpha, real	time at time step j
[i=1,nnd,nnod]		
xnode(i),a(i),u(i)	3real	x coordinate, elevation, velocity at time step j

Table B.7. Structure of time series output file - caseNxnn.cp*A* (*A*=e,f,v).

variable name	variable type	meaning
[j=1,ntso*A*]		
t, a(i), u(i) [i=1,nmcpo*A*]	(nmcpo*A*+1)real	time, elevation, velocity at time step j

B.2. How to run the model

The command to run the model is:

rita1 scheme caseN nn [-e] [-v] [skip]

Variables scheme, caseN and nn have the meaning explained above; they identify the numerical strategy, the case and the specific run, respectively. The flags -e and -v and the parameter skip are to be used when the model runs from the visualization program ACE_1. The flag -e specifies the display of elevations and the flag -v the display of velocities. The parameter skip sets the number of time steps between two consecutive displays.

The command to use ACE_1 is simply:

ace1 [-p parameter file]

$RITA_1$ can then be run by using the pop-up $RITA_1$, from the pull-down menu Models.

BIOGRAPHICAL SKETCH

The author was born the 13th October, 1963, in Lisbon, Portugal. He entered Universidade Nova de Lisboa, Monte da Caparica, Portugal, in October 1981 and received his Bachelor of Science degree in Environmental Engineering in January 1987.

In September, 1989, the author came to the Oregon Graduate Institute with a three month grant from the World Health Organization, to do research with Dr. António M. Baptista on estuarine modeling. In January, 1990, he became a student at the Oregon Graduate Institute, under the supervision of Dr. António M. Baptista. He was awarded his Master of Science in Environmental Science and Engineering in April 1992.